Modelling the Asian Paleo-hydroclimatic Variability

A Dissertation

Submitted in Partial Fulfilment of the

Requirements for the Degree of Doctor rerum naturalium (Dr. rer. nat.)

to the Department of Earth Sciences

of the Freie Universität Berlin

by

Bijan Fallah Hassanabadi

Berlin, February 2015

Supervisor: Prof. Dr. Ulrich Cubasch
Institut für Meteorologie, Freie Universität Berlin

Second examiner: PD. Dr. Sushma Prasad
Institut für Erd- und Umweltwissenschaften, Universität Potsdam

Date of the viva voce/defense: 11. May 2015

Eidesstattliche Erklärung

Hiermit versichere ich an Eides statt, die vorliegende Arbeit selbstständig und eigenhädig ohne fremde Hilfe angefertigt zu haben. Es wurden keine anderen als die angegebenen Quellen und Hilfsmittel benutzt. Wörtlich oder inhaltlich entnommene Stellen wurden als solche kenntlich gemacht. Diese Arbeit hat in gleicher oder änlicher Form noch keiner Prüfungsbehörde vorgelegen.

Berlin, 5. Februar 2015

Bijan Fallah Hassanabadi

"What's the use of having developed a science well enough to make predictions if, in the end, all we're willing to do is stand around and wait for them to come true?"

Frank Sherwood, Nobel laureate in Chemistry in 1995

Abstract

Using a multi-proxy and multi-model approach, this study aims to unravel the characteristics of modern- and palaeo-hydroclimatic variability over Asia. This is designed on different time-scales and diverse geographically distributed regions in Asia. Special emphasis is given to extreme hydro-meteorological events (*e.g.*, mega-droughts). The main focus of this investigation is on climatically sensitive regions of Asia (*e.g.*, monsoon-dominated and westerly-dominated regions).

The combination of different model and proxy data leads to an enhanced understanding of the controlling mechanisms of the Asian climate dynamics. In this thesis, palaeoclimate simulations of different time-slices are carried out for selected time periods. The main focus lies in global and regional model simulations, as well as the sensitivity tests using these models. In a first step, existing global simulations for the past 1,000 years are analyzed, concentrating on dynamics of Asian monsoon and Westerlies, and on climate modes like El Niño Southern Oscillation (ENSO), Pacific North Atlantic Oscillation (PNA) and North Atlantic Oscillation (NAO) and their tele-connections with the Asian climate. In this regard, two Paleoclimate Modelling Intercomparison Project Phase III (PMIP3)/ Coupled Model Intercomparison Project Phase 5 (CMIP5) climate model ensemble simulations of the past millennium have been analyzed to identify the occurrence of Asian mega-droughts. The Palmer Drought Severity Index (PDSI) is used as the key metric for the data comparison of hydro-climatological conditions. The model results are compared with the proxy data of the Monsoon Asia Drought Atlas (MADA). This study shows that Global Circulation Models (GCMs) are capable to capture the majority of historically recorded Asian monsoon failures at the right time and with a comparable spatial distribution. The simulations indicate that ENSO-like events lead in most cases to these droughts. Both, model simulations and proxy reconstructions, point to less monsoon failures during the Little Ice Age. During historic mega-droughts of the past millennium, the monsoon convection tends to assume a preferred regime described as "break" event in Asian monsoon. This particular regime is coincident with a notable weakening in Pacific Trade winds and Somali Jet.

The interesting periods that are run and analyzed include extreme rainfall anomalies

within the Medieval Climate Anomaly (MCA) and the Little Ice Age (LIA). The generated model data are compared with the recently published paleo-data derived from different archives. The global simulations served as boundary conditions for regional climate and its transition from one climate period to another (e.g. from MCA to LIA). For the selected climatic periods typical circulation anomalies responsible for changes in regional climate and the physical mechanisms driving them are identified. Additional sensitivity simulations are carried out with and without Tibetan Plateau to investigate and compare the existing hypotheses on the behavior of Asian summer monsoon due to plateau forcing. The analysis of sensitivity experiments point out to the significant impacts of Plateau forcing on the atmosphere-ocean tele-connections. It is shown that, in addition to the direct feedbacks of Tibetan Plateau orography on the climate of Asia, such as *sensible heat pumping* and *thermal insulation*, other significant processes exist, which link the Asian summer monsoon to the sea surface temperatures in the North Atlantic Ocean. A removal of the Tibetan Plateau modifies the wind-driven ocean circulations over the North Atlantic, leading to a decrease of surface heat advection over the North Atlantic Ocean and a decrease of the Atlantic Meridional Overturning Circulation. This, in turn, affects via teleconnections both the monsoon rainfall and the position of the intertropical convergence zone. A climate modelling approach is presented to reproduce the rainfall patterns over Iran due to the climatic forcings during the past 6,000 years. The selected periods are simulated using a spatially high-resolved atmosphere General Circulation Model (GCM). The results show that the winter rainfall patterns over Iran have changed due to the changes in solar insolation to a wetter condition starting around 3,000 yr BP and reaching its maximum during the Medieval Climate Anomaly ca. 1,000 yr BP. The rainfall variability can be explained by the changes in the climate energy balance as a result of changing incoming solar irradiance based on the Milankovitch theory. A shift in the earth energy balance leads to the modulation of the West Asian Subtropical Westerly Jet (WASWJ). The investigations support the hypothesis that during the Holocene a northward shift in the WASWJ contributes to the less cyclonic activities over Iran. This brings less moisture into the region during the winter.

Contents

Dedicated to Tahereh,
Hosseinali,
and Dagmar.

Chapter 1

Introduction

The climate of the Earth has always been changing throughout the history. Proxy reconstructions of climate change indicate the existence of eight cycles of glacial advance and retreat in the last 740,000 years [Augustin, 2004]. However, some scholars suggest that the recent warming trend is *very likely* human-induced [Hegerl et al., 1996, Ramaswamy et al., 2006, Santer et al., 1996, 2003, Stocker et al., 2013]. Cook et al. [2013b] have shown that of the 4,000 peer-reviewed scientific papers published in the period 1991–2011 "expressing a position on anthropogenic global warming, 97.1% endorsed the consensus position that humans are causing global warming". The evolution of future "human-induced" global climate change has become one of the main concerns of the 21^{st} century.

1.1 Complex monsoon-dominated Asia

Comparing the complex regional monsoon area [Wang et al., 2005a] over Africa, Australia, India and East Asia (Figure 1.1) with population density estimate from Global Rural-Urban Mapping Project, Version 1 (GRUMPv1) (Figure 1.2, http://sedac.ciesin.columbia.edu/gpw/), reveals that the monsoon region is the most densely populated area of the Earth. Minor changes of seasonal mean rainfall in this "convectively active" area, inflict damage on a large portion of the society that is closely tuned to the monsoon variability [Hannachi and Turner, 2013, Webster et al., 1998]. In recent times, monsoon affects the livelihood of more than 2.5 billion people under the increasing occurrence and

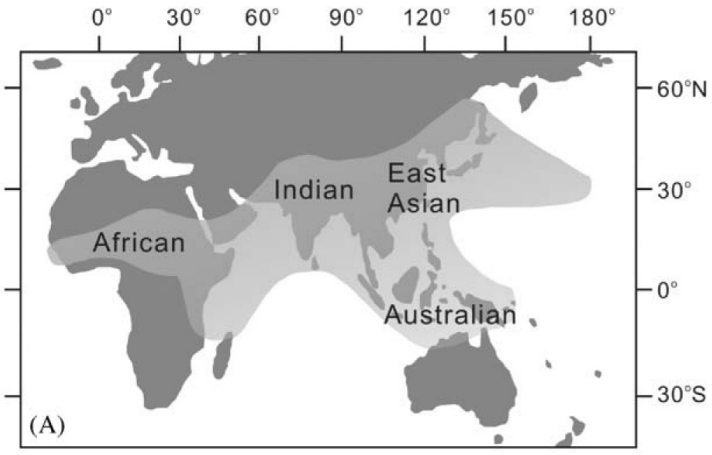

Figure 1.1: Modern complex monsoon domain (light gray shading). Figure from Wang et al. [2005a].

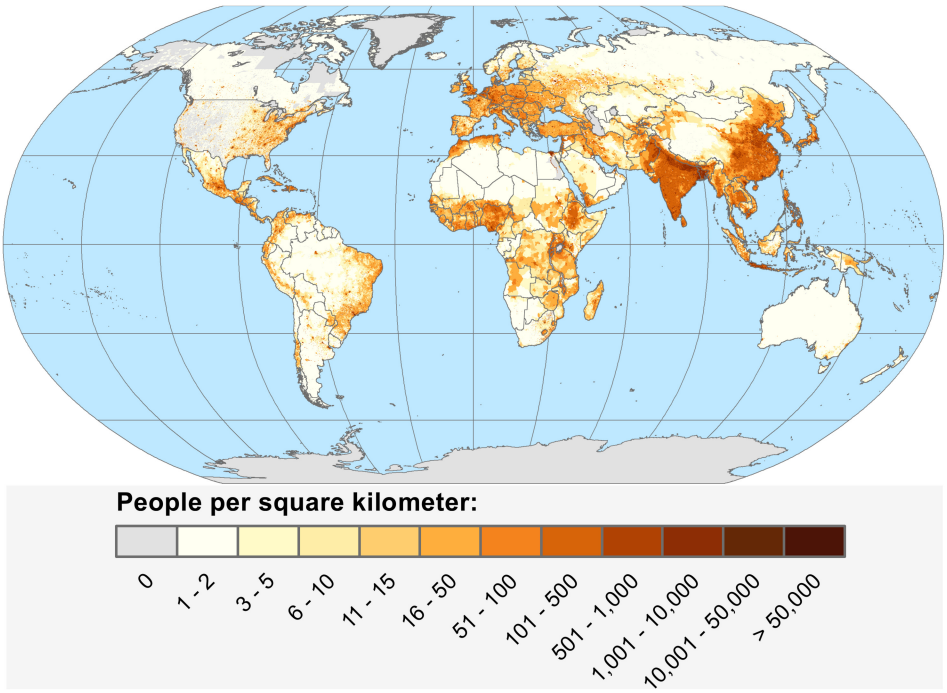

Figure 1.2: Population density ($^{people}/_{km^2}$) from GRUMPv1 (http://sedac.ciesin.columbia.edu/gpw/).

frequency of extreme monsoon rainfall events [Krishnan et al., 2009, Shaw and Nguyen, 2011, Ummenhofer et al., 2013].

Annual and intra-seasonal variations of hydro-climatological systems can lead to haz-

ards in vulnerable Asian regions relating public water availability, sustainable development, energy security, crop damage, hydro-electric generation and infrastructures. There is an urgent need to address this issue for planning and securing the future mitigation and adaptation strategies under global warming scenarios.

Asia has two specific climatic regions: (i) monsoon-dominated humid Southern and Southeastern Asia and (ii) westerlies-dominated Arid Central Asia (ACA) [Dando, 2005]. Our knowledge about the sensitivity of the severe climate conditions (e.g. droughts) to changes in climate forcing is mostly limited to the modern instrumental records [Easterling et al., 2000]. Asian summer monsoon is the most complex circulation of Tropics [Holton and Hakim, 2012]. This extensive circulation has a dominant role on the climate of South Asia. It is a consequence of an interplay between land, ocean and atmosphere. The schematic presented in Figure 1.3 depicts the factors which affect the severity of monsoon (Seas Surface Temperature (SST)s in the Pacific and Indian Oceans, snow cover and soil moisture, position and strength of westerlies and changes in solar output) [Wahl and Morrill, 2010].

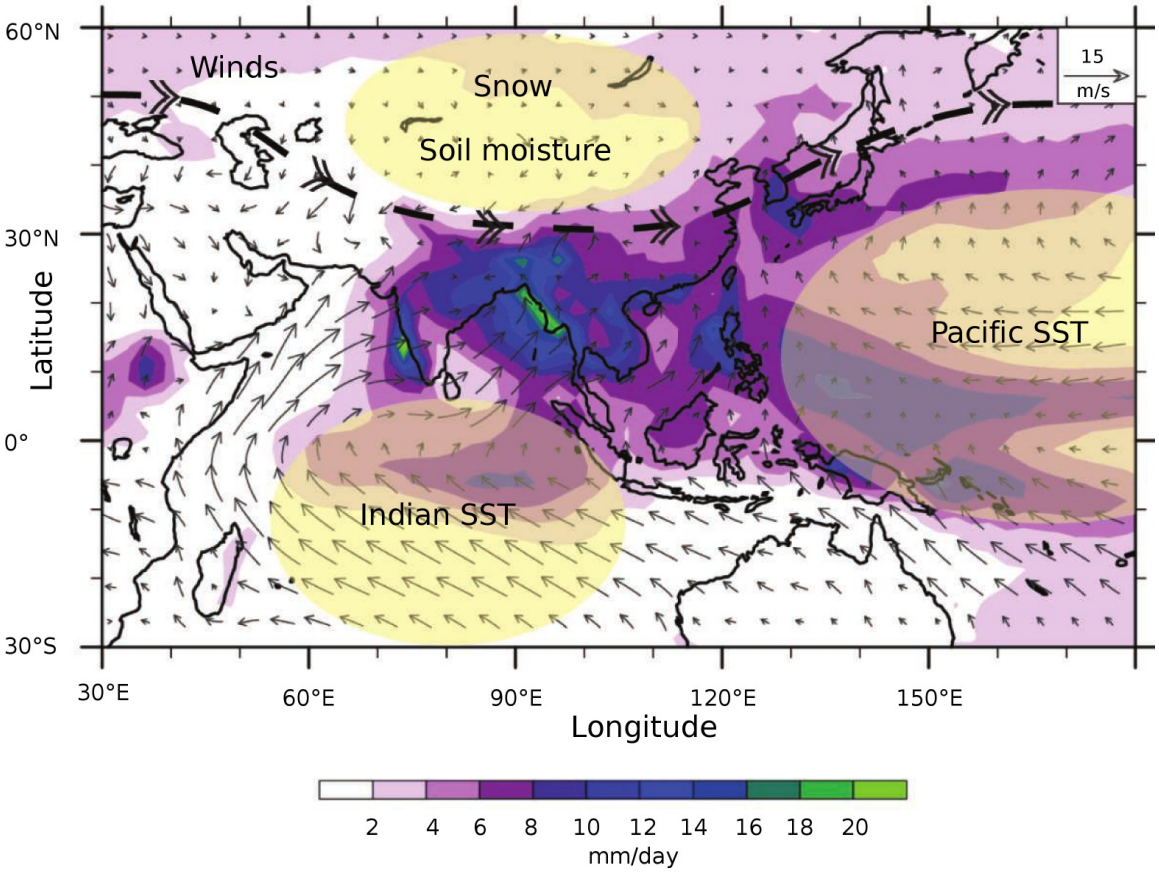

Figure 1.3: Rainfall (from GPCP http://precip.gsfc.nasa.gov) and surface winds (NCEP/NCAR reanalysis http://www.cpc.ncep.noaa.gov/products/wesley/reanalysis.html) over Asia during summer (JJA) from Wahl and Morrill [2010]. Yellow areas and schematic winds indicate some drivers of monsoon changes. Data is averaged over the period 1979-2009.

1.2 Model-proxy comparison in Asia

This study tackles important subjects for which there is up to now mainly controversial evidences. The climate of the past millennium, with several mega-droughts recorded in high-resolution proxy indicators in several areas of the Earth, and with now several simulations with coupled atmosphere ocean models and regional climate simulations, is an obvious object of study.

Figure 1.4 presents the number of station temperature records available for the Climatic Research Unit Time-Series Version 3.21 (CRU TS 3.21) gridded temperature

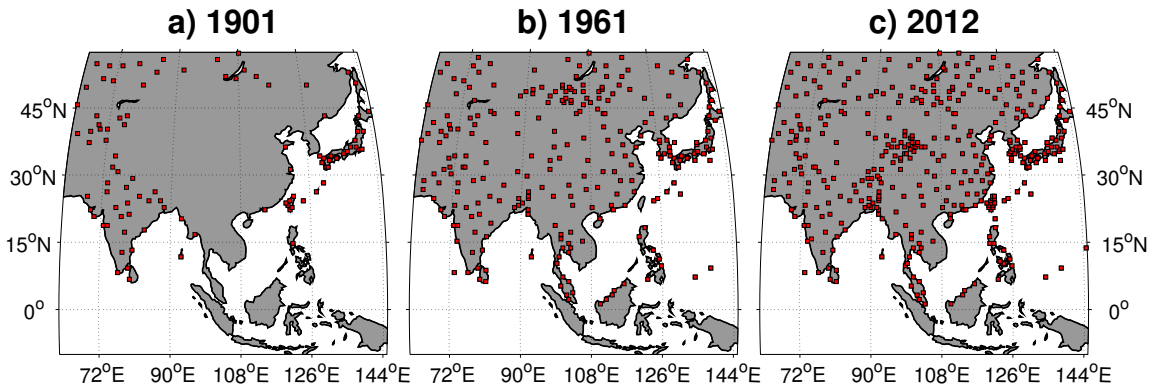

Figure 1.4: Number of station temperature records available for the CRU TS 3.21 gridded temperature field for year a) 1901, b) 1961 and c) 2012.

field [Harris et al., 2014] for the years 1901, 1961 and 2012. As can be seen, the number of stations drops precipitously for the year 1901. The lack of observations prior to 1930 is dramatic in Central Asia [Cook et al., 2013a]. Thus, this study will use a model-proxy approach to investigate the Central Asian climate dynamics in a longer period of time.

The reconstructions of Northern Hemisphere temperature anomaly have shown three different climatic episodes during the past 1,100 years: (i) Medieval Climate Anomaly (MCA), roughly 950 –1250 AD, (ii) Little Ice Age (LIA), the period of 1400 –1700 AD and (iii) the Recent Climate, 1800 –2000 AD [Briffa, 2000, D'Arrigo et al., 2006, Hegerl et al., 2007, Mann and Jones, 2003, Mann et al., 1999, 2008, Moberg et al., 2005]. Figure 1.5 shows the reconstructed Northern Hemisphere annual temperature anomaly during the past 2000 years from Intergovernmental Panel for Climate Change Fourth Assessment Reports (IPCC) 2013 report [Stocker et al., 2013]. The data can be obtained from the National Climate Data Center (NCDC) webpage (`http://www.ncdc.noaa.gov/paleo/recons.html`).

So far there is a huge lack of knowledge about the evolution of precipitation or moisture for centennial and millennial time scales. In contrast to temperature, hydrological variability has a very regional nature. Hydrological response to large-scale climate forcing

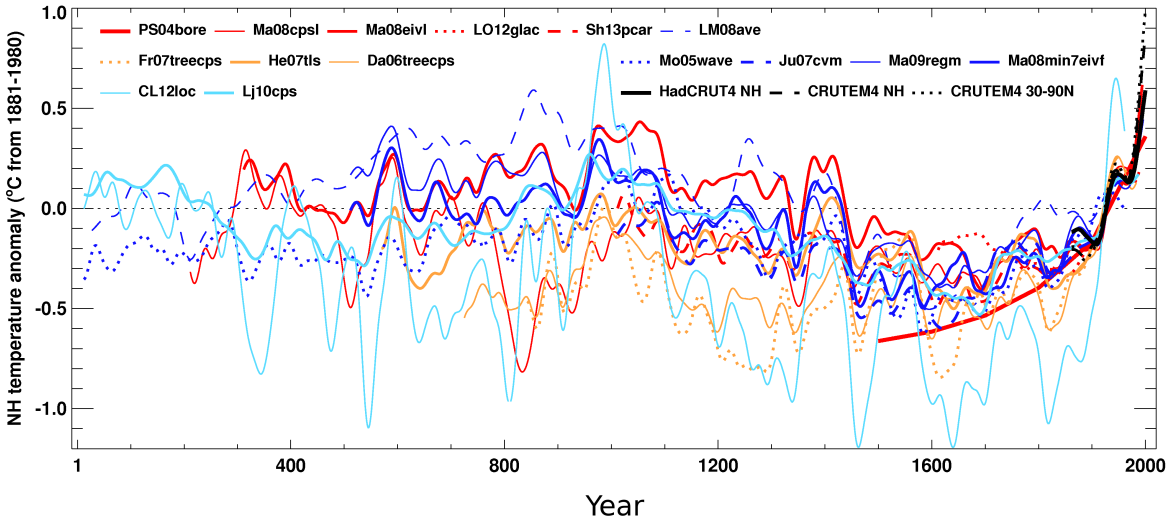

Figure 1.5: Reconstructed Northern Hemisphere annual temperatures for the past 2000 years from IPCC 2013 [Stocker et al., 2013].

is still a debating aspect of study [Chen et al., 2010, Krishnamurthy and Shukla, 2007, Turner and Hannachi, 2010]. Recurring climatic phenomena can have a large influence on societies, economies and human health, with extreme events potentially leading to crises of some kind. The component of droughts driven by internal variability seem to be very large and thus the timing of droughts might not be "predicted".

The following major questions will be investigated within this study:

Question 1) *Are the state-of-the-art climate models able to capture the historically recorded monsoon failures during the past millennium? (Chapter 2)*

Question 2) *Is there any consistency between simulated and reconstructed moisture signals in the monsoon regions? (Chapter 2)*

Question 3) *What are the possible drivers of Asian mega-droughts during the past millennium? (Chapters 2 and 3)*

1.3 Regional Climate Modelling in Arid Central Asia

Recent studies [Boos and Kuang, 2010, Park and Sohn, 2010, Saito et al., 2006, Wu et al., 2012, Yasunari et al., 2006] demonstrate that the Tibetan Plateau controls the climate in most parts of Asia (especially monsoon regions). Regional Climate Models (RCMs) include more accurate topographic information and are able to reproduce the climate of the region more precisely than the "driving Global Circulation Model (GCM)" [Bell et al., 2004, Diffenbaugh et al., 2006, Proemmel et al., 2013].

Arid Central Asia (ACA), one of the largest deserts of the globe, is likely to be extremely vulnerable to the future global warming [Chen et al., 2010]. Extreme drought events, which affect extended areas and maintain over a prolonged period are defined as "exceptional drought events" [Shen et al., 2007].

The regional hydro-climatic change in ACA over the past millennium is poorly understood. The published climate reconstructions like the Monsoon Asia Drought Atlas [Cook et al., 2010a], are based on proxy data which are not homogeneously spread over the Asia. The analysis of local effects are a challenging approach when using such data. The time resolution of proxies also does not allow the investigation of inter-annual and seasonal changes. Previous studies based on different proxies show that moisture changes in ACA and monsoon Asia present an out-of-phase behavior [Chen et al., 2008, 2010, Cook et al., 2010a, Fallah and Cubasch, 2014, Polanski et al., 2014]. According to Chen et al. [2010], this out-of-phase relation is more clear during the LIA. They proposed that the strengthening and southward shift of the westerly jet stream may contribute to moist Little Ice Age (LIA) in ACA. Sato et al. [2007] have studied the origins of water vapor over ACA in the recent climate. They concluded that the westerly circulations are major drivers of moisture changes in ACA. Lioubimtseva et al. [2005] concluded that the cyclone storms originated from Mediterranean transport moisture via westerly jet stream into ACA.

This study tries to find a proper answer to the following question:

Question 4) *Was the westerly jet stream's variability the driver of climate change in arid central Asia during the past 1,000 years? (Chapter 3)*

1.4 Orographic forcing of Tibetan Plateau on Climate of Asia

The Tibetan Plateau (TP) is a vast elevated plateau in Central Asia with an average elevation of 4,500 meters. It has long been an established textbook knowledge that the Asian summer monsoon is associated with the direct sensible heating over the TP [Flohn, 1968, Yanni and Wu, 2006]. Recent theoretical studies and numerical experiments have challenged this idea [Boos and Kuang, 2010, 2013, Park et al., 2011, Rajagopalan and Molnar, 2013, Saito et al., 2006, Tang et al., 2011, 2013a,b, Wu et al., 2012, Yasunari et al., 2006]. There is still controversy on the role of the TP in driving the Asian summer monsoon system.

This study also tries to answer the following key question:

Question 5) *How does the orographic forcing of Tibetan Plateau affect the Asian summer monsoon? (Chapter 4)*

1.5 Moisture changes over Iran

Drastic climatic change was one of the major causes leading to the abandonment of ancient populations and rise and fall of different cultures in Iran especially at the fringe of the deserts [Berberian et al., 2012]. Iran, an area with a complex topography, is located on the transection region between Europe and Asia. It covers an area of 1,648,000 km^2 and is located in the transection zone separating the continental climate of west Asia from Mediterranean climate. The Mediterranean climate governs large parts of Iran which is affected by changes in Westerly activities. Thus, except the western parts and the northern coastal areas, Iran's climate is mainly arid and semiarid [Raziei et al., 2005, Sodoudi et al., 2010].

The Iranian plateau is located upstream of the Tibetan Plateau and its moisture changes are mainly controlled by westerlies. In this study, the climate change over Iran is investigated for a longer period of time (Mid-to-Late Holocene) based on the climate

forcings of this period. The additional objective to chose this area is that, the special location of Iran makes it possible to study an Asian region which its moisture variability is mostly controlled by westerly and the influence of monsoon is negligible.

This study also aims to answer these major questions:

Question 6) *How was the rainfall change over Iran due to the climatic forcing of past 6,000 years? (Chapter 5)*

Question 7) *What were the possible drivers of rainfall patterns during the Mid-to-Late Holocene over Iran? (Chapter 5)*

monsoon and a stronger monsoon circulation. However, the monsoon circulation remains unaffected from July to September, the period corresponding to mature and degenerating phase of monsoon.

♢ ♢ ♢ ♢ ♢

This thesis is organized into four main chapters and each chapter begins with an Introduction section: Chapter 2, compares model simulations with proxy reconstructions of Asian mega-droughts during the past millennium. Furthermore, the evidence of drought predictability is investigated. Chapter 3, is contributed to the simulated changes in extreme moisture events over Asia during the past millennium, and chapter 4 is about the interplay of Tibetan Plateau, North Atlantic Ocean and Asian summer monsoon. Chapter 5 includes the analysis regarding the global climate change over Iran due to climatic forcings of the past 6,000 years. Final chapter (Chapter 6) is dedicated to conclusions and discussions.

Chapter 2

Comparison of model simulations with proxy reconstructions of Asian mega-droughts during the past millennium: evidence of drought predictability

2.1 Introduction

Mega-droughts are natural phenomena that last for years to decades and emerge at irregular intervals [Cook et al., 2010a]. They may play a pivotal role in societal changes in Asia: for example, the collapse of the Yuan Dynasty [Zhang et al., 2008], the Ming Dynasty of China [Shen et al., 2007] and the Khmer Empire of Cambodia [Buckley et al., 2010] are attributed to mega-droughts. Mega-droughts have been linked to persistent patterns of Sea Surface Temperature (SST) anomalies in the Indian and Pacific Oceans [Meehl and Hu, 2006, Ropelewski and Halpert, 1987, Wahl and Morrill, 2010] . Prolonged droughts during the twenty-first century are expected from global warming [Burke and Brown, 2008, Dai, 2011a, Rind et al., 1990, Seager, 2007, Sheffield and Wood, 2008a, Wang et al.,

2005b]. In Asia, droughts are always connected to the monsoon circulation. A decline in the rainfall amount or a change in precipitation pattern may lead to droughts in Asian monsoon region [Shaw and Nguyen, 2011]. The detection and analysis of the natural variability of extreme droughts in Asia is complicated by the short period of available observations and the proxy networks with their coarse spatial distribution.

The Monsoon Asia Drought Atlas (MADA) [Cook et al., 2010a] provides a proxy-based gridded spatiotemporal reconstruction of the Palmer Drought Severity Index (PDSI) Palmer [1994] for the past millennium. The PDSI presents the deviation from a normal hydrological balance level based on a simple water balance model. It quantifies the severity of drought in time and space based on precipitation and temperature values [Wells et al., 2004]. Several studies have been devoted to the analysis of the models' capability to simulate the mega-droughts and the processes behind them [Anchukaitis et al., 2010, Dai, 2013, Li et al., 2013]. Many simulations capture the past mega-droughts at the wrong times [Schiermeier, 2013]. Atmospheric simulations using models of intermediate complexity have shown that a warmer tropical Pacific leads to more anomalous south-westerly moisture transport into Central Asia [Mariotti, 2007]. However, these simulations were driven by the prescribed observed SST.

The Global Circulation Models (GCMs) are able to capture prolonged droughts, ENSO and the global mean aridity trend during the recent climate [Dai, 2013]. According to Krishnamurthy and Shukla [2007], inter-annual changes in monsoon precipitation consists of a seasonal mean component and an unpredictable inter-seasonal variability. This leads to the question, to what extent the simulated mega-droughts are linked to the external forcing (e.g. greenhouse gases, volcanism) or may be the result of internal variability.

This study evaluates the ability of fully coupled ocean–atmosphere climate models in identifying the potential long-term drivers of the moisture anomalies in Central and monsoon-dominated Asia. Several coupled atmosphere–ocean model simulations within PMIP3/CMIP5 project (Paleoclimate Modelling Intercomparison Project Phase III/Coupled Model Intercomparison Project Phase 5), are used to investigate the atmosphere-ocean interactions for the past millennium.

Long-term climate reconstructions derived from various well-dated proxy data (e.g., [Borgaonkar et al., 2010, Fleitmann et al., 2007, Liu et al., 2009, Ponton et al., 2012,

Prasad and Enzel, 2006, Prasad et al., 2014]) indicate that the past Millennium is the best documented interval with both historical and climate data. It can be divided into two major climate periods: the Medieval Climate Anomaly (ca. 900–1350 AD) and the Little Ice Age (ca. 1500–1850 AD) [Benedict and Maisch, 1989, Graham et al., 2011, Lamb, 1965]. Variations in volcanic forcing coupled with the remote impact of the internal dynamics of climate modes in the oceans such as the El Niño–Southern Oscillation are some of the major drivers contributing to long-term fluctuations in global temperature conditions during the last 1200 years [Jones et al., 2001] whereas solar forcing has been recently found to play a minor role [Schurer et al., 2014]. These thermal changes exhibit a strong impact on global and regional climate phenomena as monsoons [Meehl et al., 2009], which arise due to seasonal and latitudinal differences in the incoming solar radiation with effects on the landsea thermal contrast [Gadgil, 2003, Webster et al., 1998]. Consequently, large-scale pressure gradients evolve including strong low-level atmospheric wind circulations [Dallmeyer et al., 2013]. Monsoon systems are characterized by a strong spatiotemporal variability from multi-millennial to intra-seasonal time scales [Ding, 2007, Wang, 2006]. The Asian Monsoon System is the strongest monsoon system of the world [Clift and Plumb, 2008] and is divided into two strongly non-linear interacting subsystems: the East Asian Monsoon and the Indian Monsoon [Wang et al., 2001b]. The increased occurrence and frequency of extreme monsoon rainfall events (e.g., [Krishnan et al., 2009, Shaw and Nguyen, 2011, Ummenhofer et al., 2013]) in recent times has affected the livelihood of more than 2.5 billion people. Hence, an understanding of the large-scale mechanisms and regional spatiotemporal variations leading to past monsoon changes is crucial for an advanced prediction of the Indian Monsoon (e.g., [Krishna Kumar et al., 2005]), and to develop proper mitigation strategies in a global warming scenario. Several studies have been already carried out analyzing the Asian monsoon variability during the last Millennium (e.g., [Cook et al., 2010a, Sinha et al., 2011a,b, Wang et al., 2010]).

Using a paleoclimatic network approach Rehfeld et al. [2013] found a stronger Indian Summer Monsoon (ISM) circulation and a northward intrusion of the ITCZ during Medieval Warm Period caused by an earlier retreat of the Tibetan High in spring. In colder periods such as Little Ice Age, a more regional influence on the ISM strength has been identified [Rehfeld et al., 2013].

Previous reconstruction studies have mainly focused on the Tibetan Plateau and Central Asia. Until recently only few records were available from the Indian Peninsula. This led to a systematic overemphasis on the role of the Tibetan Plateau and Central Asia on the monsoon, resulting in a gap in understanding the past monsoon changes over India [Wang et al., 2010]). The combined multi-proxy-climate model approach, as adopted in HIMPAC (Himalaya: Modern and Past Climates; http://www.himpac.org) and CADY (Central Asian Climate Dynamics; http://www.cady-climate.org) projects, aims at analyzing the past monsoon climate in India during the Holocene. It introduces new, well-dated paleo-records from India, which are based on multiple proxies and archives. A 11,000-year long, high-resolution record from Central India is now available [Anoop et al., 2013, Menzel et al., 2013, Prasad et al., 2014, Sarkar et al., 2014]) and presents a unique opportunity for a comparison of long-term climate time proxy series with paleo-model simulations. The Lonar Lake is influenced by both monsoon branches: from the Arabian Sea and the Bay of Bengal [Sengupta and Sarkar, 2006].

Ensemble simulations over the last 1200 years using a comprehensive fully coupled Earth System Model have been performed using external forcing parameters such as solar variations or volcanic activity derived from reconstructions ([Jungclaus et al., 2010]). Owing to the coarse horizontal resolution of ca. $3.75^\circ \times 3.75^\circ$, these coupled models are not able to capture regional-scale atmospheric circulation and moisture patterns, which strongly depend on a realistic representation of the local topography [Polanski et al., 2010]. In this study, transient time slice experiments are performed for selected episodes of the past using the ECHAM5 model with a spatial resolution of T63 (ca. $1.8^\circ \times 1.8^\circ$). This improves the simulation of the hydrological cycle in India and the Himalayan region [Anandhi and Nanjundiah, 2014].

After introducing the model experiments, the proxy data and the statistical methods (Sect. 2), the capability of the models to simulate mega-droughts is described (Sect. 3). In Sect. 4 we investigate the relationship between the surface temperature and monsoon failures. Additionally, we investigate the long term evolution of droughts over the past millennium and its relation to global mean temperatures and monsoon convection and circulation, followed by a discussion in Sect. 5.

2.2 Data and methods

The "millennium" simulations of two coupled Atmosphere–Ocean General Circulation Models (AOGCMs) from PMIP3 and CMIP5 projects are analyzed: ECHAM5/MPIOM (five ensemble members) from Max Planck Institute for Meteorology (MPI-M) [Jungclaus et al., 2010] and GISS-E2-R (eight ensemble members) from NASA Goddard Institute for Space Studies (NASA GISS) [Schmidt et al., 2014]. The forcings for these simulations include realistic presentations of solar variability, volcanism and greenhouse gas concentrations [Schmidt et al., 2012]. These simulations are used for Intergovernmental Panel for Climate Change Fourth Assessment Reports [IPCC, 2007]. They were downloaded from https://pmip3.lsce.ipsl.fr/. Two of the GISS-E2-R experiments contain no volcanic forcing (r1i1p123 and r1i1p126). In three of the experiments (r1i1p122, r1i1p125 and r1i1p128), volcanic forcing was about a factor of 2 "larger than intended" (http://data.giss.nasa.gov/modelE/ar5/). The Empirical Orthogonal Function (EOF) analysis reveals that all these experiments, show a completely different response pattern in PDSI compared to MADA (not shown). The forcings in the remaining experiments (r1i1p121, r1i1p124 and r1i1p127) are very similar to the ECHAM5/MPIOM simulations. However, the reconstructed land use/land cover forcing in r1i1p127 experiment is notably larger than the one in r1i1p121 and r1i1p124 [Schmidt et al., 2011b]. Therefore, the r1i1p121 and r1i1p124 experiments are used in the analysis. They are called GISS-E2-R, hereafter.

To evaluate the model results in detecting the historical mega-droughts, the model results are compared with MADA. The MADA presents a gridded summer monsoon metric based on the proxy data set of 327 annual tree-ring chronologies [Cook et al., 2010a]. The number of tree-ring chronology networks in MADA rises strongly in the post-1700 period. To investigate the link between the droughts, the ocean–atmosphere dynamics and the global warming, the Northern Hemisphere temperature reconstruction [Shi et al., 2013] is used. Three different Niño indices are calculated from simulated area-averaged SST anomalies over the Niño 1+2 region (90–80°,W and 10°,S–0°), Niño 3.4 region (170–120°,W and 5°,S–5°,N) and Niño 4 region (160°,E–150°,W and 5°,S–5°,N). To evaluate the ensemble of model experiments, the arithmetic averaging is applied on each of the two

model experiments (PDSI is calculated for each member separately prior to the averaging).

In order to quantify the severity of droughts in time and space across different climates, the PDSI [Palmer, 1965] from simulated monthly summer (JJA) precipitation and temperature is applied. According to Cook et al. [2010a], the first EOF (EOF1) pattern of reconstructed PDSI is associated with a persistent weak monsoon in Asia. Therefore, the first principal component gives us information about "active" and "break" monsoonal phases. In analogy, the first EOF of simulated PDSI from model's ensemble average conveys us similar information as the EOF1 of MADA.

The maximum covariance analysis is used to identify the coupled patterns in the climate data. Dai [2013] has utilized the maximum covariance analysis to explore the relationship between the simulated global Sea Surface Temperatures (SSTs) and the PDSI. The maximum covariance analysis identifies the most important modes of climate data in which the variability of the two fields is coupled [Bretherton et al., 1992]. The advantage of maximum covariance analysis, compared with coupled EOF analysis, is that this method will focus on those modes of anomalies, which are highly coupled [Bretherton et al., 1992]. The first leading maximum covariance analysis modes of simulated SSTA represent the ENSO-like patterns. Yearly averaged monthly monsoon (JJA) SSTs were used for the maximum covariance analysis analysis. A period from 1300 to 1860 was chosen to exclude the impact of anthropogenic climate effects. The GCM data were re-gridded by bi-linear interpolation to the MADA's grid (ca $2.5^\circ \times 2.5^\circ$). The spatial domain of MADA was considered in the analysis of PDSI (61.25–143.75°,E and 8.75°,S–56.25°,N). The SST data of GISS-E2-R model is bi-linearly remapped to MPIOM's grid (horizontal resolution of GR3.0 (ca. $3^\circ \times 3^\circ$)). A 31 year filter is used to smooth the time-series.

2.3 Simulation of Asian mega-droughts

The first leading EOF pattern of simulated PDSI presents a monsoon failure pattern over India and Southeast Asia. Fig.2.1 presents the first EOF (EOF1) pattern from reconstructed PDSI [Cook et al., 2010a, Dai, 2011a, Li et al., 2013]. This pattern is comparable to the principal component pattern of modeled PDSI. The pattern correlation between

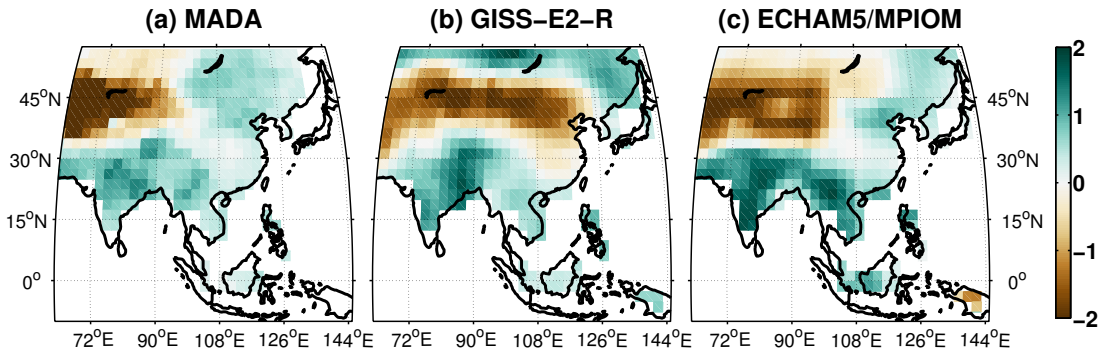

Figure 2.1: Asian monsoon failure patterns: **(a)** first EOF of PDSI for MADA, **(b)** for ensemble mean of GISS-E2-R model and **(c)** ECHAM5/MPIOM model. Pattern correlation coefficients between **(a)** and **(b)** and **(a)** and **(c)** are 0.57 and 0.78, respectively.

EOF1 of reconstructed and averaged simulated PDSI of ECHAM5/MPIOM (GISS-E2-R) is 0.78 (0.57) (Fig.2.1). The explained variances for EOF1 of MADA, ECHAM5/MPIOM and GISS-E2-R are 19.52 % and 24 %, and 12.28 %, respectively. The EOF1 pattern for each of the model members is very similar to the one from MADA (not shown). However, the time expansions show a large variability and the ensemble averaging improves the agreement between model and proxy [Fallah and Cubasch, 2014, Polanski et al., 2014]. According to Kalnay et al. [1996], the ensemble average is more accurate than a single deterministic climate simulation. [Lambert and Boer, 2001], concluded that the climatological fields from ensemble average have more agreement with the observations than the fields generated by any single member.

Those periods during which both, model and reconstruction, have the same sign in the selected Principal Components (PCs) are described as "active" resp. "break" phases of the monsoon (green/brown bars in Fig. 2.3. Monsoon "break" phases are more common after the late 17th in GISS-E2-R simulations. During the Little Ice Age (LIA), active phases of the monsoon were more frequent. This feature is captured by both the model experiments and the proxy reconstruction. Five of the large-scale mega-droughts recorded in MADA

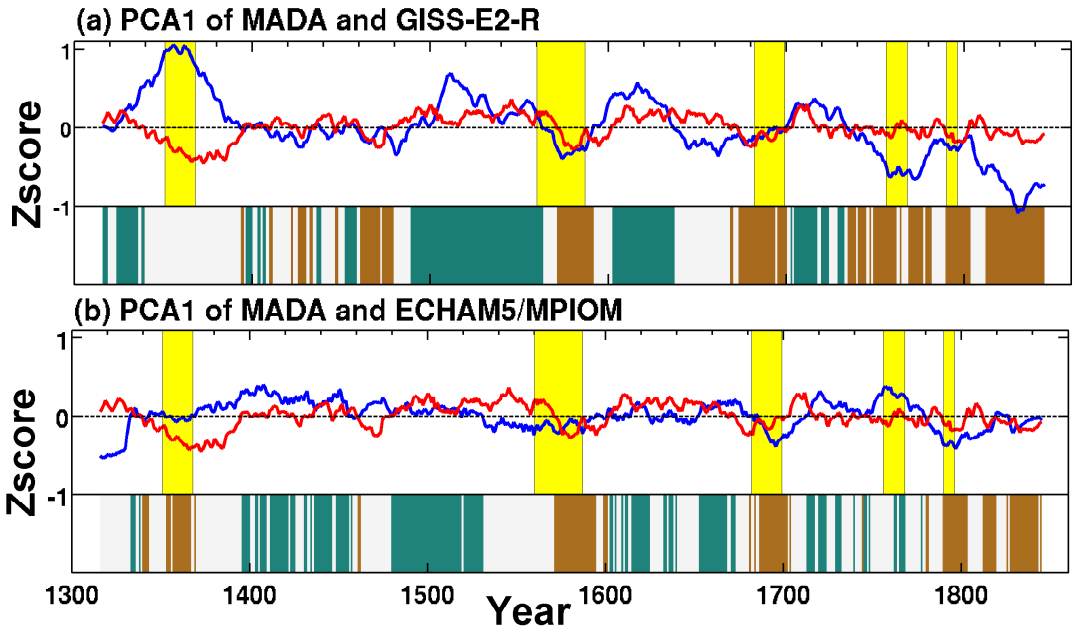

Figure 2.2: Time expansions of monsoon failure patterns for **(a)** MADA (red) and ensemble mean of GISS-E2-R model (blue), **(b)** MADA (red) and ensemble mean of ECHAM5/MPIOM model (blue). Time-series have unit-variance, zero-mean and are smoothed using a 31 year moving average filter. Green (brown) shadings indicate the times when both time-series are greater (smaller) than zero. Five historical recorded mega-drought periods are shaded in yellow.

(ref. [Cook et al., 2010a]) are selected for comparisons: (i) mid-14th century drought associated to collapse of the Khmer empire (1351–1368) in Cambodia [Buckley et al., 2010, Cook et al., 2010a], (ii) the late 16th century severe drought (1560–1587), (iii) end of the 17th century drought (1682–1699), (iv) the "Strange Parallels" drought (1756–1768) and (v) the East India drought (1790–1796). The simulated PCA1 time-series of GISS-E2-R model, detects the last four monsoon failures, but disagrees with MADA during the mid-14th century (Fig.2.2.a). The ECHAM5/MPIOM model simulation does not simulate the timing of monsoon failure during the "Strange Parallels".

The EOF analysis is a linear method for dimensionality reduction of the complex data [Hannachi and Turner, 2013]. Therefore, it can not capture all the possible drought patterns in the data-set. By applying EOF analysis, only those droughts are detected which have a similar dipole pattern as shown in Fig. 2.1 and other possible drought patterns can not be identified.

In the following the historical mega-droughts are individually investigated (Fig.2.3). Based on the reconstructions, the mid-14th century drought (Fig.2.3.a) exhibits three drought regions over the Asia: (i) most of the India, (ii) Vietnam, Thailand, Laos, South China and Myanmar and (iii) Mongolia, north East China and Lake Baikal. Figure 3.a shows that GISS-E2-R model captures these three key regions of the mid-14th century drought. The ECHAM5/MPIOM model however, simulates a wet spell over most India during this period.

The late 16th century drought (Fig. 2.3.b) presents two major drought regions in MADA: (i) over India and Bangladesh and (ii) Kazakhstan and north of Mongolia. Both models and MADA indicate the dipole pattern between India and arid central Asia region for this prolonged drought. The ECHAM5/MPIOM simulation, however, disagrees with MADA for the lake Baikal region. The GISS-E2-R model produces drought patterns similar to the patterns in MADA.

The final stage of the 17th century drought displays a similar pattern as the mid-13th century drought in MADA (Fig. 2.3.c). The GISS-E2-R model captures the two key regions of (i) North India and Pakistan and (ii) North East China and Mongolia. In the ECHAM5/MPIOM model simulation, the first pattern is shifted to the north. The "Strange Parallels" drought, the most persistent mega-drought during the last seven hundred years, had a dominant pattern over India and Southeast Asia that lasted for more than a decade (1756–1768) [Buckley et al., 2007, Cook et al., 2010a, Lieberman, 2009, Sano et al., 2009]. The broad drought patterns captured by reconstructions and simulations are comparable during the "Strange Parallels" drought (Fig. 2.3.d). In ECHAM5/MPIOM model simulations, all the three key regions of dry conditions: (India, Southeast Asia, Kazakhstan and Siberia) are captured. The GISS-E2-R model does not simulate the drought pattern over Kazakhstan and north of the Lake Balkhash. The East India drought, an El Niño induced event, occurred in the late 18th century and led to severe famine in India [Cook et al., 2010a]. The reconstruction exhibits several dry regions for this period: North East India, West and North Himalayas (Fig. 2.3.e). Cook et al. [2010a], suggested that the Indian monsoon was hardly weakened during this period. The model simulations indicate drier conditions over North and Northeast India and North of Himalayas, which are sources of the water supply for Indian subcontinent.

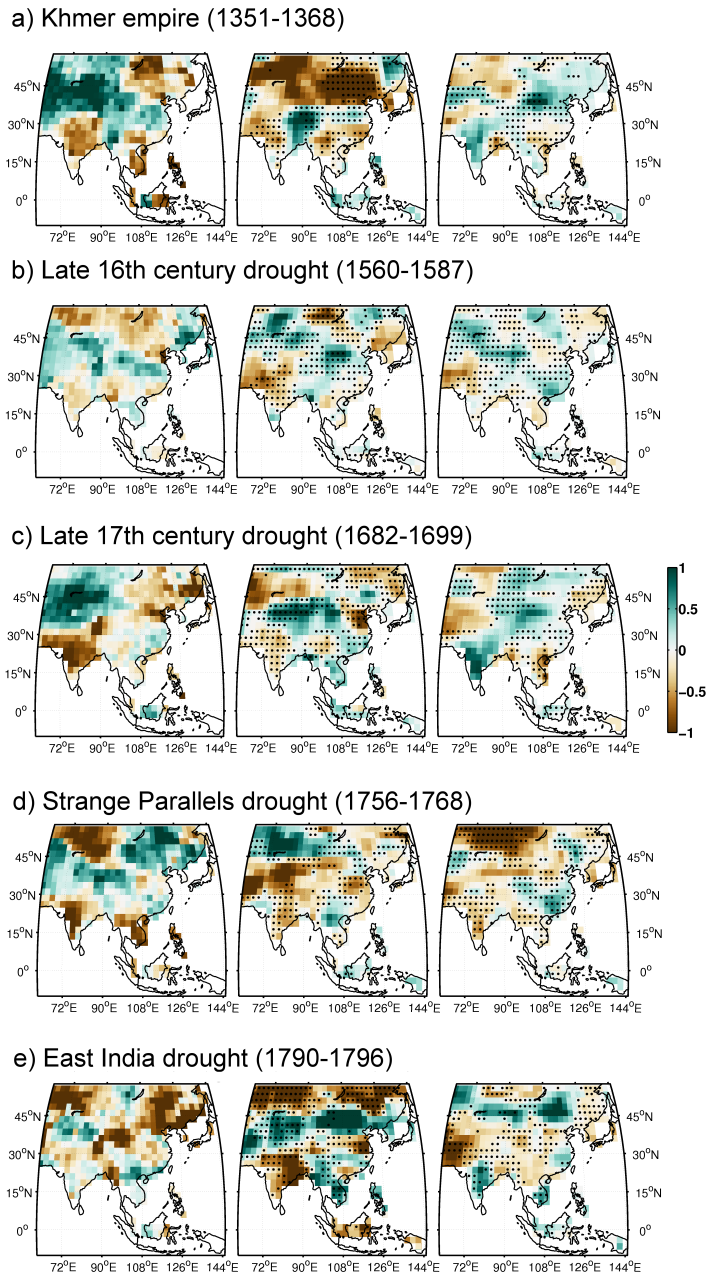

Figure 2.3: Drought patterns during **(a)** the demise of Khmer empire (1351–1368) [Buckley et al., 2010], **(b)** the late 16th century drought (1560–1587), **(c)** the late 17th century drought (1682–1699), **(d)** the "Strange Parallels" Drought (1756–1768) and **(e)** the East India Drought (1790–1796). Left panels are for MADA, middle panels for the GISS-E2-R model and right panels for the ECHAM5/MPIOM simulations. Dots indicate both model and proxy show similar sign in PDSI value.

2.4 Drivers of the Asian mega-droughts

2.4.1 ENSO

The time expansion of EOF1 mode of PDSI correlates significantly with central Pacific SST anomalies; such a correlation characterizes ENSO [Cook et al., 2010a, Li et al., 2013]. To investigate the ocean influence on Asian monsoon, a maximum covariance analysis of simulated PDSI and SSTs has been performed. By considering only the leading maximum covariance analysis modes, several other natural variations are excluded. Here, the focus is on the first mode of maximum covariance analysis (MCA1) of model simulations. MCA1 of ECHAM5/MPIOM model accounts for 90 % of explained Squared Fractional Covariance (SFC), and MCA2 of GISS-E2-R for 40 %. This pattern shows a warm anomalous (El Niño-like) SSTA over the central tropical Pacific and Indian Oceans (Figs. 2.4 and 2.5). Krishna Kumar et al. [2006], concluded that the central equatorial warmer ("westward-shifted") Pacific Ocean initiates more extreme droughts over India. The time expansions of this mode for PDSI and SST are significantly (p value < 0.01) correlated. The temporal coefficient of the MCA1 pattern of SST from ECHAM5/MPIOM model (blue line in Fig. 2.4.a) is highly correlated (corr. coeff. $= 0.93$) with the SST anomalies over the Niño 4 region (Fig. 2.4.a). The red line in Fig. 2.5.a shows the SST anomalies over the Niño 4 region for GISS-E2-R model. The correlation coefficient between MCA1 of SST and the Niño 4 index for GISS-E2-R is 0.84.

Table 5.1, shows the correlation coefficients between different Niño indices, MCA1 of PDSI and SSTA and reconstructed global mean temperatures. The behavior of individual members are shown in supplementary materials of Fallah and Cubasch [2014]. During the late 17th century, MCA modes of simulated SSTs show negative anomalies in Central Pacific, which resembles a La Niña event during this drought. ENSO may have been an important trigger of yet another recorded mega-droughts. During the late 18th century, both models simulate an El Niño event. The great El Niño of this period was the main cause of worldwide societal and economical disturbances [Grove, 2007].

The time-series in Figures 2.4 and 2.5 suggest an influence of volcanic external forcing (magenta lines in Fig. 2.4 and 2.5), especially in the mid 15th, late 17th and early

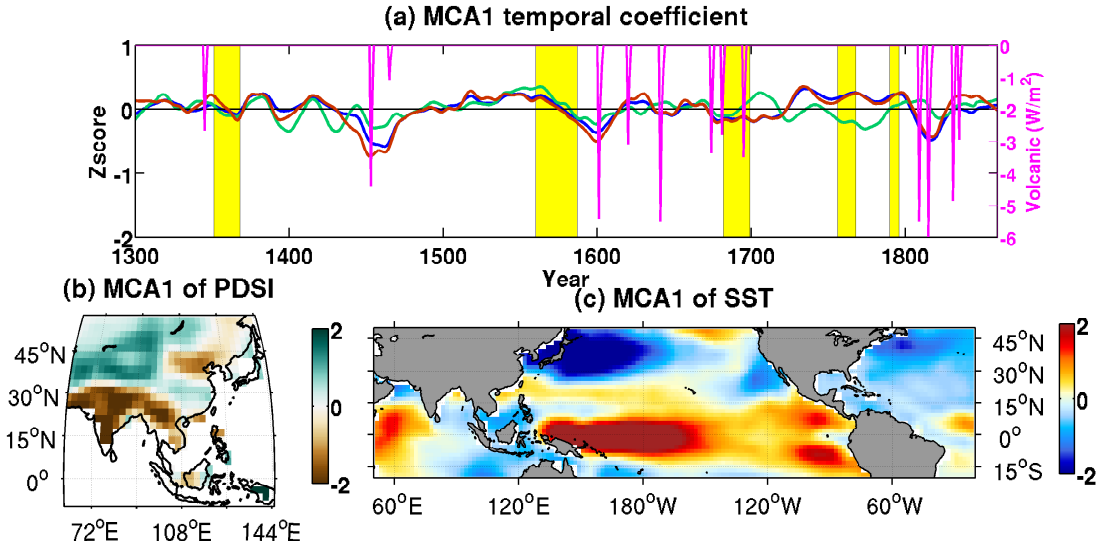

Figure 2.4: Maximum covariance analysis results for ECHAM5/MPIOM: **(a)** time-series for PDSI (green line), SSTA (blue line), volcanic forcing (magenta) and 2×Niño 4 (red line). The five recorded mega-drought periods are shaded in yellow. **(b)** MCA1 pattern for PDSI. **(c)** MCA1 pattern for SSTA.

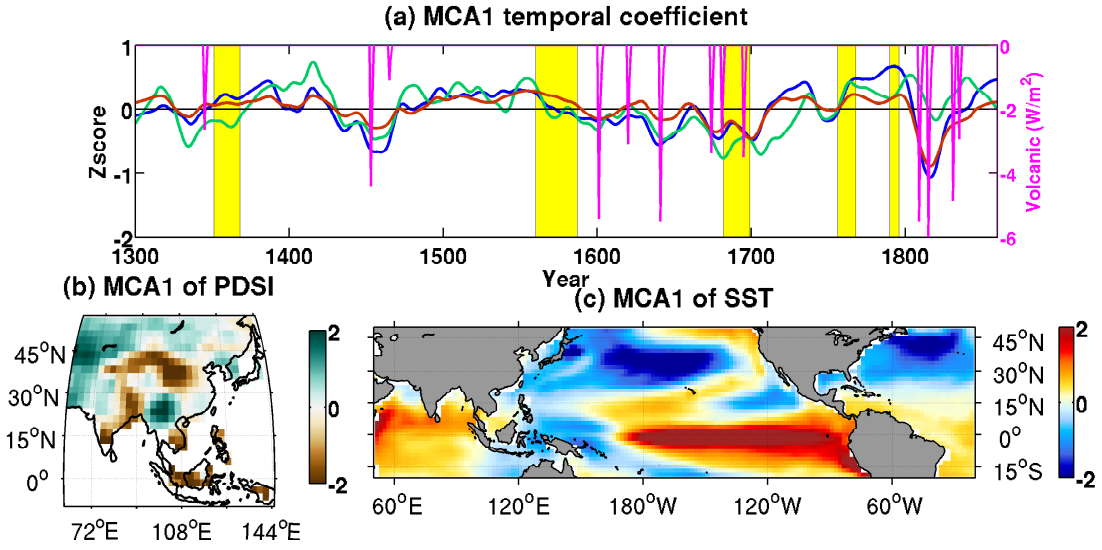

Figure 2.5: Maximum covariance analysis results for GISS-E2-R: **(a)** time-series for PDSI (green line), SSTA (blue line), volcanic forcing (magenta) and 2×Niño 4 (red line). The five recorded mega-drought periods are shaded in yellow. **(b)** MCA1 pattern for PDSI. **(c)** MCA1 pattern for SSTA.

MCA1 of	Niño 3.4	Niño 1 + 2	Niño 4	Temp.
ECHAM5/MPIOM SSTA	0.91(99%)	0.66(99%)	**0.93(99%)**	0.57(99%)
ECHAM5/MPIOM PDSI	0.35(99%)	0.21(99%)	**0.41(99%)**	0.03(NS)
GISS-E2-R SSTA	0.83(99%)	0.81(99%)	**0.84(99%)**	0.51(99%)
GISS-E2-R PDSI	0.51(99%)	0.46(99%)	0.47(99%)	**0.52(99%)**

Table 2.1: Correlation coefficients between the MCA1 time-series, Niño indices and reconstructed global temperatures from Shi et al. [2013]. Bold numbers indicate the largest value in each row. Numbers in parentheses indicate the statistical significance levels. NS stands for Not Significant.

19th century. There are clear minima in the time-series coincident with major volcanic eruptions.

2.4.2 Monsoon convection and circulation

Turner and Hannachi [2010], defined two preferred regimes in monsoon convection in the ERA-40 reanalysis [Uppala et al., 2005]. They suggested that, these regime behaviour may be related to the large scale forcing. According to them, Outgoing Long wave Radiation (OLR) is an appropriate representative of the monsoon convection and rainfall, especially for the tropical region. The yearly summer (JJA) variability of OLR is calculated over tropical domain 25°,S–35°,N; 50°,E–150°,W for the past millennium (1300–1850). In addition, as an indication of lower tropospheric circulation, yearly summer (JJA) 850 hPa wind anomalies (w.r.t 1300–1850) over this domain is used. Following Turner and Hannachi (2010), the dominant pattern of summer monsoon convection is identified as the first EOF of summer (JJA) OLR anomalies. The explained variances for ECHAM5/MPIOM and GISS-E2-R models are 56 % and 13.68 %, respectively.

Mixture Model

Mixture models are density models which contain a set of component functions (normally Gaussian functions). Any number of Probability Density Function (PDF)s can be combined to shape a mixture distribution [Turner and Hannachi, 2010]. Figure 2.6 shows the schematic PDF presentation of mixture model, its component and the estimation of the mixture model. Following Turner and Hannachi [2010], the PDF estimate function ($PDF(x)$) is decomposed into a combination of two distinct multivariate normal distributions (dashed lines in Figures 2.7 and 2.8):

$$PDF(x) = \alpha f_1(x, \sigma_1, \mu_1) + (1 - \alpha) f_2(x, \sigma_2, \mu_2) \tag{2.1}$$

Then the following weightings are applied for each of these regimes ($n = 1, 2$):

$$w_n(t) = \alpha_n g_n(t)/c(t) \tag{2.2}$$

where

$$g_n(t) = exp(-((\mu n - x_t)^2)/(2\sigma_n))/\sqrt{2\pi\sigma_n}, \tag{2.3}$$

with

$$c_n(t) = \alpha_1 exp(-((\mu 1 - x_t)^2)/(2\sigma_1))/\sqrt{2\pi\sigma_1} + \alpha_2 exp(-((\mu 2 - x_t)^2)/(2\sigma_2))/\sqrt{2\pi\sigma_2}, \tag{2.4}$$

and x_t is the Principal Component (PC)1 of yearly summer (JJA) Outgoing Long wave Radiation (OLR) time-series.

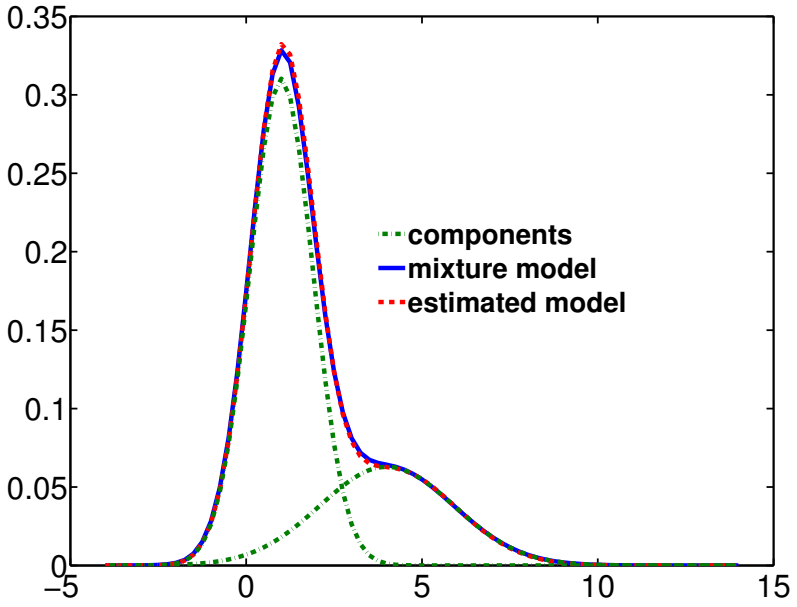

Figure 2.6: Schematic presentation of PDF of mixture model (blue line), its components (green dashed lines) and the estimation of mixture model (red dashed line).

ECHAM5/MPIOM

Figure 2.7.a presents the first EOF pattern of summer OLR for ECHAM5/MPIOM ensemble mean and Fig. 2.7.b–g the histogram of the first Principle Component (PC1) of OLR for ensemble mean and each of the experiments (mil0010 to mil0015). The EOF1 pattern of OLR (Fig 2.7.a) shows a positive anomaly pattern over west and central North Pacific and South- and south-eastern Asia and negative anomaly pattern over East Indonesian Pacific.

The Probability Density Function (PDF) estimate of OLR shows a "shoulder" in the positive PC1 values (Fig. 2.7.b). The skewness of the data for ensemble mean is high (0.42). The distance between the two peaks are larger for any individual members (Fig. 2.7.c–g). The ensemble average produces a better estimate of the mean state, thus its PDF tends to a normal distribution (Fig. 2.7.b).

Using the Eq. 2.1 the PDF estimate function (PDF(x)) is decomposed into a combination of two distinct multivariate normal distributions (dashed lines in Fig. 6b), with

$\alpha = 0.7$, $\sigma_1 = 1$, $\mu_1 = -0.4$, $\sigma_2 = 0.9$ and $\mu_2 = 0.9$. Weighting functions as in the study of Turner and Hannachi [2010] are applied for each of these regimes and the composites of 850 hPa wind and OLR are calculated. In contrast with the study of Turner and Hannachi [2010], that used the ERA-40 reanalysis, regime 1 happened more frequent than regime 2 during 1300–1850.

Figure 2.9 shows the composites of 850 hPa wind and OLR for these two distinct regimes: (2.9.a) regime 1 and (2.9.c) regime 2. The patterns are consistent with negative and positive modes of EOF1 of OLR, respectively. There is a clear regime behaviour in variability of Somali Jet with cyclonic/anticyclonic circulations over North Arabian Sea during regime 1/regime 2. In regime 1, OLR decreases over peninsular India with an increase of positive rainfall anomalies. The 850 hPa wind field presents a convergence zone over India with strengthening of Easterly winds over Indonesian and Central Pacific. This pattern is reversed during the regime 2 (Fig. 2.9.c). There is an evidence of negative OLR anomaly over west equatorial Pacific during the regime 2. This pattern is consistent with the observed enhanced rainfall over this region and drought over India during the El Niño events [Krishna Kumar et al., 2006]. These distinctive results agree well with the PC1 time-series of PDSI that indicates more "active" phases of monsoon during the LIA. The composites of modeled PDSI for the two regimes, also present clear patterns resembling "active and "break monsoon phases (supplementary materials of Fallah and Cubasch [2014]).

To examine the convection regimes of the five mega-droughts,the composite (totally 84 years) anomalies of 850 hPa wind and OLR for the total period of five mega-droughts is presented in Figure 2.10.a. During the past millennium, Asian mega-droughts are co-incident with increased (decreased) OLR over East India, South and East China (West equatorial and Indonesian Pacific), anticyclonic circulations over Arabian Sea and weakening of the lower tropospheric Trade winds over Indonesian and Central Pacific.

GISS-E2-R

Figure 2.8 presents the same results for the GISS-E2-R model simulations. The skewness of PC1 of OLR data in ensemble average of GISS-E2-R model is 0.1. Experiment

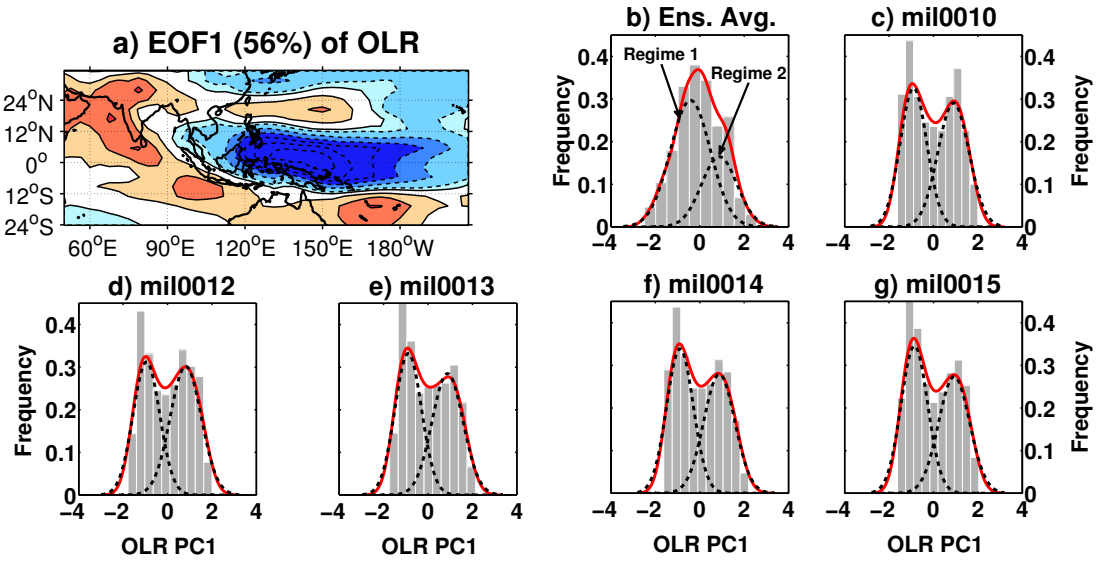

Figure 2.7: Regime behavior in ECHAM5/MPIOM model simulations: **(a)** Dominant OLR pattern (EOF1). Positive (negative) contours are shown by solid (dotted) lines. **(b)** PDF estimate of PC1 of OLR (red solid line) and each regime (dashed lines) for ensemble average and **(c–g)** for each of the experiments separately.

r1i1p121 indicates that the probability of occurrence of regime 2 was larger than regime 1 (Fig 2.8.c and Fig 2.8.d). However, the ensemble average indicates more "active" regimes during the past millennium ($\alpha = 0.7$, $\sigma_1 = 1$, $\mu_1 = -0.23$, $\sigma_2 = 1$ and $\mu_2 = 0.5$). The composite anomalies of OLR indicate negative deviations over Indonesian Pacific, Arabian Sea and India and positive anomalies over central equatorial Pacific during regime 1 (Fig 2.9.b). The lower tropospheric Trade winds during the regime 1, are strengthening over central equatorial Pacific. This pattern is reversed for regime 2 (Fig. 2.9.d). Figure 2.10.b shows similar pattern as in Fig. 2.10.a. A notable weakening of Somali Jet occurred during the mega-droughts in GISS-E2-R model simulations with positive OLR anomalies over India. The 850 hPa wind pattern of GISS-E2-R model presents a clear reduction of moisture transport into Indian, especially for the Somali Jet (Fig. 2.10.b).

The composites of modeled PDSI for the two regimes from GISS-E2-R model, present less clear "active monsoon phase for regime 1 (supplementary materials of Fallah and Cubasch [2014]). The ensemble average of GISS-E2-R model presents a peak near neutral conditions ($PC1 = \sim 0$) in Fig. 2.8.b.

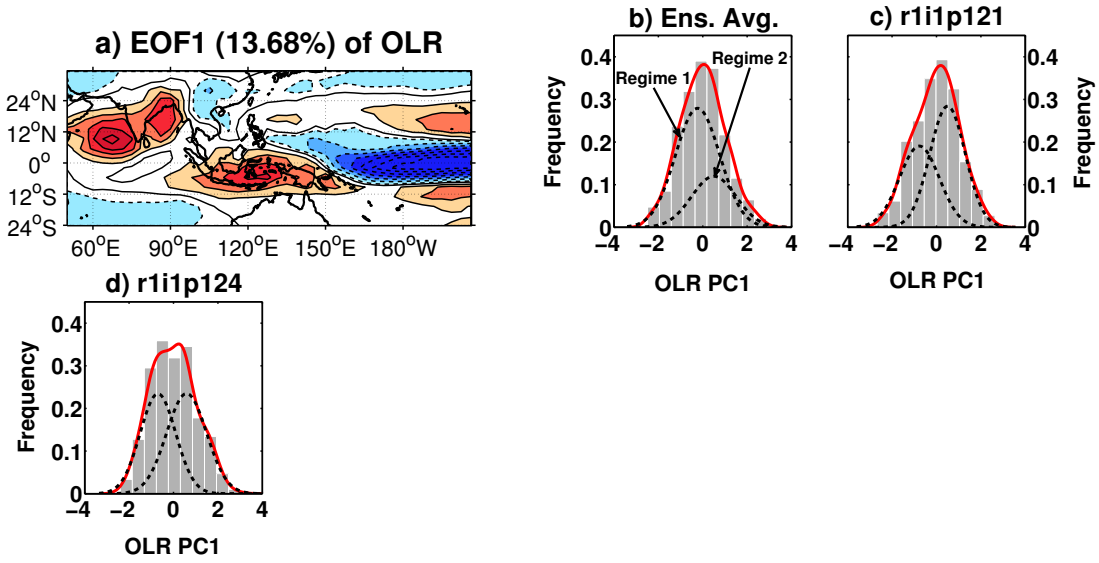

Figure 2.8: Regime behavior in GISS-E2-R model simulations: **(a)** Dominant OLR pattern (EOF1). Positive (negative) contours are shown by solid (dotted) lines. **(b)** PDF estimate of PC1 of OLR (red solid line) and each regime (dashed lines) for ensemble average and **(c–d)** for each of the experiments separately.

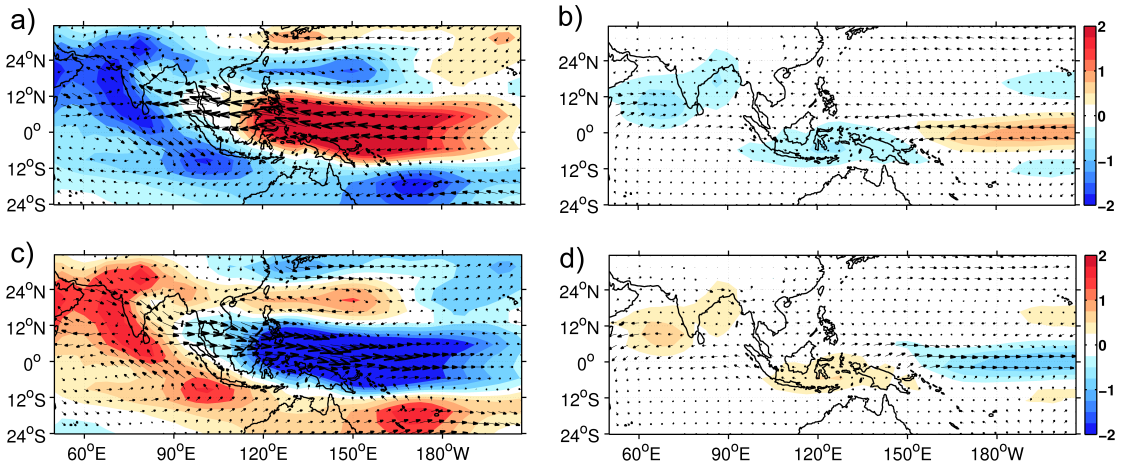

Figure 2.9: Model simulations' composite anomalies of 850 hPa wind ($m\,s^{-1}$) and OLR ($W\,m^{-2}$) for the first (**(a)** and **(b)**) and the second regime (**(c)** and **(d)**) from ECHAM5/MPIOM (left panels) and GISS-E2-R (right panels) model. Largest wind vector in left panels is 0.6 $m\,s^{-1}$ and in right panels is 0.1 $m\,s^{-1}$.

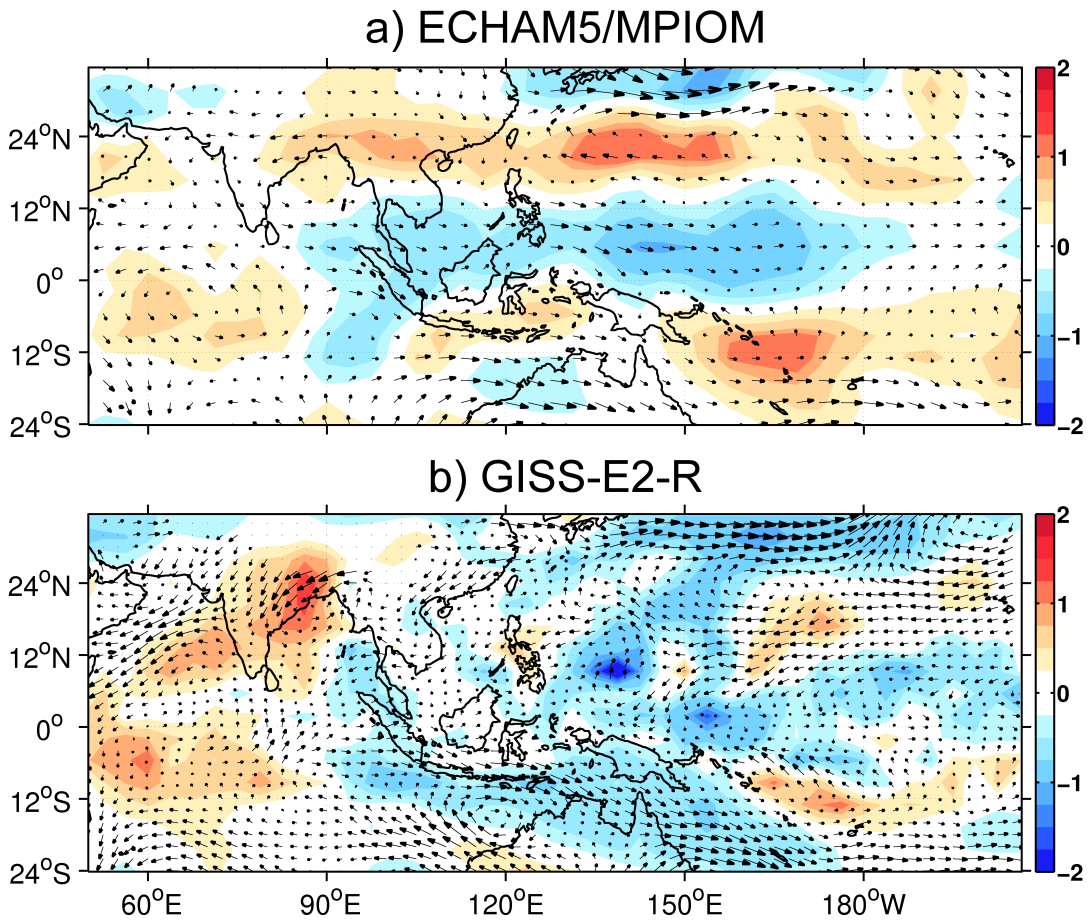

Figure 2.10: Model simulations' composite anomalies of 850 hPa wind ($m\,s^{-1}$) and OLR ($W\,m^{-2}$) for the five mega-droughts (totally 84 years) of the past millennium from **(a)** the ECHAM5/MPIOM and **(b)** the GISS-E2-R model. Largest wind vector in **(a)** is 0.33 $m\,s^{-1}$ and in **(b)** is 1.02 $m\,s^{-1}$.

2.5 Atmosphere-only GCM simulations of the past millennium

Due to the high computational costs of the available computing systems, coupled atmosphere-ocean GCMs can not be applied for the longer time periods (e.g. several thousand years). For producing a detailed climatic data which is comparable with the local proxy information, a downscaling technique is required. Here, a two-step approach ("time-slice simulation", ref. [Berking et al., 2013, Cubasch et al., 1995]) is used to simulate the climate of the past millennium: (i) the fully coupled COmmunity earth System ModelS (COSMOS) from Max Planck Institute for Meteorology (here referred to Atmosphere Ocean Global Circulation Model (AOGCM) throughout the manuscript) consisting of the atmosphere model ECMWF operational forecast model cycle 36 and a comprehensive parameterisation package developed at HAMburg version 5 (ECHAM5) with a spatial resolution of T31 (ca. $3.75^\circ \times 3.75^\circ$) with 19 vertical levels and coupled to the ocean model Max Planck Institute Ocean Model (MPI-OM) (horizontal resolution of GR3.0 (ca. $3^\circ \times 3^\circ$)), 40 vertical levels; (ii) the atmosphere-only general circulation model ECHAM5 (here refereed to Atmosphere only Global Circulation Model (AGCM) throughout the manuscript) with a spatial resolution of T63 (ca. $1.8^\circ \times 1.8^\circ$) and 31 vertical levels.

In the Millennium project [Jungclaus et al., 2010], an ensemble of five simulations covering the time from 800 to 2005 AD has been calculated starting from different ocean initial conditions. The model simulations have been forced by: solar variability [Krivova et al., 2007, Solanki et al., 2004], volcanoes [Crowley et al., 2008b], land cover changes [Pongratz et al., 2008], orbital variations [Bretagnon and Francou, 1988], greenhouse gases [Marland et al., 2008] and aerosols [Tanre et al., 1984a]. A detailed description of the Millennium simulations is documented in Jungclaus et al. [2010]. These simulations have been analyzed to detect extreme wet and dry summer monsoon rainfall anomalies over India on centennial time scales.

Figure 2.11 illustrates the time series of Empirical Orthogonal Function (EOF)1 of calculated Palmer Drought Severity Index (PDSI) for the five ensemble members of the

Millennium experiment from 1300–2000 AD and reconstructed PDSI from Monsoon Asian Drought Atlas (MADA) (MADA does not include the MCA period). The time series are smoothed with a 101-yr moving-average filter. The first leading EOF pattern of MADA and ensemble average of Millennium experiments was shown in previous chapter (Figure 2.1).

The pattern correlations between EOF1 of MADA and each individual experiment is: mil0010 (0.44), mil0012 (0.46), mil0013 (0.51), mil0014 (0.51) and mil0015 (0.54), respectively. For the period from 1400 - 1900 AD (excluding the increase in CO_2 during past century), PC1 time-series of mil0014 experiment shows the best agreement with MADA (correlation coefficient $= 0.58$). This period is coincident with the LIA [Cronin et al., 2003, Mann et al., 1999]. Correlation coefficients between PC1 of other experiments and MADA for LIA are mil0010 (-0.53), mil0012 (-0.39), mil0013 (-0.67) and mil0015 (0.12), respectively.

Furthermore, to consider the nonlinearity in temporal evolution of the monsoon activity (PC1 of PDSI) and quantify the climate behavior due to external forcing, the Empirical Mode Decomposition (EMD) method is applied [Huang et al., 1998, Rilling et al., 2007] to develop the nonlinear trend and imbedded structures within the data. A modified version of this method (Ensemble EMD) was used recently by Franzke [2014], Ji et al. [2014] to determine the nonlinear trends of land temperatures. EMD isolates signals with specific time scales which are produced by different physics within the data.

Figure 2.12 shows the nonlinear trends (last EMD component, $N = 7$) of the data. As can be seen in this figure, the nonlinear centinental trends are captured very well by EMD method. The incoherent behavior of the original time-series in the centinental scale is not strong in the EMD trends. There is a clear rising trend (since 1800 AD) in all of the time-series that could be linked to anthropogenic forcing (with the exception of mil0012). Two out of five ensemble members (mil0014, mil0015) present very similar trends as in the MADA. Among all the members, mil0014 shows the best agreement to the reconstruction during the entire period (1300- 2000).

Correlation coefficients between corresponding EMD trend of PC1 for MADA and ensemble members are shown in Figure 2.13 for different components (component number $N = 0$ indicates the original data). Higher correlations are obtained between components

from mil0014 and MADA, especially those of centennial time-scales (components $N = 6$ and $N = 7$). The agreement between mil0014 and MADA for the short selected period of LIA (1515–1715) may be accidental. But now by detrending the data, for a longer period (1300–2000), it can be concluded that this agreement existed for the whole period of the MADA. mil0015 also present similar behavior as in MADA for centinental time-scales. Thus, two out of five experiments are showing trends similar to MADA for the whole period of 1300-2000. This results indicate that the agreement between mil0014 and MADA did not happened by chance.

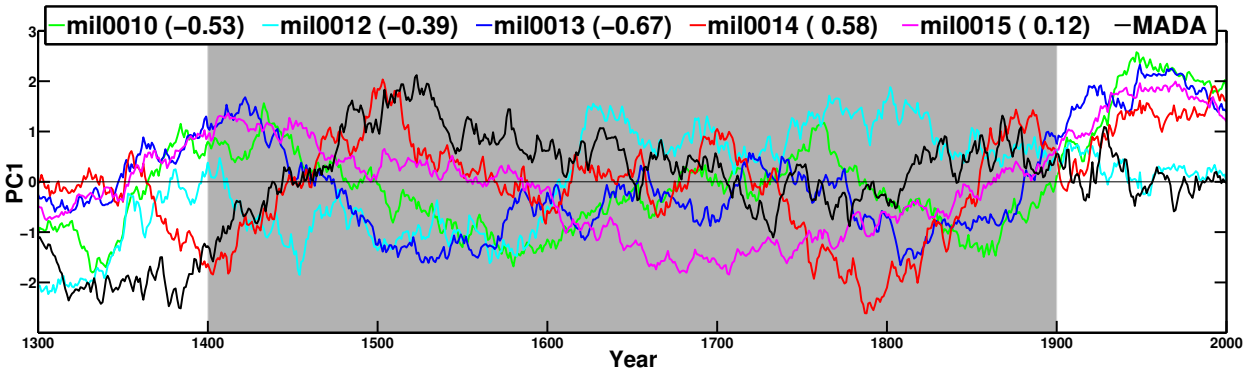

Figure 2.11: PC1 of PDSI for the five ECHAM5/MPI-OM experiments and MADA. Shading indicates the LIA period inferred from reconstructions of Mann et al. [1999].

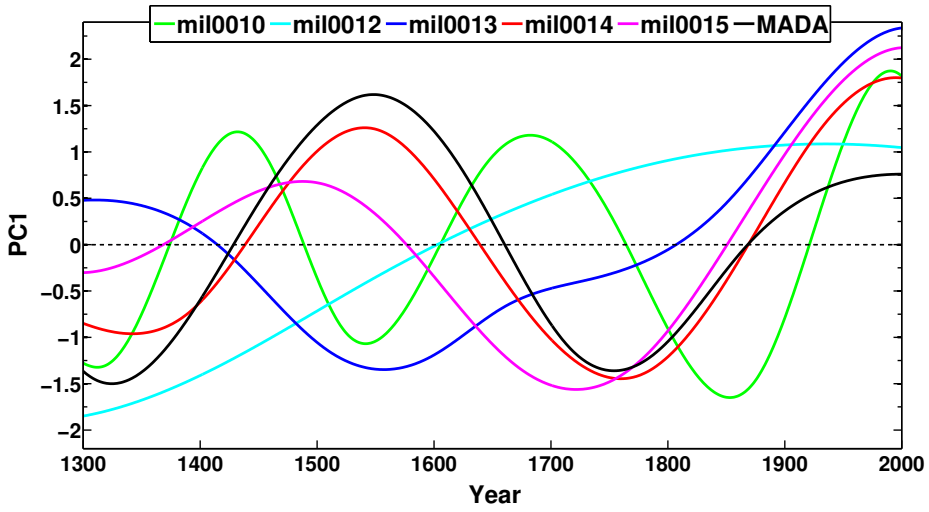

Figure 2.12: EMD trends of PC1 of PDSI for millennium experiments.

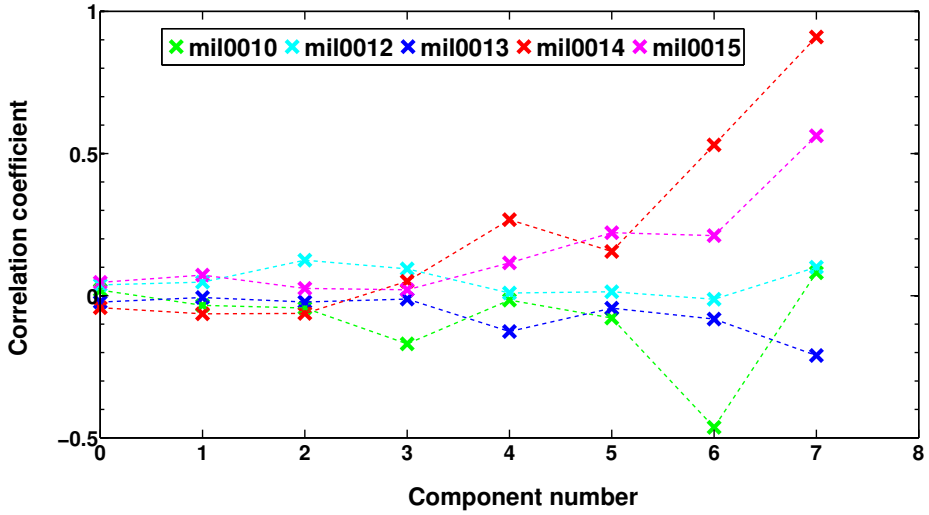

Figure 2.13: The correlation coefficients (cross) of the ensemble experiments and MADA and their corresponding EMD components. Component 0 here means the original signal.

Limitations in available computing resources was the forcing factor to focus on a single higher-resolved calculation of the Millennium experiment. Since mil0014 shows the best fit to MADA during LIA, this experiment has been selected as basis for the AGCM simulation. This experiment has been simulated with the higher-resolved AGCM for the MCA (900–1100 AD) and the LIA (1515–1715 AD). One additional experiment has been performed Post Industrial (PI) (1800–2000 AD) to test the performance of the model to simulate the present-day climate. The sea surface temperature and sea ice cover data have been taken from the AOGCM simulations. The same set of full forcing parameters used for the AOGCM simulations has been applied for the experiments. Furthermore, several time-slices within each of these AGCM simulations were selected (see. Chapter 3) using the arid Central Asia rainfall amount and PDSI. Finally, six periods (two 30 years periods in each AGCM time-slice) are chosen (based on the severity of moisture changes) for regional climate model simulations to test the sensitivity of regional-scale extreme moisture events to past millennium climate forcing. The results of regional climate simulations are presented in the next Chapter.

2.5.1 Reconstructions

The AOGCM and AGCM simulated moisture changes between MCA and LIA are compared with 9 reconstructed paleo-data [Anoop et al., 2013, Bhattacharyya et al., 2007, Chauhan et al., 2000, Denniston et al., 2000, Ely et al., 1996, Kar et al., 2002, Menzel et al., 2013, Ponton et al., 2012, Prasad et al., 2014, Sanwal et al., 2013, Sarkar et al., 2014, Sinha et al., 2011a] derived from different archives like lake and ocean sediments, peat, and stalagmites (Tab.2.2) using various proxies as pollen, isotopes, mineralogy, and sedimentology.

The reliability of the archives are evaluated using the following criteria: (i) reliability of chronology: the archives should be dated using the radiocarbon or U/Th dating method. Archives which had the possibility of hard water effect were excluded where the presence of dead carbon results in artificially old ages for aquatic organic matter [Bjoerck and Wohlfarth, 2001, Fontes et al., 1996]; (ii) the proxies used should be sensitive to climate change [Prasad et al., 2014]; (iii) the archives should not have long-term (decadal) documented hiatus.

Subsequently, the archives are divided into low, medium, and high confidence categories depending on the number of dates and the sampling Table 2.2. The archives in the region (76°E–92°E; 16°N–32°N) encompass sites from both the Core Monsoon Zone (CMZ) and from the northern Himalayan Indian Summer Monsoon (ISM) and Westerlies influenced regions Figure 2.14. While the sites in the CMZ are mostly affected by ISM from June to September, the Himalayan records show a seasonality in the moisture source origin between summer (ISM) and winter (Westerlies) due to the northward (southward) shift of the Inter-Tropical Convergence Zone (ITCZ) band in the corresponding summer (winter) season.

The annual relative moisture signal from the multi-proxy investigations has been translated into a qualitative moisture index for a three-part scale: minus (plus) values indicate drier (wetter) conditions in each 200-yr time slice. No changes are marked with zero values. This information has been corroborated with the available historical information in Central India, where decadal scale drought-induced famines are documented in historical records from the 13^{th} and 14^{th} centuries AD [Dhavalikar, 1984, Maharatna, 1996]).

No.	Name	Lat.	Lon.	Archive	Proxy	Reference
1	Naychudwari	32.30	77.43	Peat Bog	Pollen	Chauhan et al., 2006
2	Gangotri	31.00	79.00	Sediment	Pollen	Kar et al., 2002
3	Dharamjali cave	29.31	80.12	Stalagmite	δ^{18}O,δ^{13}C Isotopes	Sanwal et al., 2013
4	Siddi Baba	28.00	84.00	Stalagmite	Laminae thickness	Denniston et al., 2000
5	Paradise Lake	27.30	92.06	Lake core	Pollen	Bhattacharya et al., 2007
6	Narmada basin	23.00	77.43	Sediment	Flood Deposite	Ely et al., 1996
7	Lonar Lake	19.51	76.00	Lake Sediment	Mineralogy and isotopes	Anoop et al., 2013 Menzel et al., 1996 Prasad et al., 2014 Sarkar et al., 2014
8	Dandak+Jhumar	19.00	82.00	Stalagmite	δ^{18}O Isotope	Sinha et al., 2011a
9	Godavari	16.00	83.00	Marine Core	δ^{13}C of plant waxes	Ponton et al., 2012

Table 2.2: Paleoclimate records. The colors indicate the confidence level of the records based on chronology and sampling resolution (red = low confidence record with either extrapolated or one date for 1000 years, multi-decadal or higher resolution; orange = medium-range confidence with at least 2 dates and decadal resolution for 1000 years and green = high confidence with more than 2 dates and sub to decadal resolution for 1000 years).

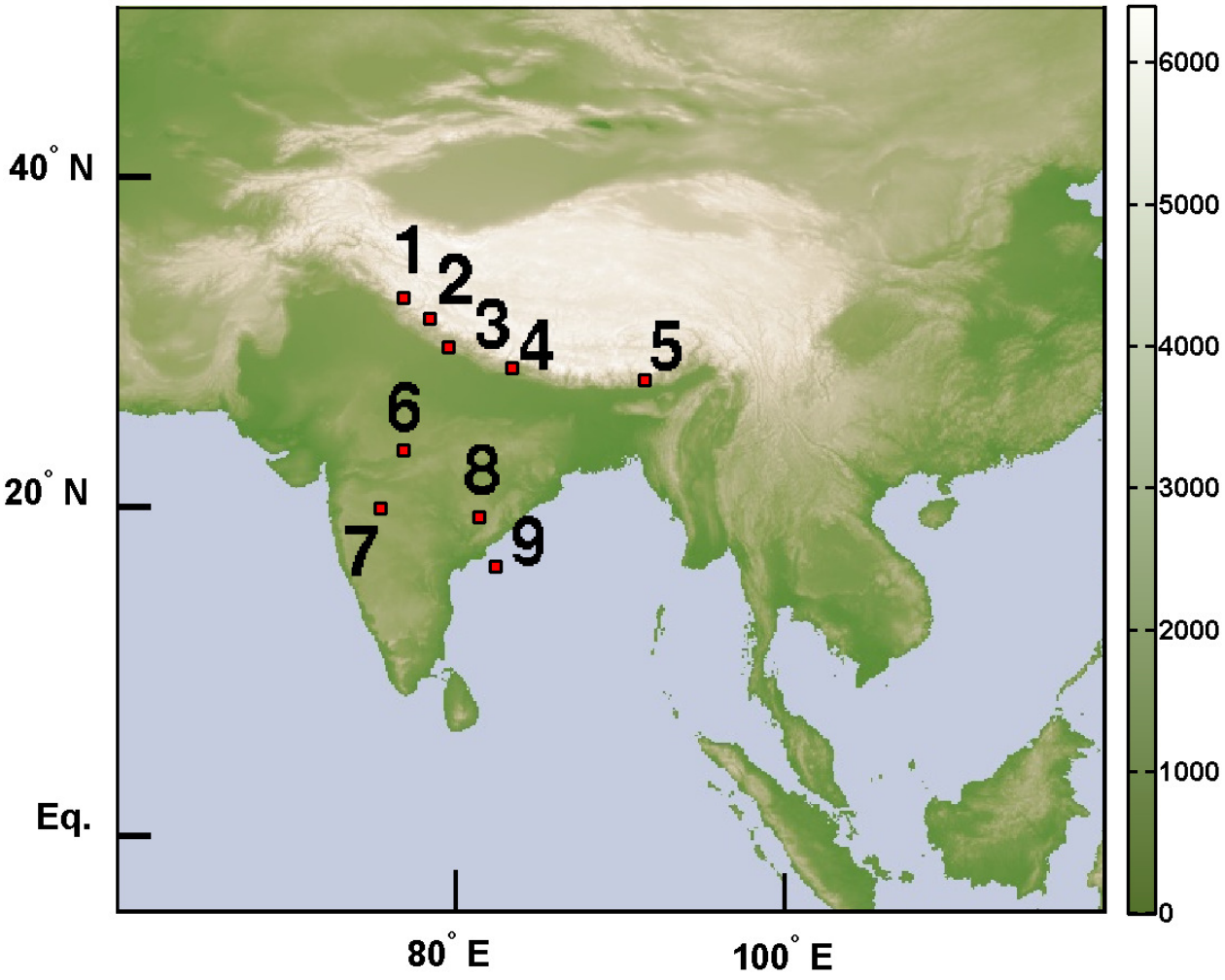

Figure 2.14: Paleoclimatic site's (red squares) and topography in m. Topographic data is downloaded from http://neo.sci.gsfc.nasa.gov/.

2.5.2 Monsoon variability during MCA and LIA

The paleoclimatic reconstructions (Figures 2.15.a and 2.16.a) indicate a clear moisture shift departing from the MCA to the LIA. The data are compared with the AOGCM and AGCM simulated Precipitation minus Evaporation (P-E) anomalies. The advantage of the higher-resolved AGCM (Figures 2.16.a) in regions with complex topography (Himalaya) is confirmed by a better spatial correspondence to the reconstructed moisture index compared to the coarse resolved AOGCM of the Millennium experiment (Figure 2.15.a). The

dipole pattern between wetter (Himalaya) and drier (Central India) conditions is in good agreement between the AGCM simulations and the reconstructions (Figure 2.16.a). Further, a strong and statistical significant drying is simulated over northern Arabian Sea and Bay of Bengal. The characteristic dipole structure in moisture is further supported by European Centre for Medium-Range Weather Forecasts (ECMWF) climatology for recent times (http://old.ecmwf.int/research/era/ERA-40_Atlas/docs/section_B/parameter_emp.html) indicating realistic patterns in the AGCM compared to coarse resolved AOGCM. The summer (JJAS) and winter monsoon (DJF) P-E anomalies and its statistical significances at 90% confidence level are illustrated for the AOGCM (2.15) and AGCM (2.16) simulations between MCA and LIA. Due to better spatial resolution, AGCM shows more detailed representation of seasonal moisture changes.

During summer months MCA tends to be drier compared to LIA especially in a zonal belt from northern Arabian Sea, Central India and northern Bay of Bengal (Figure 2.16.b). Over eastern Himalaya wetter summer conditions occur during MCA. Both regions are statistically significant at 90% confidence level. During the MCA winter months, the significant drying pattern over Indian Peninsula disappears and is restricted over Arabian Sea and Bay of Bengal. Statistical significant wetter conditions between LIA and MCA are simulated over western and central Himalaya (Figure 2.16.c). The sites in Central India, i.e., Lonar, Narmada basin, and Dandak cave lie in the heart of the Indian summer monsoon region and the signal can be considered as summer signal. MCA minus LIA annual P-E anomalies are more influenced by a winter signal in the western and central Himalayan region and a summer signal in the eastern Himalaya and Central India.

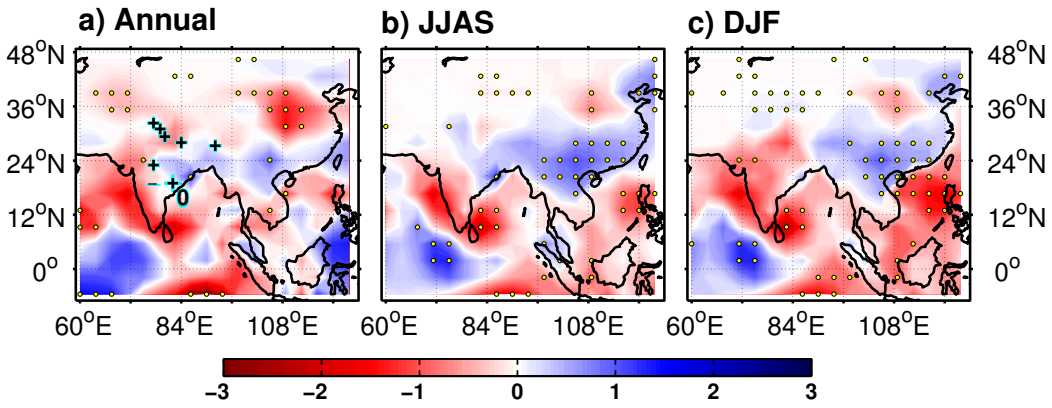

Figure 2.15: Simulated anomalies of P-E ($^{mm}/_{day}$; colours) annual (a), summer monsoon (b) and winter monsoon (c) MCA minus LIA for AOGCM in Monsoon Asia. In addition the reconstructed moisture index (symbols: + wetter, - drier and 0 no changes; dimensionless) for MCA minus LIA is shown for annual anomalies (a). Statistical significant P-E values ($p < 0.1$; two-tailed t-test) are illustrated by yellow dots.

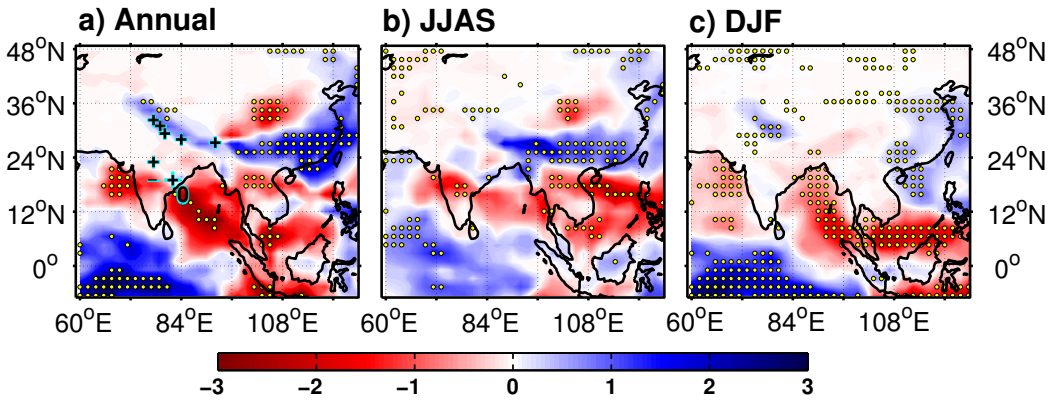

Figure 2.16: As in Figure 2.15 but for AGCM.

Chapter 3

Past millennium climate change in Arid Central Asia simulated by a regional climate model

Bijan Fallah, Sahar Sodoudi and Ulrich Cubasch, " Westerly jet stream and past millennium climate change in Arid Central Asia simulated by COSMO-CLM model.", Theoretical and Applied Climatology, http://link.springer.com/article/10.1007/s00704-015-1479-x#, DOI: 10.1007/s00704-015-1479-x, 2015.

Chapter 4

A numerical model study on the behaviour of Asian summer monsoon due to orographic forcing of Tibetan Plateau

4.1 Introduction

Several studies applied Atmosphere–only General Circulation Models (AGCM) [Boos and Kuang, 2010, Chakraborty et al., 2002, Wu et al., 2012, Yasunari et al., 2006] or Atmosphere–Ocean General Circulation Models (AOGCM) [Boos and Kuang, 2013, Park et al., 2011, Tang et al., 2013b] to investigate the Asian summer monsoon behaviour due to orographic forcing of Tibetan Plateau (TP). For example, Boos and Kuang [2010, 2013] showed that the heating of the TP locally affects the precipitation over the Himalayas but has no impact on the large-scale monsoon circulations. They demonstrated that, during the summer, the Himalayan topography acts as a barrier to shield the warm and moist southern Asian monsoon region from the cold and dry extra-tropical air masses. They also found that, during summer, the maximum upper tropospheric temperatures occur throughout the Indian sub-continent and are not located over the TP. In contrast

to Boos and Kuang [2010, 2013], Wu et al. [2012] suggested that South and East Asian monsoons are controlled by the thermal forcing of the different parts of the TP and that the mechanical effect of the plateau is not the major driver of Asian summer monsoon. The models applied in the studies of Boos and Kuang [2010] and Wu et al. [2012] were integrated using the prescribed climatological SST and sea ice. This approach may be insufficient to represent the indirect impact of the orographic modifications on the ocean circulation [Boos and Kuang, 2010]. The integration period of the coupled atmosphere-ocean simulation of Boos and Kuang [2013] was limited to 25 years. Additional studies are therefore needed to investigate the ocean response to orographic changes by using longer integrations of coupled atmosphere-ocean models.

To discover the high resolution patterns of Asian summer monsoon, [Tang et al., 2013b] applied a regional climate model which was driven by an AOGCM. They showed that the regional orographic uplift produces asynchronous evolution of Indian summer monsoon and East Asian summer monsoon. They concluded that the intensified East Asian summer monsoon is linked to *sensible heat pumping* of the northern, eastern and central TP and the Indian summer monsoon is enhanced by the *thermal insulation*. The selected AOGCM, which was used for their sensitivity experiment, had a globally lower orography and not only over the TP.

Apart from sensitivity experiments by means of climate models, some studies have used observational and reanalysis data to study the signature of the TP in the Asian monsoon [Gu et al., 2009, Rajagopalan and Molnar, 2013]. Using the reanalysis data, Rajagopalan and Molnar [2013] showed that plateau heating correlates directly with monsoon rainfall during early and late summer, but only marginally during the mid-June to the end of August period.

On the other hand, the ocean circulation is affected by the highly nonlinear complex variations in atmospheric circulation. This is illustrated for example in the atmosphere-ocean interactions during an abrupt climate change [Gu et al., 2009, Liu et al., 2013, Rahmstorf, 2002]. Using the NCEP/NCAR reanalysis dataset, Ya et al. [2013] investigated the possible Eurasia-North Atlantic Ocean teleconnection. According to their results, Atlantic SST changes have a greater impact on the southern TP summer rainfall than Indo–Pacific oceans via Rossby waves. The recent IPCC report Stocker et al. [2013]

points out that global warming may lead to a cooler North Atlantic by weakening the Atlantic Meridional Overturning Circulation (AMOC). Assuming two preferred regimes (e.g. *active* and *break*) in the Asian summer monsoon [Hannachi and Turner, 2013, Palmer, 1994, Turner and Hannachi, 2010], the *break* phases of the Indian monsoon coincide with a cold Northern Atlantic and Arctic, and the *active* phases with a warm Northern Atlantic and Arctic [Marzin et al., 2012]. Thus, the AMOC, which plays a major role in transporting heat from the Southern Hemisphere and tropics towards the North Atlantic, may influence the extreme moisture changes in monsoon regions. Alteration of the AMOC will impact the North Atlantic "storm tracks". The AMOC reduction is closely connected with the cooling of the North Atlantic. Woollings et al. [2012] estimated a temperature change of 0.31 K for a 1 Sv weakening of the AMOC in the region 20°–60°W, 45°–70°N. They concluded that in a warm North Atlantic, the positive Atlantic Multidecadal Oscillation (AMO^+) phase is associated with an increase of the Sahel and India summer monsoon rainfall. Previous studies [Cheng et al., 2013, Chiang et al., 2008, Stouffer et al., 2006, Vellinga and Wood, 2002] indicated that changes in the AMOC influence the Inter-Tropical Convergence Zone (ITCZ). Stouffer et al. [2006] showed that an AMOC weakening causes an equatorward shift of the ITCZ. Thus, as a consequence of changing ITCZ, AMOC influences the Asian monsoon regions [Zhang and Delworth, 2006]. The paleo records from sediment cores of North Atlantic indicate a "shutdown" in the AMOC during the Heinrich event H1 [McManus et al., 2004]. Using a stalagmite record from China, Liu et al. [2013] assessed the linkage between the North Atlantic and the monsoon system during the 8.2k year event. They showed that, during this event, the climate was significantly drier than today and was connected to an abrupt cooling in the North Atlantic ocean. According to their results, this linkage is also existent in any warm climate similar to the current one. Wang et al. [2001b] found a remarkable resemblance between oxygen isotope records of stalagmites from the Hulu Cave in China and from Greenland ice cores. They concluded that the strong East Asian monsoon is linked to warmer Greenland temperature while the weaker East Asian monsoon is related to cool temperatures in Greenland. The weakening of AMOC due to global warming is more likely to be linked to changes in surface heat flux than in freshwater [Gregory et al., 2005].

The question which is not answered yet in the previous studies is how the TP uplift will influence the atmosphere-ocean relation and to what extent the atmospheric changes influence the ocean's response. Our study investigates the results of a numerical modelling experiment using the ECHAM5/MPI-OM coupled AOGCM to investigate the role of the TP on the climate system with a focus on the Asian summer monsoon. A longer integration time is chosen here to consider the feedback processes between ocean and the atmosphere. In contrast to most of the previous studies, our model set up allows an investigation of the climatic patterns under changing Tibetan Plateau forcing with an interactive ocean.

Simulations using the ECHAM5/MPI-OM coupled atmosphere-ocean model with and without the Tibetan Plateau have been performed to study the large scale effects of orographic forcing on the behaviour of the Asian summer monsoon system. The analysis emphasizes the significant impact of plateau forcing on the atmospheric circulations.

4.2 Model configuration

The feedback processes between ocean, atmosphere and orographic forcing are studied by designing two different simulation scenarios: (a) a simulation with present day topography as the Control (CTRL) run and (b) with decreased elevation of the TP and Central Asia, No Tibetan Plateau (NOTP). The Community Earth System Models (COSMOS version 1.2.1) developed by the Max Planck Institute for Meteorology in Hamburg was applied in this study, which consist of the atmosphere climate model ECHAM5 version 5.4.01 [Roeckner et al., 2006] and the ocean model MPI-OM version 1.3.1 [Marsland et al., 2003]. ECHAM5 was integrated at T31 resolution (corresponding to a Gaussian grid of $3.75^\circ \times 3.75^\circ$) with 19 vertical levels and the MPI-OM ocean model at GR30 resolution with 40 vertical levels. Both simulations are initialised using the climate state of the ensemble member mil0014 of the "millennium" simulation from the fully coupled Max Planck Institute for Meteorology Earth System Model (MPI-ESM) [Jungclaus et al., 2010], starting from the year 1500 AD. The model-proxy comparisons show that the mil0014 has the best performance [Polanski et al., 2014].

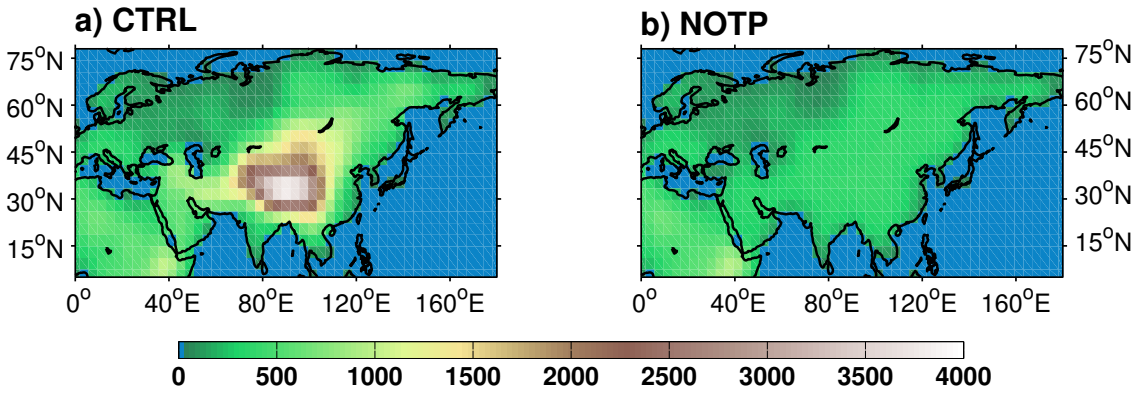

Figure 4.1: Topography in unit m for (a) CTRL and (b) NOTP (final state) simulations.

Green-House Gas (GHG)s concentrations (e.g. CO_2 , N_2O, CH_4) are fixed at their pre-industrial values. In both setups, the subgrid-scale orographic drag is considered, using the parameterisation scheme of Lott and Miller [1997]. In the NOTP set-up, the topography of the TP is decreased by 200 metres in every 10-year integration period to the threshold of 500 metres after 180 years of integration (Fig. 4.1). The related subgrid-scale orography parameters surface roughness length, standard deviation of orography, slope, orientation, anisotropy, angle, peaks and valleys elevation have been adjusted according to the scheme presented by Baines and Palmer [1990]. The model simulations are integrated for 500 years and the last 50 years are used for the analysis, unless otherwise stated. height of Tibetan Plateau, NOTP. The Community Earth System Models (COSMOS version 1.2.1) developed by Max Planck Institute for Meteorology (MPI-M) in Hamburg was applied in this study: Physical climate model ECHAM5 version 5.4.01 [Roeckner et al., 2006] / MPI-OM version 1.3.1 [Marsland et al., 2003] is used. MPI-OM includes HAMburg Ocean Carbon Cycle (HAMOCC), a sub-model that simulates bio-geochemical tracers in the oceanic water column and in the sediment. The ECHAM5 was integrated at T31 resolution with 19 levels and the MPI-OM ocean model at GR30 resolution with 40 levels. Both simulations are initialized by using the climate state (restart files) of the ensemble member mil0014 of "millennium" simulation from the fully coupled Max Planck Institute for MPI-ESM [Jungclaus et al., 2010] from the year 1500.

4.3 Theoretical considerations

The atmospheric general circulation consists of the flow which is averaged in time long enough to eliminate the random changes related with local weather systems [Holton and Hakim, 2012]. In a very simplified model, general circulation can be qualitatively studied by the "barotropic equation of midlatitude β-plane". The conservation law of the Rossby potential vorticity ($(\xi+f)/h = const.$) indicates that, in the northern hemisphere, a westerly propagating air parcel is squashed on a topographic barrier and stretched on the upstream. This leads to a cyclonic motion of the fluid column as it reaches the topographic barrier. The resulting cyclonic poleward motion will increase Coriolis force (f) on the air parcel which also reduces relative vorticity (ξ) to conserve the potential vorticity. When the air column crosses the topography, the height of the air column (h) decreases and relative vorticity becomes negative (anticyclonic motion) and the air parcel moves equatorward. On the downslope, the air column reaches its original height and the cyclonic motion brings the trajectory to its original latitude. Thus, steady westerly flow will generate a series of cyclonic and anticyclonic motions on the lee side of a large-scale barrier. The downstream wave train for the easterly flow is different and the air column propagates westward at its original latitude. However, in reality, the vertical motions are influenced by static stability and the large-scale motions are forced rather to pass around the topography while the potential vorticity remains conserved. These flows may converge again and increase the baroclinicity [Saulire et al., 2011]. The storm track usually weakens near the large-scale topography and its trajectory is tilted southwest to northeast over the lee side.

The midlatitude topographies play a major role on the formation of Rossby waves [Held and Ting, 1990, Hoskins and Karoly, 1981, Saulire et al., 2011]. The Rossby waves can influence the air flows up to very remote areas and alter the wind field pattern throughout the hemisphere. Previous studies confirmed the linkage between North Atlantic and Eurasia via the wave trains [Bothe et al., 2011, Sun and Wang, 2012, Ya et al., 2013]. According to Ding and Wang [2005], the summer wave train (e.g. *circumglobal teleconnection pattern*) originates in Europe and North Atlantic region which facilitates the low-level ascending air motions over India. As mentioned by Holton and Hakim [2012],

a quantitative study of the general circulation requires complex numerical models which solve the spherical primitive equations.

4.4 Simulation of present day conditions

The state-of-the-art IPCC AR5 models can mainly provide accurate estimates of the current climate. Among them, ECHAM5/MPI-OM shows a relatively good performance in reproducing the interannual variation and mean of the Asian summer monsoon [Kripalani et al., 2007a,b]. Using this motivation, the possible state of the climate (temporally averaged patterns of temperature, wind, precipitation and other variables) in the absence of the Tibetan Plateau is presented here. Prior to applying the model for the sensitivity experiment, the ability of the model to reproduce the Asian summer monsoon patterns for precipitation and temperature is tested. Figure 4.2 compares the large scale patterns of near surface temperature and precipitation between model simulations and the observations. The model-data comparison shows that the model is skillful in reproducing the mean climatological state of the rainfall and temperature patterns throughout the Asian monsoon domain.

Figure 4.3(a) shows the mean summer (JJAS) precipitation minus evaporation (P-E) for the CTRL. The global picture of the summer monsoon is well represented by this simulation. Figure 4.3(b) shows the 500 hPa ω (Pas^{-1}) as a proxy for the ascending ($\omega < 0$) and descending ($\omega > 0$) motions superposed on the 850 hPa wind field. Comparing the two figures reveals that the maximum rainfall values are located on the upward motion regions (convective precipitation). 850 hPa winds over the central Pacific correspond to the Walker circulation trajectory with a descending center on the west coast of the United States and an ascending region over west equatorial Pacific. The easterly winds connect these two regions and generate the trade winds over the Pacific. There are two large scale anticyclonic motions on the lee-side of TP over the North Pacific Ocean and the North Atlantic Ocean (Fig. 4.3(b)). The influence of TP on the monsoon circulation is studied in the next section by a simulation of conditions without the TP.

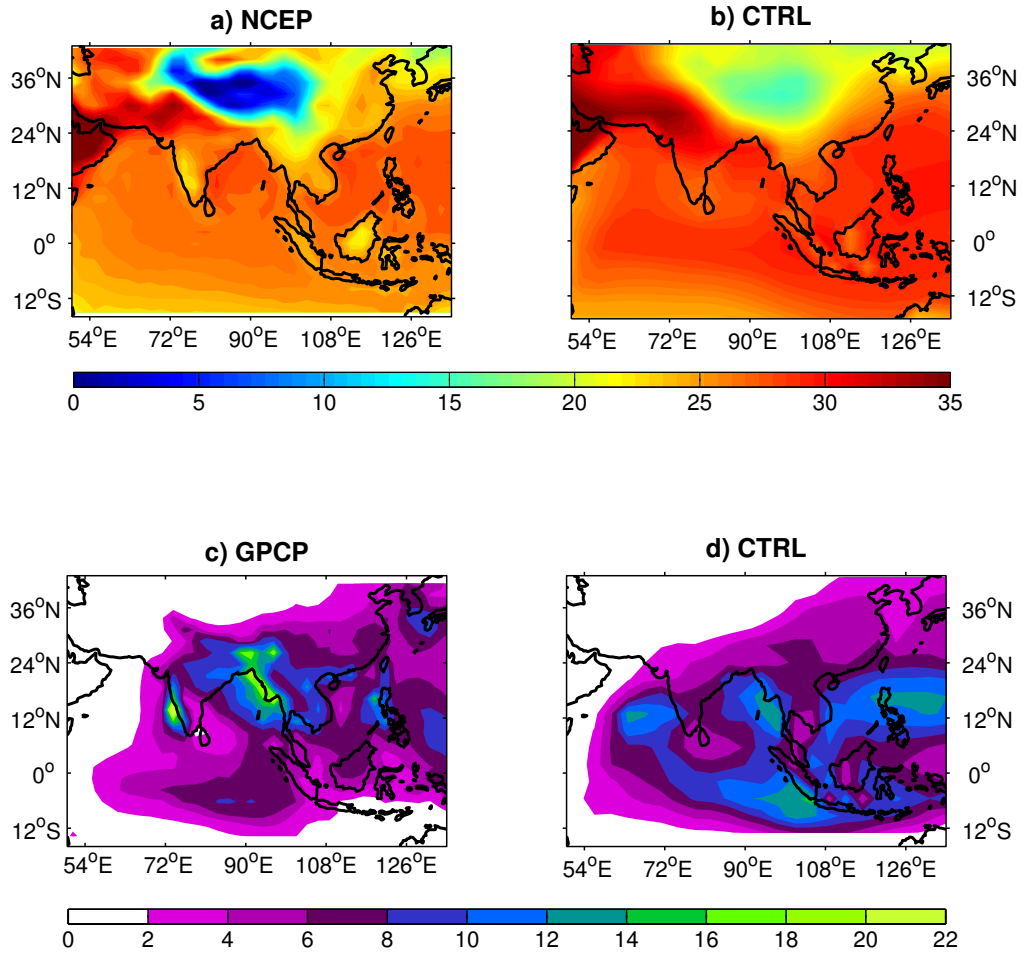

Figure 4.2: Climatology of (a) summer (JJAS) near surface temperature (°C) from NCEP for 1950-1999, (b) from CTRL; large scale Asian summer monsoon rainfall ($^{mm}/_{day}$) from (c) GPCP and (d) from CTRL.

a) P−E for CTRL

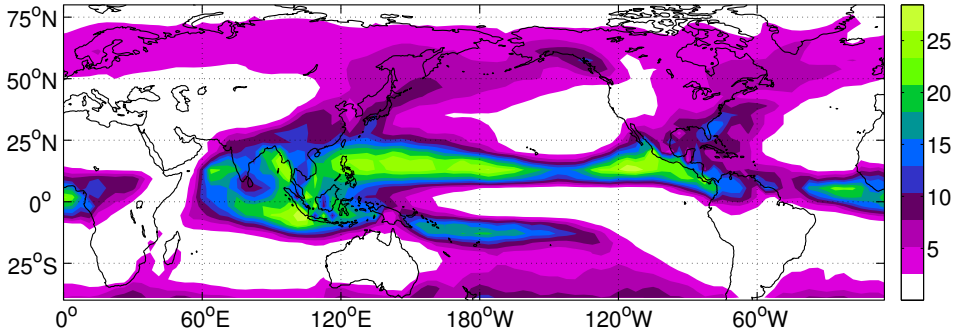

b) 500 hPa ω and 850 hPa Wind for CTRL

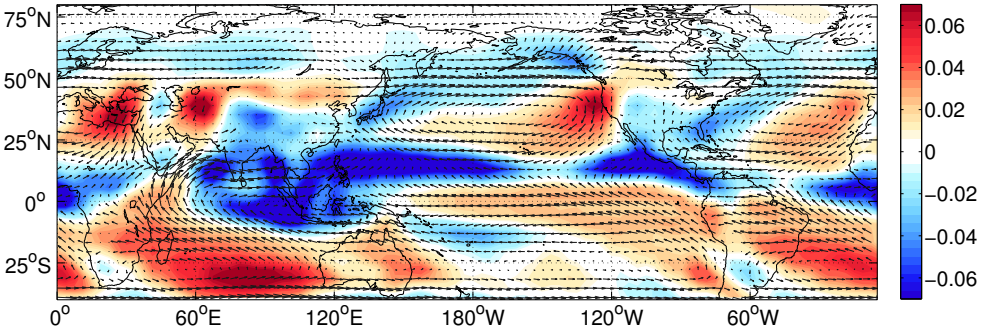

c) P−E for CTRL−NOTP

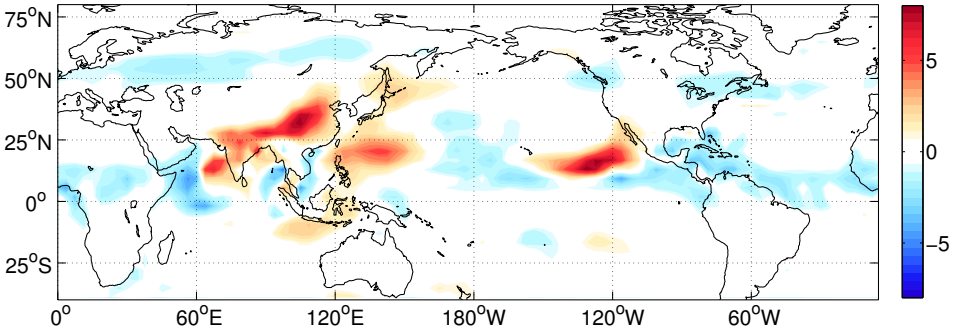

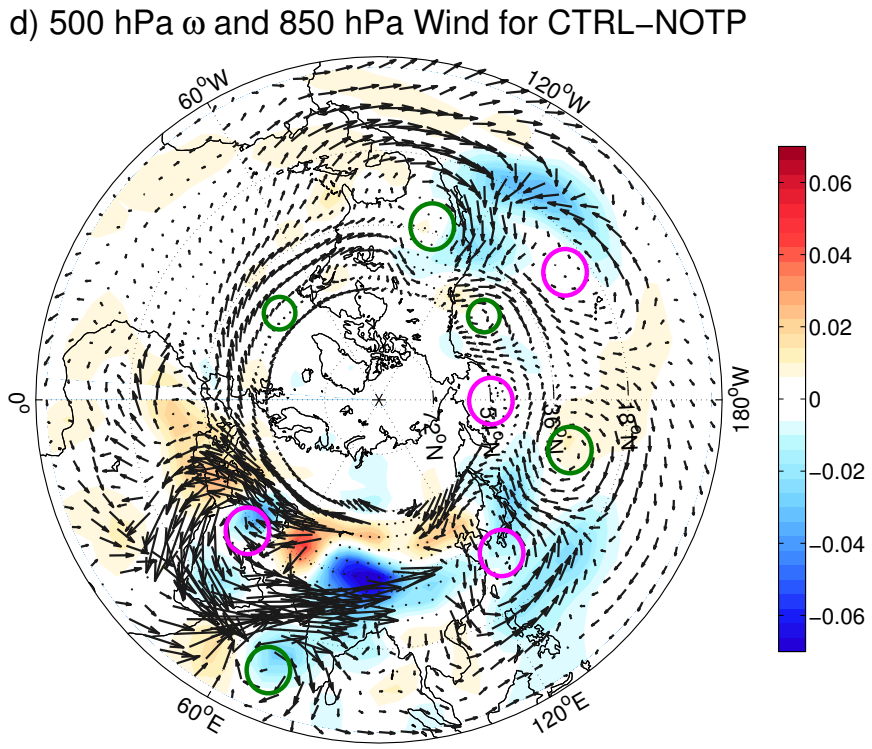

Figure 4.3: Large scale patterns of (a) summer (JJAS) Precipitation minus Evaporation (mm/day) for CTRL (b) 500 hPa. ω (Pas^{-1}) and 850 hPa wind (ms^{-1}) for CTRL (c) Precipitation minus Evaporation (mm/day) difference of NOTP compared to CTRL (CTRL-NOTP) and (d) 500 hPa ω (Pas^{-1}) and 850 hPa wind (ms^{-1}) difference of NOTP compared to CTRL (CTRL–NOTP). The largest vector in (b) is 12 (ms^{-1}) and in (d) is 6 (ms^{-1}). The magenta circles indicate cyclonic and the green ones the anticyclonic motions.

4.5 Simulation of conditions without Tibetan Plateau

Subtracting the general state of the climate in the two different simulations (CTRL–NOTP) highlights the altered patterns in the climate without topographic effect of TP. As can be seen in Figure 4.3(c), a large portion of the Asian summer monsoon precipitation is not present in the NOTP. Over the east equatorial Pacific Ocean (around 120°W and 20°N), atmospheric deep convection is reduced and shifted towards the Central Pacific and American continent. The largest patterns which are altered in the NOTP are the reduced ascending motions over the monsoon region with a peak over TP and the weaker Somali Jet (Fig. 4.3(d)). The pronounced weakening of the Somali Jet, which transits Kenya, Somalia, Yemen and Oman, accounts for the reduction of moisture transport in the Indian monsoon region. On the lee-side of the largest topographic barrier (TP), the alternating cyclonic and anticyclonic motions are not existent in the NOTP simulation (color circles in the Fig. 4.3(d)). The weakening of trade winds in the NOTP lead to an attenuated "Walker cell" in the equatorial Pacific which accounts for the rising motion over Indonesia and a sinking one over the eastern Pacific. The 850 hPa wind presents an anticyclonic motion in North Atlantic (Fig.4.3(d)). The reduction of this circulation in NOTP influences the oceanic currents in North Atlantic via the wind-driven ocean circulations. The anticyclonic motion over the west side of North Pacific, east coast of Japan, is also reduced in the NOTP. The large cyclonic motion over Middle East which transports moisture toward the monsoon regions from west Arabian Sea is reduced (Fig. 4.3(d)). As a response to anomalous atmospheric low level winds, convergence, precipitation and vertical motions, the ocean-atmosphere interaction alters the ocean circulation.

The impact of the removal of TP is apparent in SST patterns in North Atlantic region (Fig. 5.9(a)). A change in the wind field results in impact on the ocean circulations (Figure 5.9(c)). Figure 5.9(b) shows the climatology of summer (JJAS) SST and wind stress in North Atlantic. The wind stress over the North Atlantic is considerably weaker in NOTP (Figure 5.9(c)). This leads to reduced downwelling motions of warm waters in the mid North Atlantic Ocean. The cyclonic surface wind stress contributes to the convergence of the surface water, resulting in downwelling; conversely, anticyclonic surface

wind leads to divergence of surface water resulting in upwelling motions. The wind stress difference between CTRL and NOTP presents an anticyclonic motion over North Atlantic Ocean (Figure 5.9(c)). The changes in surface wind velocities in North Atlantic and near coastal wind stress have an important effect on the Ekman pumping in North Atlantic region. The reduction of the downwelling motion in NOTP which originates from wind-driven Ekman convergence, is reflected in the SST pattern (Fig. 5.9(c)). The North Atlantic Ocean is remarkably warmer in the CTRL than in the NOTP (up to 8 K). This influences the monsoon via the teleconection between North Atlantic and Asian monsoon via the mechanisms proposed by Liu et al. [2013]. Figure 5.9(d) shows the climatology of ocean temperature in the longitude-depth plane at 45°N. With the TP , a warm water current which initiates from the surface over west of North Atlantic Ocean (around 45°W) penetrates to the deeper layers down to 2000 m depth over 10°W. This warm current is reduced when the large scale topography of TP is removed (Figure 5.9(e)).

To verify this effect, the Ekman pumping velocity is calculated based on the surface wind stress [Legatt et al., 2012]. The climatological Ekman pumping velocity (Figure 4.5(a)) presents an upwelling region around 45°N–70°N and 30°W–10°W and a downwelling region south of 48°N. The difference between the simulated Ekman pumping in CTRL and NOTP indicates the response of ocean's upwelling to uplift of the TP. Figure 4.5(b) indicates the region of downwelling (blue shadings) and upwelling (red shadings) induced by the wind stress differences. Following the zonal line in Figure 5.9(b), Ekman pumping velocity indicates a downwelling over the east part of the North Atlantic Ocean (around 45°W) (Fig. 4.5(b)). In the NOTP experiment, there is a reduction in downward motions in the wide area of North Atlantic Ocean (Fig. 4.5(b)). This reduction of downwelling lessens the heat transport from near ocean surface atmosphere to deeper layers (down to 2500 m depth) and induces a cooling effect in North Atlantic Ocean.

The North Atlantic averaged meridional overturning stream function for the NOTP shows a remarkable decrease compared to the CTRL (Fig.4.6(a)). This circulation expresses the role of TP on the North Atlantic circulations. The AMOC circulation pattern (its core is located at $\sim$ 1,000 m depth and 55° N) leads to decreased downwelling motion of warm surface water into the deeper ocean layers around 40° N. To assess the AMOC changes, the AMOC index is calculated based upon the maximum value of meridional

overturning stream function north of 28°N within the red box in Figure 4.6(a) [Hofer et al., 2011]. The AMOC indices of the CTRL and the NOTP are shown in Figure 5.8(b). There is a clear drop of about 6 Sv in the AMOC when the TP is removed. The weakening of the AMOC is connected to the cooling of North Atlantic. A decreased AMOC will reduce the heat advection from western North Atlantic region into the eastern parts. The existence of a teleconnection between the North Atlantic SSTs and the rainfall over the Asian monsoon leads to additional reduction of the summer precipitation over Asia in the NOTP experiment, thereby reinforcing the direct effect.

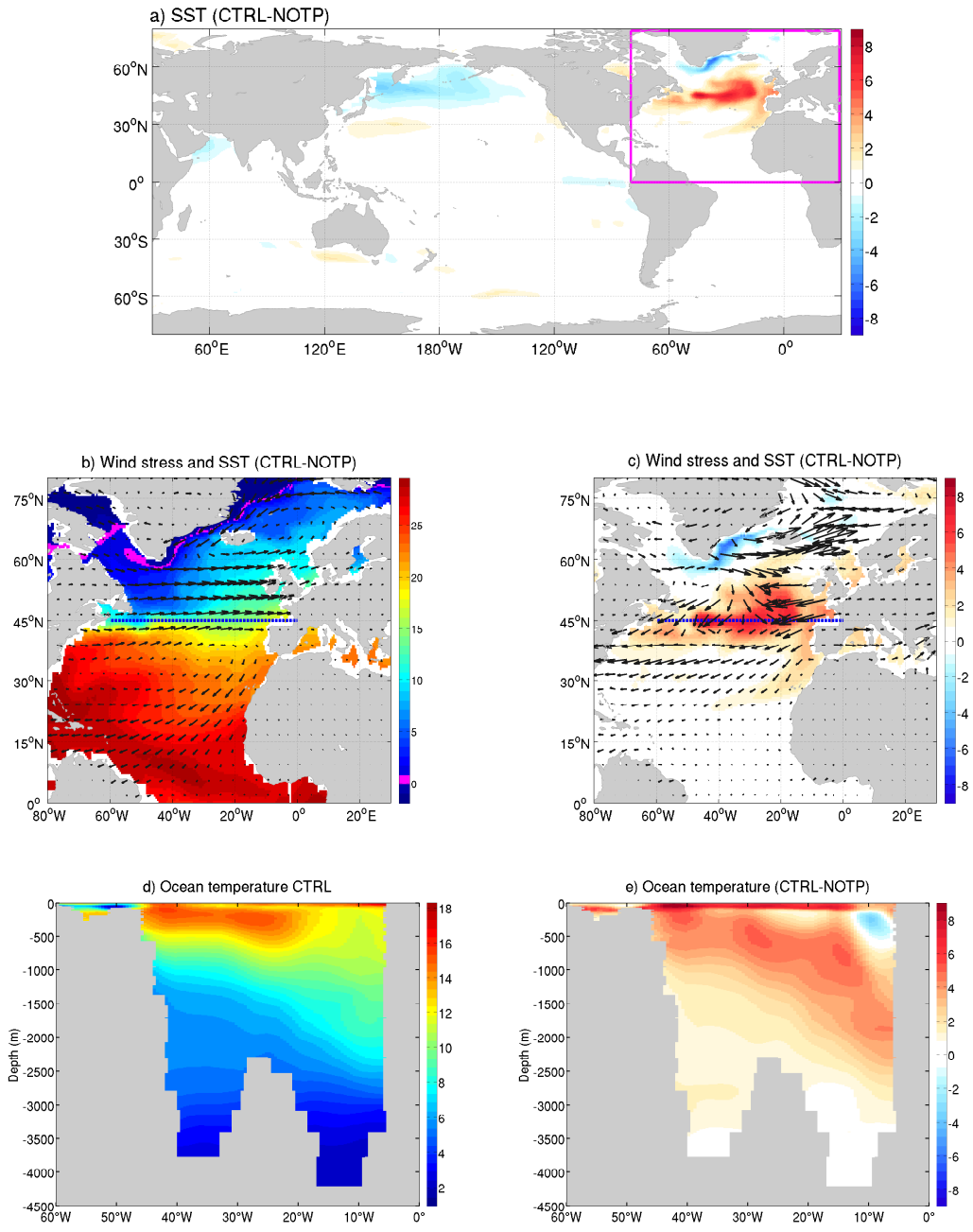

Figure 4.4: Spatial patterns of (a) global summer (JJAS) SST differences (K) for CTRL-NOTP, (b) climatology of summer (JJAS) SST (°C) and wind stress (Pa) for CTRL (c) summer (JJAS) SST (K) and wind stress (Pa) differences for CTRL-NOTP (d) cross section of North Atlantic Ocean's temperature (°C) and (e) cross section of the North Atlantic Ocean's temperature difference (CTRL-NOTP) along the blue dashed line in (b) and (c). The largest vector is 0.23 Pa. Magenta color in (b) indicates zero values.

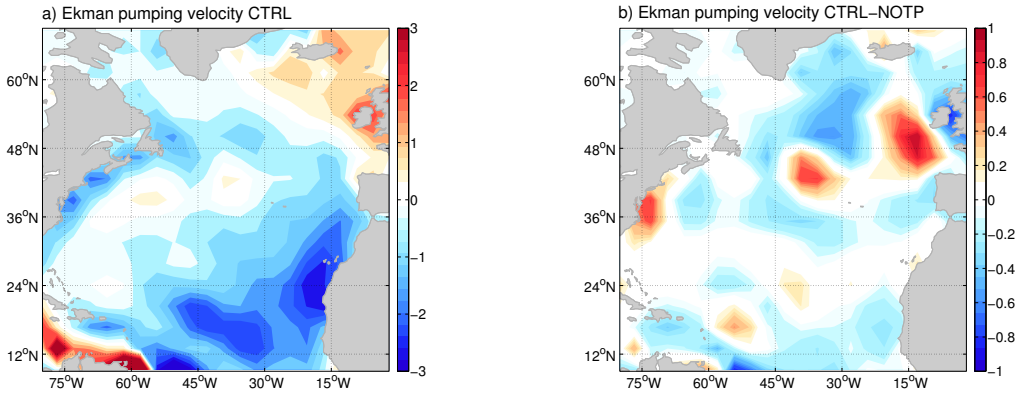

Figure 4.5: Ekman pumping velocity ($10^{-6}ms^{-1}$) for (a) the climatology of CTRL and (b) the difference (CTRL-NOTP) over the North Atlantic. Note the different colorbars. Negative values indicate down-welling and positive values upwelling.

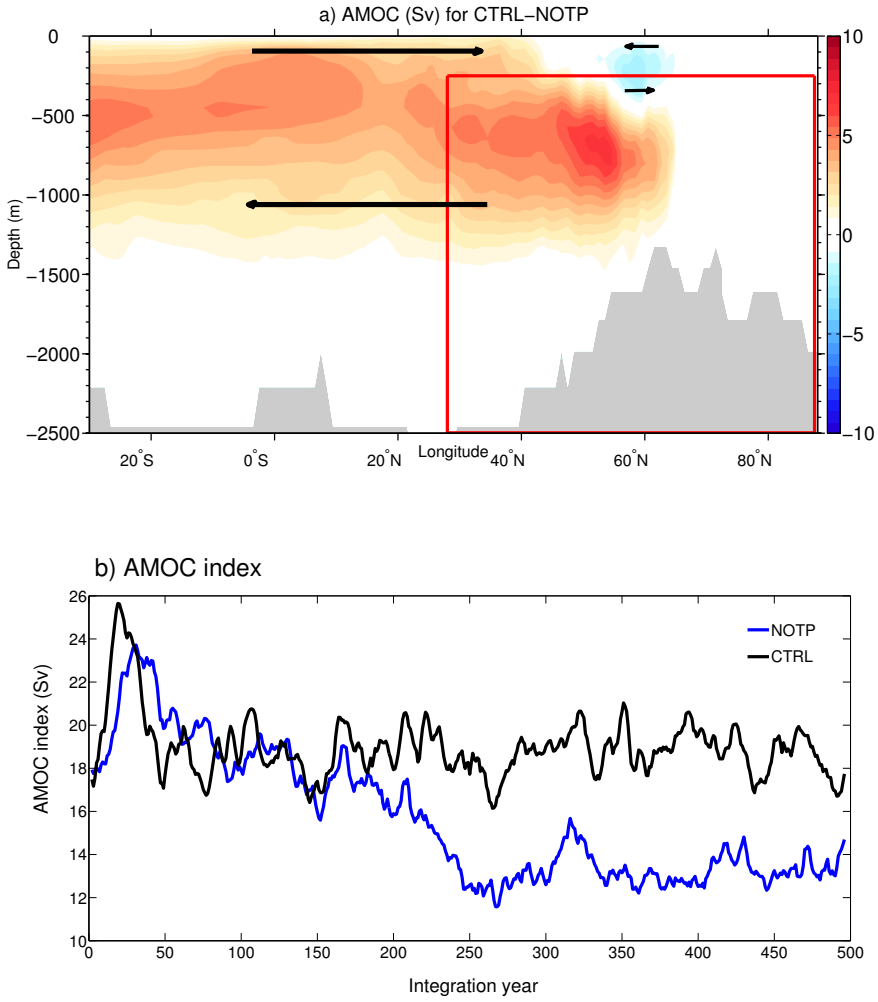

Figure 4.6: North Atlantic averaged meridional overturning stream function difference (Sv) between CTRL and NOTP (CTRL-NOTP) and (b) time-series of AMOC for NOTP (blue) and CTRL (black).The maximum value inside the red box is defined as AMOC index for each time-step. Positive values indicate anticyclonic circulations. Vectors in (a) show the schematic meridional currents.

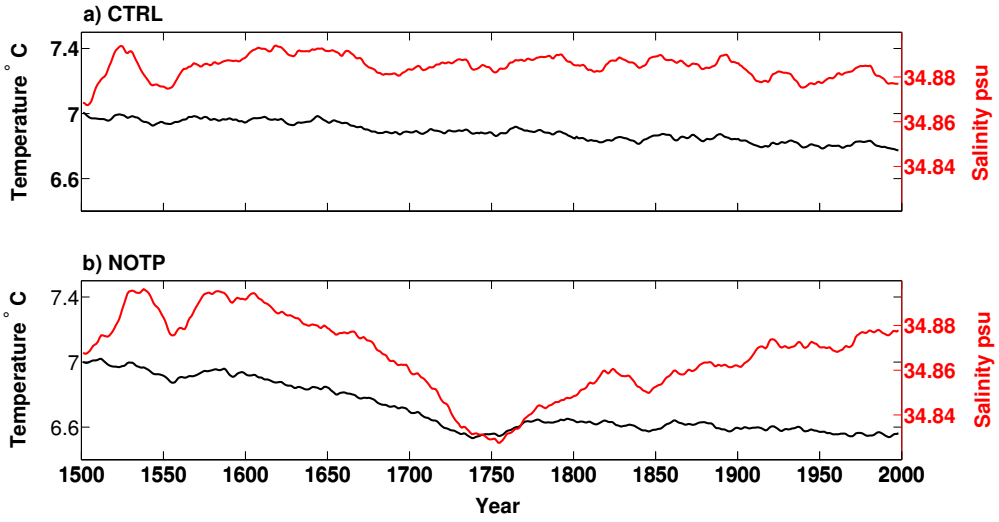

Figure 4.7: Annual mean of ocean temperature (red line) and salinity (black line) at 740 m depth for (a) CTRL and (b) NOTP simulation.

4.6 Shallow ocean's equilibrium state

For the CTRL experiment, model reaches an equilibrium state in shallow water (740 m depth), for both temperature and salinity distribution, after $\sim$ 60 years of integration (Figure 4.7.a). In the decreasing topography scenario, salinity and temperature decline remarkably and reach their minimum after 250 years for NOTP simulation (Figure 4.7.b). Shallow ocean temperature approaches a steady state after $\sim$ 250 years with a slightly cooling linear trend. However, the shallow water's salinity of NOTP rebounds to values ($\sim$34.88 psu) of CTRL after 500 years.

Chapter 5

Towards modelling the regional rainfall changes over Iran due to the climate forcing of the past 6,000 years.

5.1 Introduction

In the inland area of Iran, the climate is characterized as continental hot and dry with annual range of 22°C to 26°C [Sodoudi et al., 2010]. The Siberian High and Southwestern branch of summer Monsoon also contribute to the Iranian climate for the winter and summer seasons, respectively. The fluctuations of Westerlies' equator-ward shift or strength lead to the climatic changes (more precipitation) in the westerly-dominated regions [Chen et al., 2010].

Ancient cultures in Iran were mostly relying on the availability of rainfall as a source of water supply. The archeological evidences show an abrupt collapse of the developed Akkadian empire ca. 4,170 $\pm$ 150 yr BP [Cullen et al., 2000].

The ostracod fauna of Lake Mirabad suggests a low lake level during the early Holocene and an increase during mid-Holocene [Griffiths et al., 2001]. There is a lack of knowledge

on the past climate change in Iran compared to other regions of the globe [Karimi et al., 2011, Kehl, 2009]. Kehl [2009] reviewed the state of the paleoclimate knowledge in Iran. He concluded that there are evidences of several Quaternary climate changes in this region. However, their timing and location are controversial.

A pollen record from southwestern Iran, provided the reconstruction of climate change and vegetation during the Holocene [Djamali et al., 2009]. According to Djamali et al. [2009], human activity became more evident after 3,700 BP. Using the geologic, geomorphic and chronologic data from the Qazvin Plain in northwest Iran, Schmidt et al. [2011b] studied the cultural dynamics in the Central Iranian Plateau during the Holocene. Their multiproxy data suggest a peak in aridity at ca. 4,550 yr BP in northwest of Iran which seems to be shifted from the "4.2 ka BP" drought event [Staubwasser et al., 2003].

There are two classical approaches for the global climate simulations of the Holocene: (i) transient low resolution comprehensive coupled Atmosphere-Ocean General Circulation Models (AOGCMs) and (ii) highly resolved Atmosphere only General Circulation Models (AGCMs) for the selected episodes, the "time-slice simulations" [Berking et al., 2013]. This is due to the high computational costs of the available computing systems that the second approach can not be applied for the longer time periods (e.g. several thousand years). For producing a detailed climatic data which is comparable with the local proxy information, a downscaling technique is required. In this study we use a state-of-the-art AGCM to carry out the time-slice experiments for the Mid-to-late Holocene. The focus of our study is the climatic response to external forcings of the climate system since Mid-Holocene to present day in Iran.

For the first time, I present simulated rainfall data for the period of Mid-Holocene to present day over the Persian region with employing a dynamical downscaling approach. Different selected time-slices are simulated by using a spatially finer resolved AGCM.

5.2 Materials and Methods

In this paper we used the ECHO-G model which consists of the atmospheric model ECHAM4 [Roeckner et al., 1996] and the ocean model HOPE [Wolff, 1997], at a spectral

resolution of T31 ($\sim 3.75^\circ \times 3.75^\circ$). The ECHO-G model has already been used in several studies [Strandberg et al., 2014, Wagner et al., 2007, Zorita et al., 2005]. However, the horizontal resolution of the ECHO-G does not capture local patterns over Iran region (totally 24 grid points within the domain).

Therefore, we utilized the "time slice simulations" [Berking et al., 2013, Cubasch et al., 1995] for reproducing the rainfall patterns over Iran. These simulations have been successfully applied for a climate-archaeological study over Sudan to reproduce heavy rainfall regimes in the ancient city of Naga [Berking et al., 2013]. Twelve 30 year long simulations for six different periods throughout the last 6,000 years have been performed with the fifth-generation atmospheric general circulation model (ECHAM5) at two spectral horizontal resolution of T63 ($\sim 1.8^\circ \times 1.8^\circ$) and T106 ($\sim 1.125^\circ \times 1.125^\circ$). The lateral boundary conditions, Sea Surface Temperature (SST) and sea-ice cover distribution from the transient simulation of Wagner et al. [2007] (coupled ocean atmosphere model ECHO-G) are prescribed for time-slice experiments with ECHAM5 model.

5.3 Results

5.3.1 Present time

The geographical distribution and the topography of the study area is shown in Figure 5.1. Iranian plateau is the continuation of the Tibetan Plateau. The topographical forcing plays a major role in the diverse climate of Iran [Sodoudi et al., 2010]. Figure 5.2 shows the climatology of seasonal rainfall over Iran from Global Precipitation Climatology Centre (GPCC) data-set provided by the NOAA/OAR/ESRL PSD, Boulder, Colorado, USA, from their Web site at http://www.esrl.noaa.gov/psd/. There is a clear seasonal rainfall variability over Iran, especially between summer (Fig. 5.2(a)) and other seasons (Fig. 5.2(b) to 5.2(d)). The complex topographical condition which contains Alborz range in the north and Zagros mountains in the West and Northwest and the latitudinal extent of Iran lead to the spatio-temporal variability of rainfall over this region.

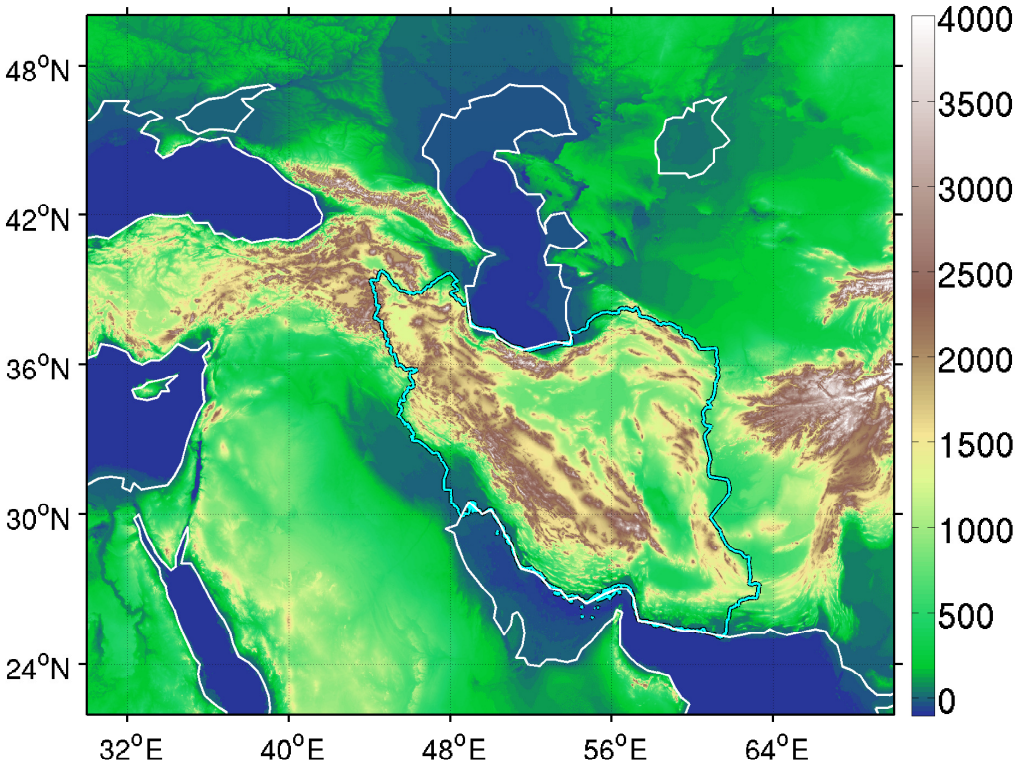

Figure 5.1: Topography in meter over the study region. Cyan line indicates the recent time Iranian political boarder.

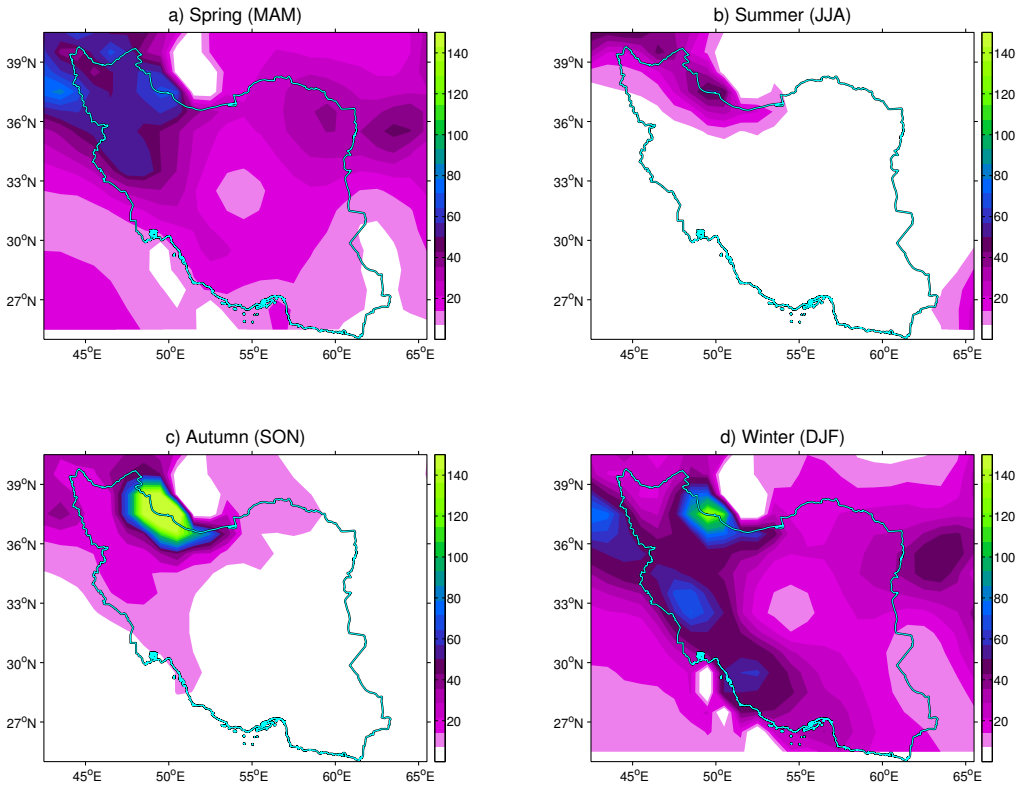

Figure 5.2: Rainfall [mm/month] over Iran for 5.2(a) Spring (MAM), 5.2(b) Summer (JJA), 5.2(c) Autumn (SON) and 5.2(d) Winter (DJF) from GPCC VASClimo for 1951–2000.

5.3.2 ECHO-G simulations

According to Sundqvist et al. [2010], Zhang et al. [2010], the changes in orbital forcing are the major driver of the climate change during the Holocene. The insolation due to orbital forcing shows different anomalous pattern during winter and summer from Mid-holocene to present time. Figure 5.3 shows the insolation difference between Mid-holocene and present time. The Northern Hemisphere shows a positive insolation anomaly during summer (JJA) and a negative anomaly during winter (DJF). Given that the extreme anomalies in solar insolation between 6 Kyr BP and present time happen during summer and winter, we focus on these seasons in our analysis.

Figure 5.4 presents the mean summer (JJA) rainfall over Iran region [$42.5°E$–$65.5°E$; $25°N$–$41°N$] for 6 KBP to Pre-Industrial (PI) (blue line) from ECHO-G simulation and the solar insolation [W/m^2] at $31°$N on 15^{th} July (red line). During summer, the rainfall fluctuations over Iran region show a clear decrease from Mid-holocene to present time. This can be explained by the changes in solar insolation due to varying orbital forcing. This result agrees well with the "moderate drying trend" from the study of Lauterbach et al. [2014] based on reconstructions of summer moisture using a sediment core from Central Kyrgyzstan. By synthesizing the lake sediment records of mid-latitude arid Central Asia, Chen et al. [2008] found the existence of a moderate drying trend since Mid-Holocene, caused by the Westerlies. They concluded that the summer insolation might be the major driver in controlling the moisture changes in arid Central Asia during mid-and late Holocene.

For winter, this pattern is reversed and the rainfall presents an increase since the Mid-holocene until present (Figure 5.4). In contrast with the summer time, the solar insolation indicates an increasing trend from Mid-holocene until the present.

The time-series of rainfall from Mid-holocene to present time, show that during the Mid-holocene (ca 6 Kyr BP) the summer rainfall value was larger than winter. This regime is reversed for the recent observed climate (Fig. 5.2).

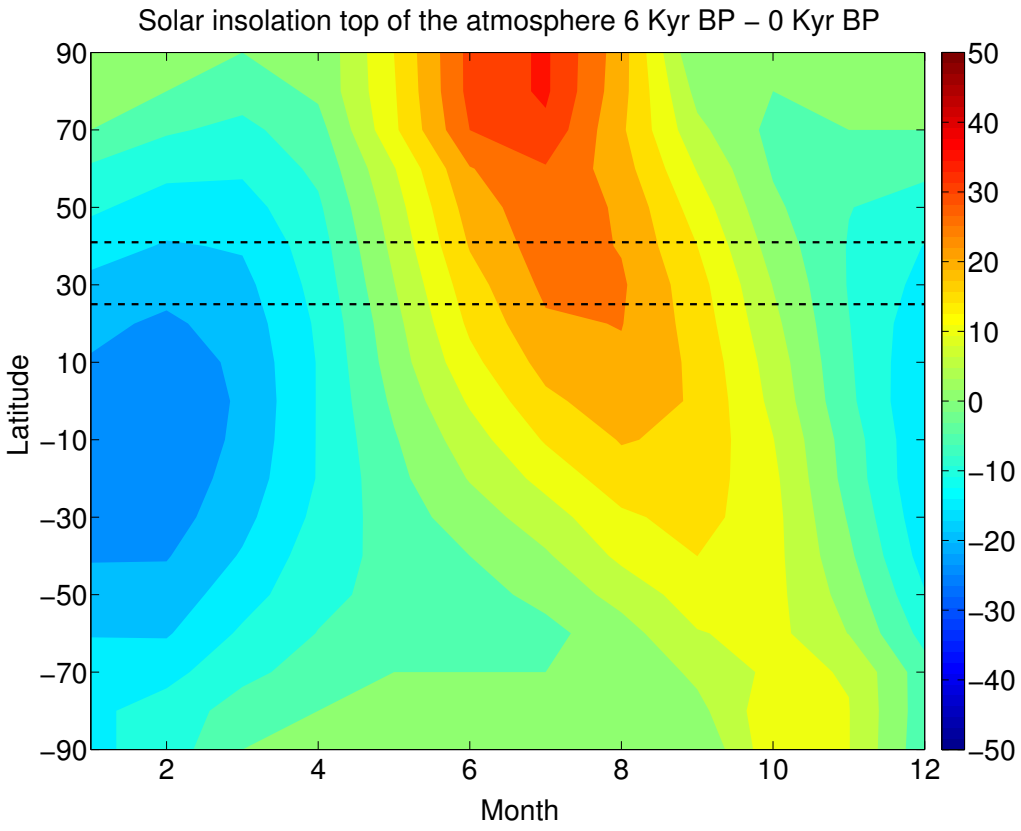

Figure 5.3: Insolation difference (W/m^2) between Mid-holocene and present day (6 Kyr BP – 0 Kyr BP) due to changes in orbital parameters. The area between the dashed lines indicates the latitudinal expansion of Iran.

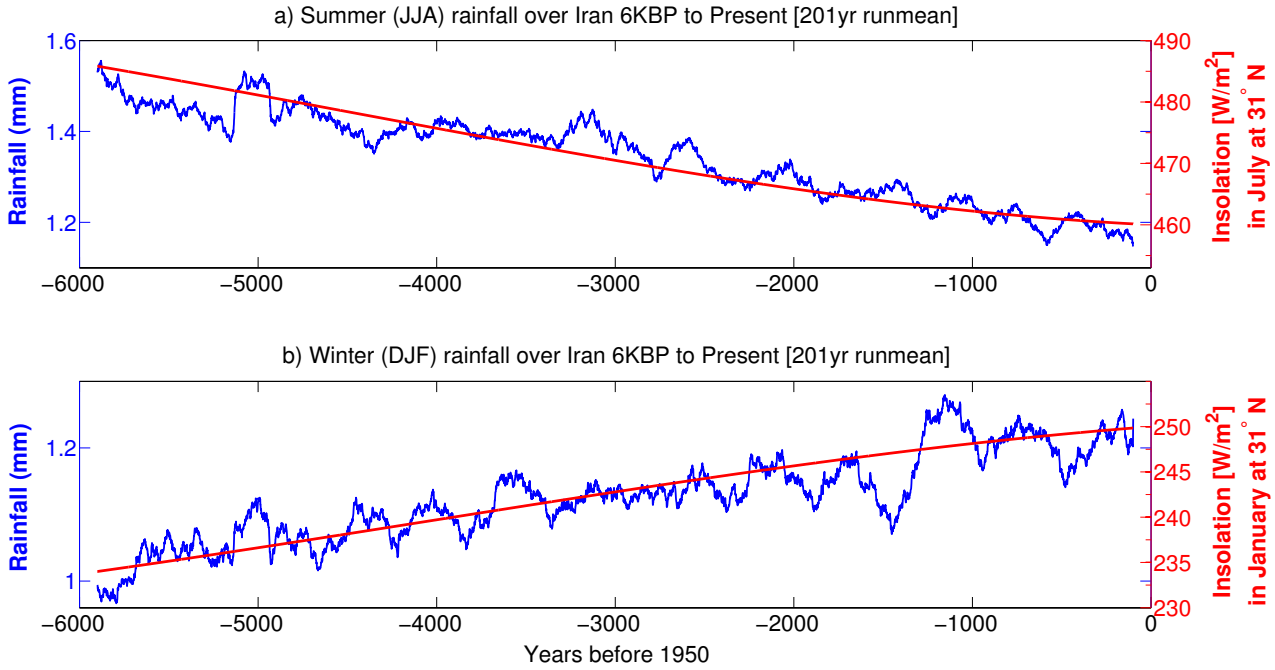

Figure 5.4: Rainfall over Iran [$42.5°E$–$65.5°E$; $25°N$–$41°N$] for 6 Kyr BP to present (blue line) and the solar insolation [W/m^2] at $31°$ (red line) from ECHO-G simulation during (a) Summer (JJA) and (b) Winter (DJF). Time-series are smoothed using 201 years running mean.

5.3.3 ECHAM5 simulations

Recent climate simulation of ECHAM5 reproduces similar large rainfall patterns as in GPCC but with about 4 ($\frac{mm}{moth}$) over-estimation in area-averaged rainfall during winter (not shown). This bias can be explained by the coarse spatial distribution of observational stations used by GPCC or the absence of data assimilation in the model during the recent climate. In order to investigate the spatio-temporal rainfall changes in Iran throughout the past 6,000 years, the differences between the time-slice simulations and the pre-industrial (200 yr BP) simulation is shown for Summer and Winter seasons (Figures 5.5 and 5.6). The results from the ECHAM5 simulations at T106 horizontal resolution are shown. The pre-industrial era has been selected to exclude the human-induced climate change period due to the recent anthropogenic forcing. During summer, the rainfall anomalies present similar patterns for all time-slices with minor changes over Southeast corner of Iran and Pakistan. These rainfall patterns originate from the Asian summer monsoon activity. Using the European Centre for Medium-Range Weather Forecasts (ECMWF) reanalysis ERA-40 data set [Uppala et al., 2005], Turner and Hannachi [2010] showed that, there is an existence of negative outgoing long-wave radiation composite anomalies (more convective activities) over Southeast corner of Iran in the "break phases" of Indian summer monsoon. The simulated All Indian Monsoon Rainfall (AIMR) index from ECHO-G simulations presents a similar trend as the mid-July solar insolation over 25° N during the past 6,000 years (not shown). The negative rainfall anomaly over Southeastern Iran can be explained with the increased break monsoonal phases during recent climate which contributes to more precipitation over this region of Iran.

During winter, the rainfall anomalies are more distinct for the different time-slices. In the following we investigate the possible drivers of such anomalous winter rainfall patterns throughout the past 6,000 years.

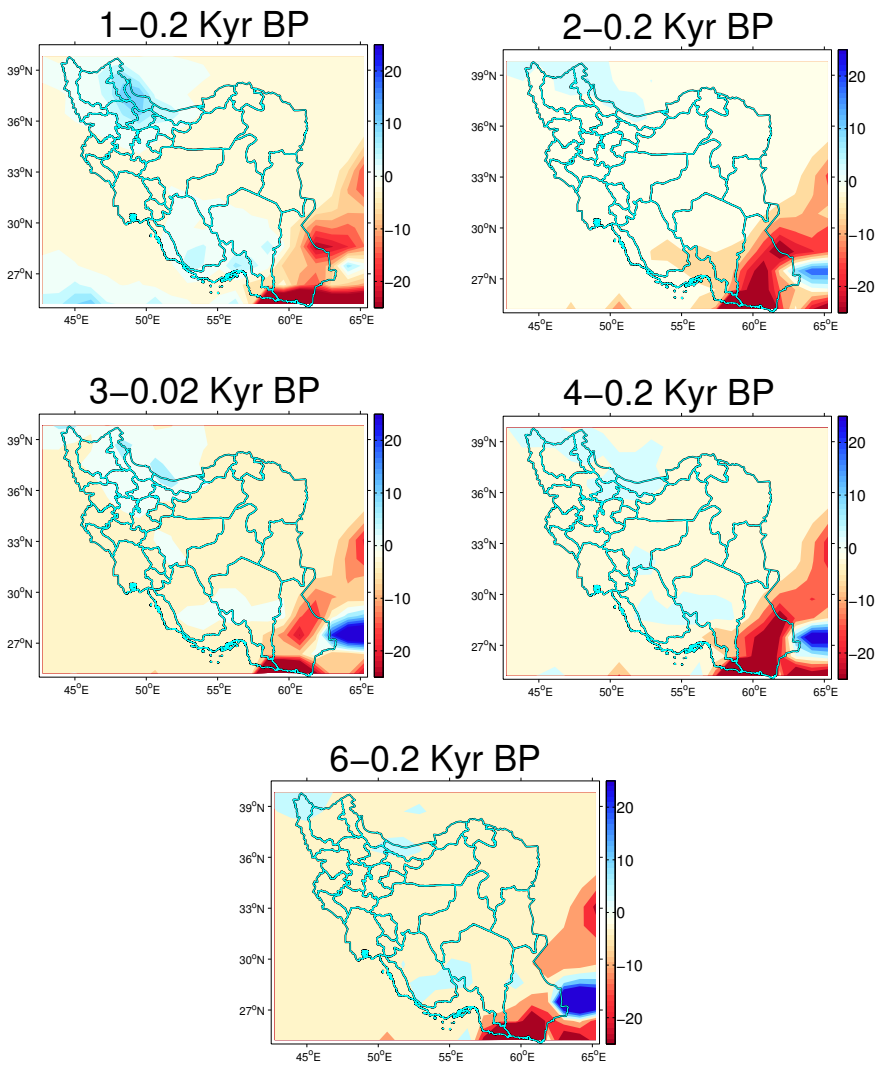

Figure 5.5: The 30-yr mean summer rainfall differences [mm/month] over Iran for 5.5(a) 1 $minus$ 0.2 Kyr BP, 5.5(b) 2 $minus$ 0.2 Kyr BP, 5.5(c) 3 $minus$ 0.2 Kyr BP, 5.5(d) 4 $minus$ 0.2 Kyr BP and 5.5(e) 6 $minus$ 0.2 Kyr BP.

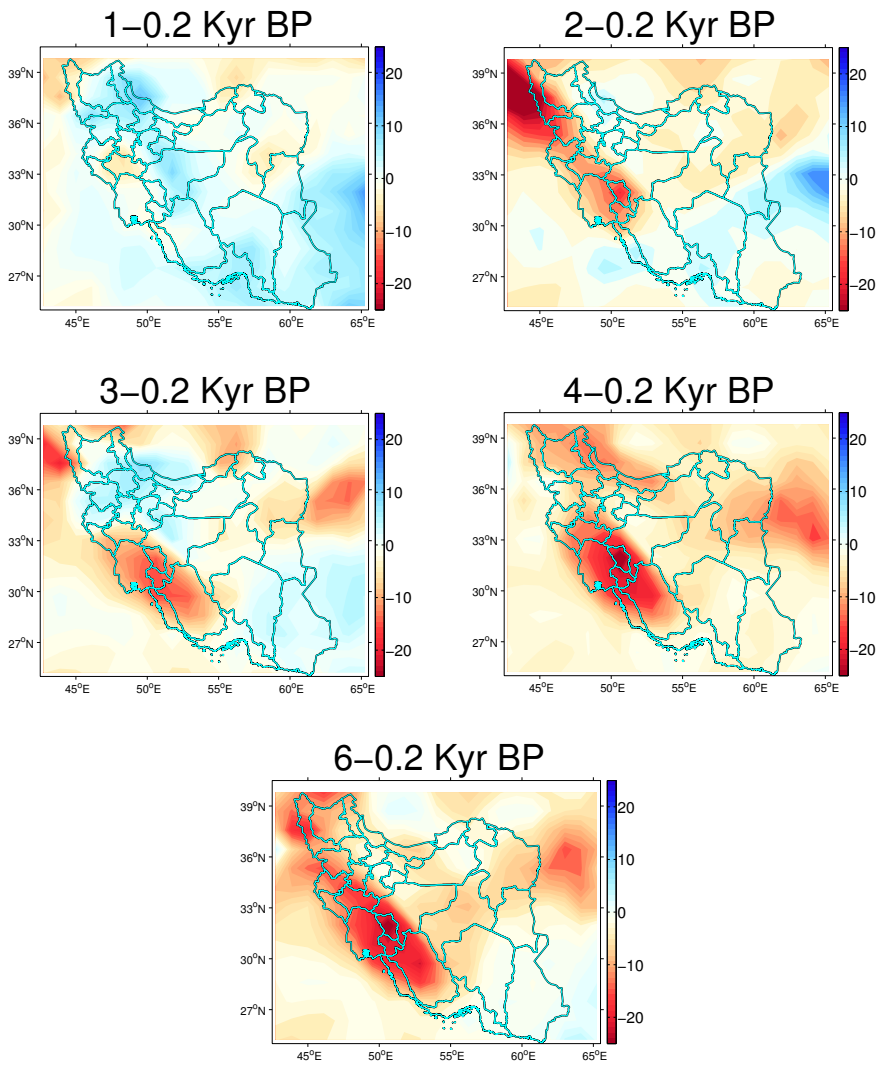

Figure 5.6: The 30-yr mean winter rainfall differences [mm/month] over Iran for 5.9(a) 1 $minus$ 0.2 Kyr BP, 5.9(b) 2 $minus$ 0.2 Kyr BP, 5.9(c) 3 $minus$ 0.2 Kyr BP, 5.9(d) 4 $minus$ 0.2 Kyr BP and 5.9(f) 6 $minus$ 0.2 Kyr BP.

5.3.4 Westerly jet stream and winter rainfall

According to Holton and Hakim [2012], the fluctuations of time-averaged jet stream from zonal symmetry are important features of general circulation in Northern Hemisphere. The maximum jet speed during the winter (located at $\sim 30^{\circ}N$) is twice as large as during the summer (located at $\sim 40-45^{\circ}N$) in the Northern Hemisphere. The largest time-mean anomalies of longitudinally averaged zonal flow are located around $30^{\circ}N$ east of North American and Asian continents and north of Arabian peninsula [Holton and Hakim, 2012]. Jets consist of strong velocity shears which are unstable to any small disturbances. The small perturbations of jet stream may lead to amplification or drawing of energy from the jet ("baroclinic instability", see. Holton and Hakim [2012]). The existence of baroclinic instability is a major factor in developing the midlatitudes synoptic-scale systems.

We apply the maximum covariance analysis [Bretherton et al., 1992] to obtain the pair of correlation pattern estimates between the rainfall and 250 hPa zonal wind and corresponding time-series. Maximum covariance analysis has been used in several studies to capture the correlated modes of variation within pairs of climate variables [Bretherton et al., 1992, Dai, 2013, Fallah and Cubasch, 2014]. Prior to maximum covariance analysis, all the time-slice simulations have been merged to a single data-set. The two leading maximum covariance analysis modes (MCA1 and MCA2) contain 90% of explained Squared Fractional Covariances (SFC). The first maximum covariance analysis mode contains 56% of SFC and the second one 34%, indicating that most of the variances are explained by these two modes.

Figure 5.7 shows that the first maximum covariance analysis mode (MCA1) of rainfall is remarkably similar to the maximum winter rainfall pattern over Iran. MCA1 of zonal wind presents a dipole pattern with a maximum core over the North Arabian peninsula and Persian Gulf and a negative maximum loading over west-north of Caspian Sea. Time expansion of these patterns show significant correlation of 0.45 ($p - value = 0.01$).

The second maximum covariance analysis mode (MCA2) presents a dipole pattern for rainfall with a negative sign over Central Zagros and a positive sign over East Turkey. The MCA2 of zonal wind shows a positive center over Northwest of Iran. Time-series of these patterns show significant correlation of 0.64 ($p - value = 0.01$).

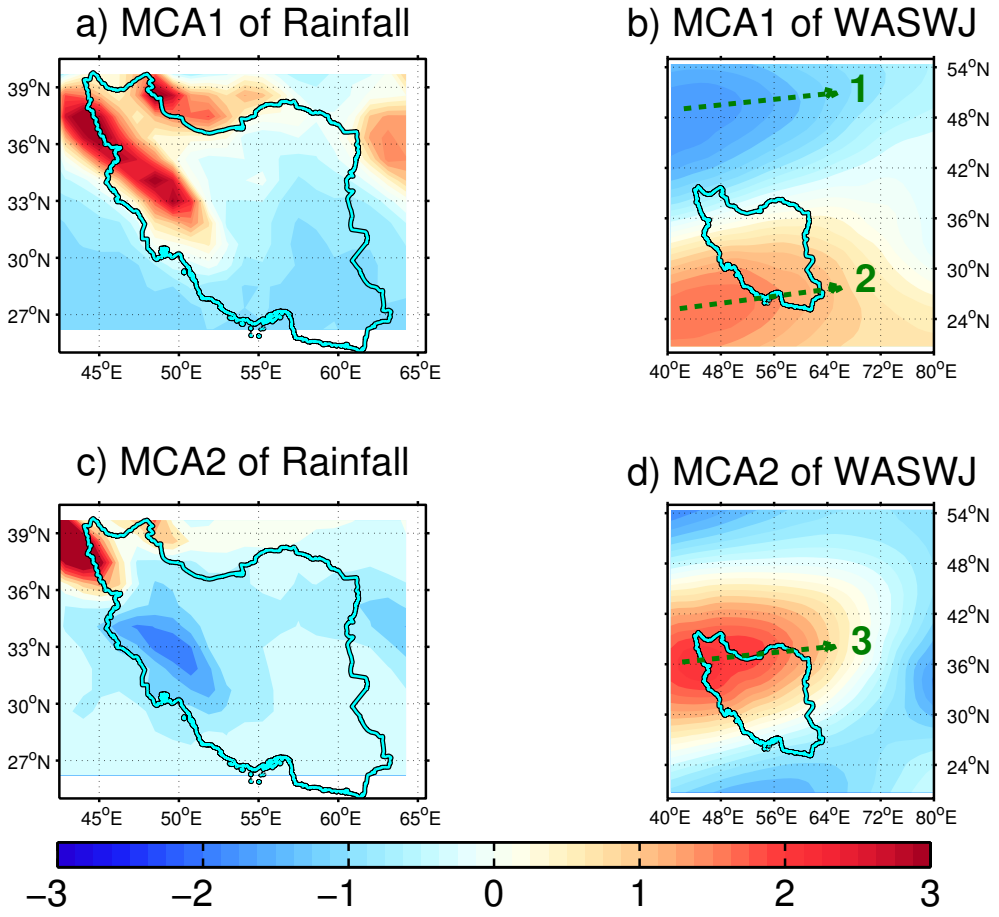

Figure 5.7: Maximum covariance analysis results for the two leading modes (SFC=56% and SFC=34%) of winter zonal wind anomaly at 250 hPa and total rainfall for all simulations: (a) the first maximum covariance analysis pattern of rainfall, (b) the first maximum covariance analysis pattern of jet, (c) the second maximum covariance analysis pattern of rainfall and (d) the second maximum covariance analysis pattern of jet. Green vectors in (b) and (d) indicate the possible positions of WASWJ.

The V-shape topography distribution over Iran with Alborz mountain range extending in North from West to East and the Zagros mountain range extending from Northwest to South Iran, will force the westerly currents to shape three different pathways (green vectors in Figures 5.7 (b) and (d)). Under different WASWJ instability conditions, the westerly current will flow in one of the three trajectories : (1) north, (2) south and (3) center.

We analyzed the regime behavior of the westerly Jet stream by investigating the

time-series of the coupled modes (MCA1 and MCA2) throughout the past 6,000 years. In order to detect the changes in mean state of the WASWJ, the Kernel [Bowman and Azzalini, 2004] Probability Density Function (PDF) of maximum covariance analysis modes of WASWJ and rainfall are shown in Figures 5.8(a)–(d). PDF estimates of MCA1 and MCA2 of WASWJ present normal distributions. However, the center of the PDF is shifted from present time to 6 Kyr BP time episodes. PDF estimates of MCA1 and MCA2 of rainfall present non-Gaussian distribution with a skewness to the negative values and a peak in positive values (Figures 5.8(c) and (d)). Figure 5.8(e) illustrates the the PDF centers (maximum probabilities) for each simulation. The linear trend of the time-series agree well with the time-series of solar insolation and rainfall index from ECHO-G model (Figure 5.4). Tables 5.1 to 5.2 show the significance of PDF's shifts between different maximum covariance analysis time-series using the chi-square test. During 3 Kyr BP, the MCA2 of WASWJ shows a negative maximum which can explain the dipole pattern in Figure (5.6) during this episode. The reduced rainfall pattern over Zagros mountains during 4 Kyr BP (Figure 5.6) can be explained with the most negative shift of MCA1 of WASWJ.

In order to clarify the regime shifts between different episodes, we show the linear composite of MCA1 and MCA2 ([MCA1's pattern $\times$ MCA1's time-series] $+$ [MCA2's pattern $\times$ MCA2's time-series]) for the WASWJ (Figure 5.9). These modes explain most of the availabilities. Therefore, we exclude the small perturbations by choosing these two leading modes. Figure 5.9.f shows that during 6 Kyr BP the WASWJ was located far in the North (at $\sim 54^{\circ}N$). The WASWJ was located over North of the domain between the Black Sea and Caspian Sea (at $\sim 45^{\circ}N$) during the 4 Kyr BP. The WASWJ shows a "tipping point" in its shift with a combination of South and Nort trajectories during the 3 Kyr BP. Since 2 Kyr BP the WASWJ was located in the central trajectory (at $\sim 35^{\circ}N$).

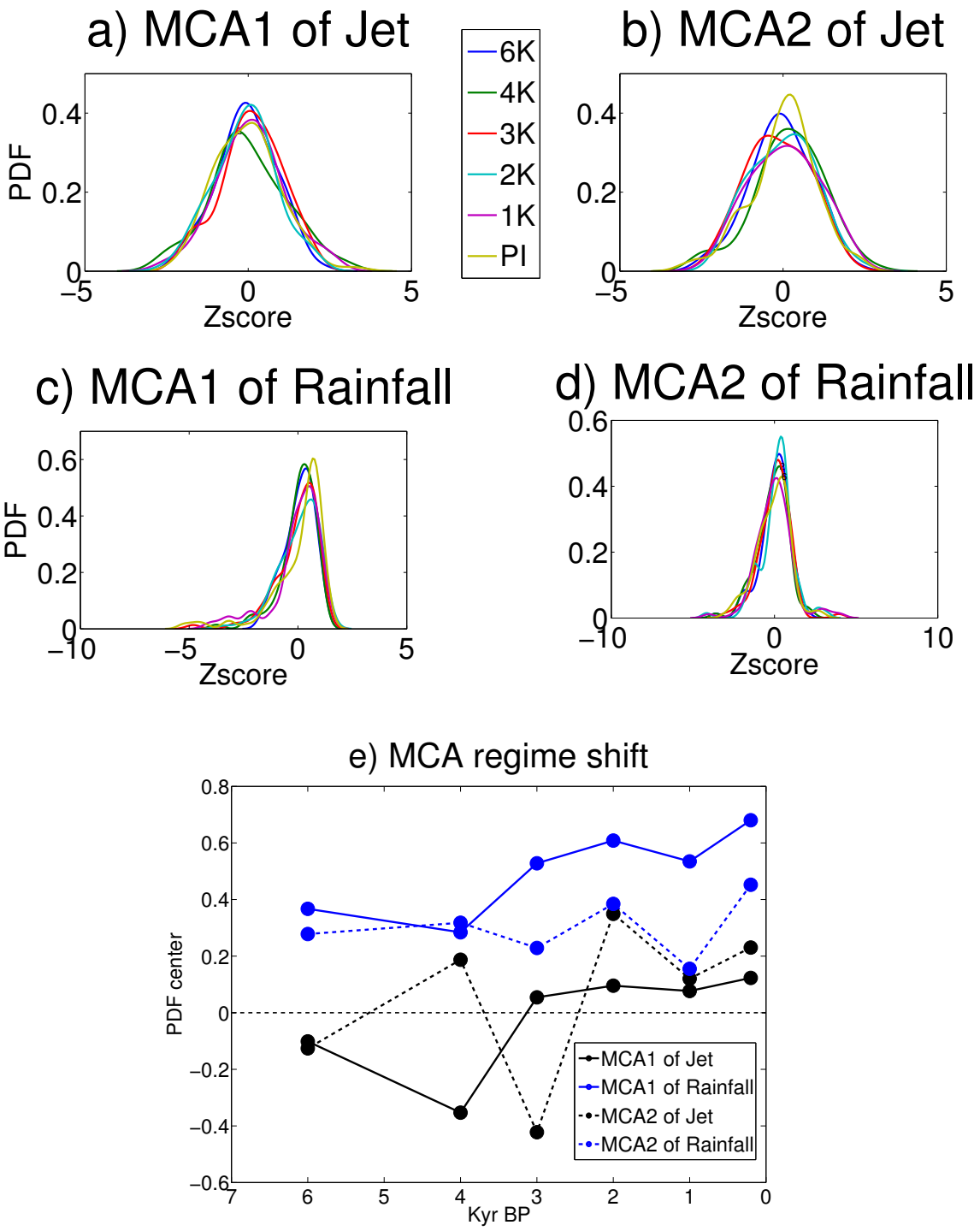

Figure 5.8: The Kernel PDF estimate of maximum covariance analysis time-series for (a) MCA1 of WASWJ, (b) MCA2 of WASWJ, (c) MCA1 of rainfall and (d) MCA2 of rainfall. (e) The maximum covariance analysis PDF's regime shifts for model simulations.

	6 Kyr BP	4 Kyr BP	3 Kyr BP	2 Kyr BP	1 Kyr BP	0.2 Kyr BP
6 Kyr BP	–	*	–	–	–	***
4 Kyr BP	–	–	**	*	**	**
3 Kyr BP	*	***	–	–	–	***
2 Kyr BP	**	***	***	–	–	***
1 Kyr BP	***	***	**	**	–	***
0.2 Kyr BP	*	–	***	***	**	–

Table 5.1: Chi-square test of PDF estimate shifts of different time-slices for MCA1 and MCA2 of WASWJ. *,** and *** indicate that the test rejects the null hypothesis at 5%, 1% and 0.1% significance level, respectively. Red stars indicated MCA1 and blue MCA2.

	6 Kyr BP	4 Kyr BP	3 Kyr BP	2 Kyr BP	1 Kyr BP	0.2 Kyr BP
6 Kyr BP	–	***	***	***	***	***
4 Kyr BP	*	–	–	**	*	**
3 Kyr BP	***	***	–	**	*	–
2 Kyr BP	***	***	***	–	***	**
1 Kyr BP	***	***	***	***	–	***
0.2 Kyr BP	***	***	***	***	***	–

Table 5.2: Chi-square test of PDF estimate shifts of different time-slices for MCA1 and MCA2 of rainfall. *,** and *** indicate that the test rejects the null hypothesis at 5%, 1% and 0.1% significance level, respectively. Red stars indicated MCA1 and blue MCA2.

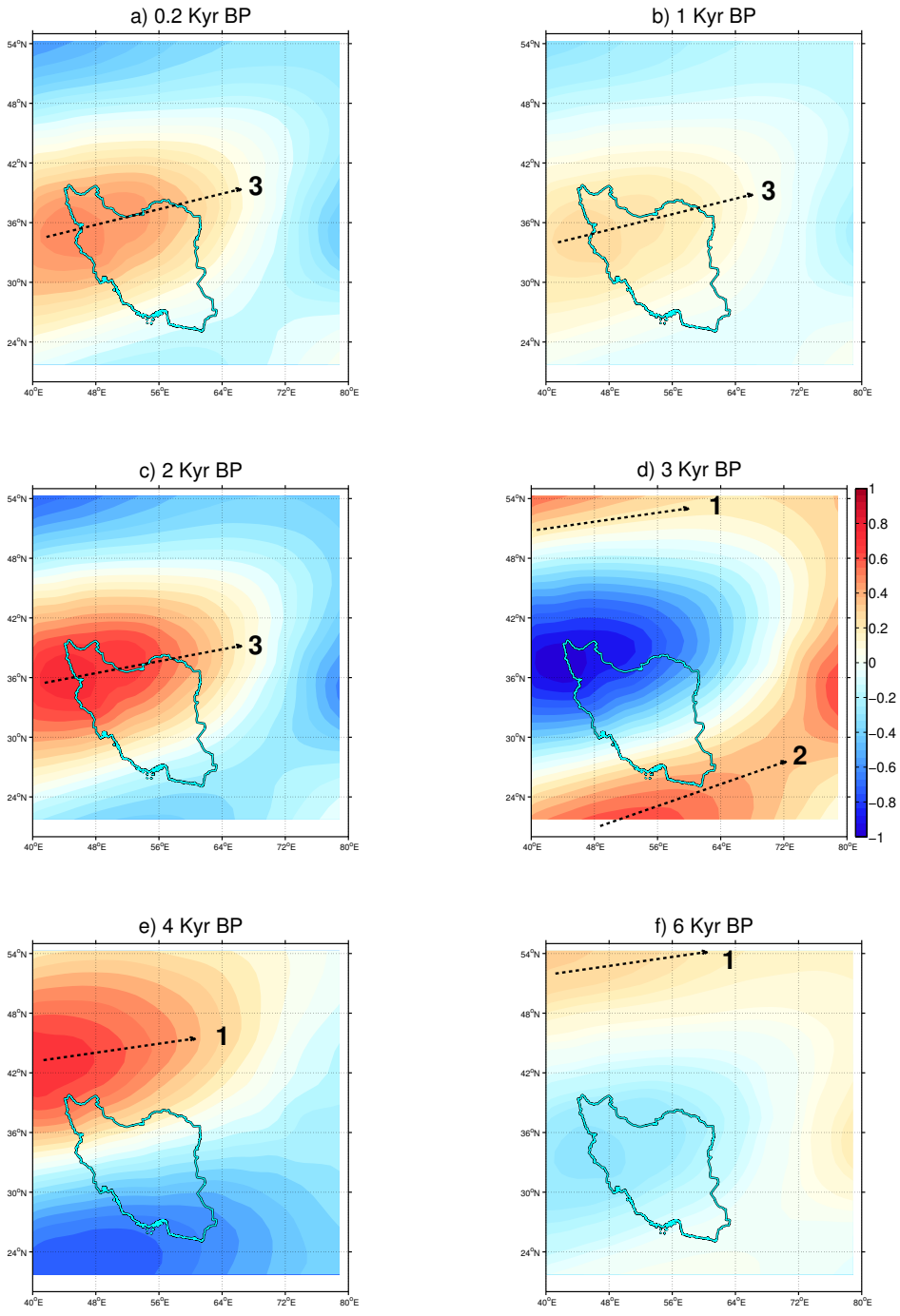

Figure 5.9: Composite of leading two maximum covariance analysis patterns of WASWJ for different time-slices (a-f). Vectors indicate the position of WASWJ shown in Figure 5.7.

Chapter 6

Conclusions and outlooks

This study presents a comprehensive investigation of the Asian climate dynamics for the period of the past millennium and present time based on different proxy data, observations and the state-of-the-art model simulations (see Appendix A). In the first step, the recently available global climate simulations and proxy reconstructions are used to study the evolution of extreme moisture events over central Asia and monsoon region. Global and regional climate simulations are further designed to investigate the mechanisms behind the climate change throughout the past millennium. The role of Tibetan Plateau on atmosphere-ocean interactions is investigated using a coupled atmosphere-ocean climate model. Finally, the paleo-hydroclimatic variability over Iran is studied during the Mid-to-Late Holocene.

6.1 Model-proxy comparisons

This section answers the main questions 1, 2 and 3 presented previously in the Introduction chapter of the thesis. The analysis of the climate during the past millennium is based on ensemble simulations of two state-of-the-art coupled atmosphere–ocean models and published proxy reconstructions of the climate (i.e. tree ring reconstructions from Cook et al. [2010a]).

EOF analysis of PDSI is applied to identify the monsoon failure periods within the model-proxy space. Then the MCA analysis of PDSI and SSTA was used to capture the

coupled spatiotemporal modes of atmosphere–ocean interactions during the past millennium. Finally, by using a statistical mixture model method on an index of convection, the regime structures in monsoon convection is investigated during the past millennium.

When the PDSI is used as metric, the two model and the proxy data sets agree in terms of timing and duration of the Asian mega-droughts. Time expansions of ENSO-like patterns agree well with Northern Hemisphere temperature anomalies based on paleoclimate data [Shi et al., 2013], both in magnitude and timing. The analysis showed that, the mega-droughts are mostly linked to El Niño-like patterns in central equatorial Pacific. The linkage between droughts and temperature may originate from PDSI, which contains information about the simulated temperature.

The IPCC Assessment Report 5 [Stocker et al., 2013] summarizes that volcanic and solar forcing have weak influence on monsoon. Adams et al. [2003] and Mann et al. [2005] concluded that the ENSO may has been influenced by solar and volcanic radiative forcing. The correlations between the time expansion of MCA1 mode for SSTA of ECHAM5/MPIOM (GISS-E2-R) model and the Northern Hemisphere temperature reconstruction from Shi et al. [2013] are 0.57 (0.51). These time expansions show distinctive negative anomalies after explosive tropical volcanic eruptions for the mid-15th century (Pinatubo eruption) and early 19th century (Tambora, Galunggung, Babuyan Claro and Cosiguina volcanic eruptions). These anomalous cooling SSTAs are consistent with the reconstructed temperature changes in the Northern Hemisphere [Shi et al., 2013]. The early 1800s was the coldest period during the past four centuries [D'Arrigo et al., 2009]. The simulations show that, the volcanic eruptions in the early 19th century triggered the oceans into as cold conditions compared to the LIA.

During the mega-droughts, there is an evidence of decreased monsoon convection over India and northern Arabian Sea and increased convection in west and central equatorial Pacific. The MCA1 patterns for SSTAs are in a well agreement with the correlation patterns of MADA and observed SSTAs for the period 1856–2004 [Cook et al., 2010a]. In agreement with England et al. [2014], it is concluded that the weakening in the Pacific Trade winds and Somali Jet explains for the decreasing of monsoon convection. Weakening of the Pacific Trade winds leads to El Niño-like patterns of SSTAs over central and eastern equatorial Pacific by decreasing the ocean upwelling in these regions ("wind-driven

circulation"). This increases the surface temperatures over central and eastern Pacific, which drives further the Asian monsoon failures.

An increase in the likelihood of very wet conditions is projected over the Indian monsoon region for the next century under the rising greenhouse gas concentration scenarios [Dai, 2013]. Further studies are necessary to investigate the ENSO-monsoon relationship under increased GHG concentrations. It has to be stressed that the methods applied in this study can only capture the linear hydro-climatic interactions of the complex Asian summer monsoon system. The nonlinear mechanisms require further investigations [Dai, 2013, Hannachi and Turner, 2013].

6.2 Regional Climate Model simulations

This section is dedicated to the main questions 3 and 4 of the Introduction chapter. This study also focuses on the dynamical drivers of the moisture changes in central Asia during the past millennium by using the ECHAM5 AGCM and COSMO-CLM RCM simulations. After evaluating the performance of models in detecting the wet and dry regimes of the observational and reanalysis data, they are applied for the climatic moisture extremes of the past millennium. The model experiments cover different possible climate behaviors throughout the past millennium which could be clustered into wet and dry spells. By comparing the dynamical behavior of westerly jet over Arid Central Asia (ACA) in the selected time-slices, the differences of internal variations of the climate system between extreme dry and wet spells are studied.

Following Lorenz's idea of predictable climate response to different forcing, the existence of *regime behavior* in the westerly jet stream data from model simulations is analyzed. The evolution of westerly jet shows a clear bimodal behavior. This regime behavior existed in both RCM and GCM simulations. The existence of the bimodality is mostly linked to the subtropical westerly jet displacement. The analysis based on regional response of the hydro-climate of ACA to the large-scale climate forcing of the past millennium, reveals that during the MCA, this region was as sensible as the recent climate to the westerly jet stream. During the MCA the dipole pattern between India and ACA was

not as pronounced as during the LIA. The sensibility of moisture changes in Kazakhstan to westerly variability was stronger during the MCA. During the LIA East China shows dry patterns as a response to large-scale climate forcing and Kazakhstan remains unaffected by the regimes of westerly jet changes.

Finally, it should be noted that the simulations are based on a single driving model and the timing in the model may be uncertain, preventing any conclusion about a specific year in the simulations. However, for longer 30-year time periods within MCA and LIA, the results depict the averaged internally produced climate variability under external natural climate forcings within these epochs. Using different driving GCMs for dynamical downscaling with RCMs will largely improve the certainty of the results. Regarding this, it is suggested that considering more realizations using ensemble of driving GCMs and nested RCMs will produce a lot of added value in the results. This will lead to a larger coverage of the sample space. However, the computational costs will extremely increase in such approaches.

6.3 Orographic forcing

This section is committed to the key question 5 of the Introduction chapter. The interplay of Tibetan Plateau, Asian summer monsoon and atmosphere-ocean teleconnections are studied using the ECHAM5/MPI-OM coupled model simulations. As a result of their coarse spatial resolution, these experiments are able to capture the large-scale climatological patterns of the monsoon but its local effects are not resolved. The large-scale patterns of Asian summer monsoon are influenced significantly by removal of Tibetan Plateau. In contrast to the studies of Boos and Kuang [2010] and Park et al. [2011], the results demonstrate that the large-scale Asian summer monsoon circulations weaken remarkably by removal of TP. Considering the β-plane barotropic theory, eastward propagating fluid columns will expand on the downslope and compress on the upslope, generating a series of alternating cyclonic and anticyclonic motions on the lee-side of the topographic barrier. The model experiment revealed that lee-side circulations are declined in the absence of TP.

Two main effects are found when removing the TP: 1. The removal of the TP produces a weaker Somali Jet that normally acts as the main driver of the "moisture conveyor belt" which brings moisture to the Indian continent. In the absence of the TP forcing, trade winds tend to decelerate over the North Pacific Ocean. As a result, the "Walker cell" attenuates in the equatorial Pacific. These changes result in a reduction of the monsoon rainfall by around 50% over India and East China. 2. The removal of the TP alters the global wave pattern, which induces an intensification of anticyclonic patterns of low-level winds in the North Atlantic Oceans. This leads to a stronger wind-driven Ekman pumping over this region, connected with a reduction of the AMOC by about 6 Sv. This leads to the decreased advection of near surface atmosphere heat into the North Atlantic Ocean and a drop of the surface temperature by about 6 K. With the North Atlantic SSTs being related to the rainfall over Asian monsoon region via teleconnections, this effect results in a precipitation drop over the Indian Peninsula and Southeast China.

These results point to possible direct and indirect mechanisms, in which the TP influences the climatic circulation and particularly the Indian summer monsoon. It is recognized that the model experiment, due to a lack of computing resources, does not have the resolution to resolve all processes in detail. The experiment could not be run to reach an equilibrium state of the oceanic circulation. The COSMOS simulations need a spin-up phase on the order of 5000 years for deep oceans [Stepanek and Lohmann, 2012]. More experiments and experiments with different models are necessary to establish additional confidence in the results. However, with currently available computing resources it is impossible to cover all these considerations.

6.4 Paleaoclimate modelling over Iran

This section is formulated to answer the questions 6 and 7 of the Introduction chapter. Climate simulations of the past 6,000 years, designed using a "time-sclice modelling" approach, are used in this study. As the result of the extremely high computational costs of these GCM simulations, it was possible to apply a deterministic single model simulation using ECHAM5 for each selected time-slice. A total number of twelve GCM simulations

throughout the past 6,000 years were designed at two different horizontal resolutions. Moving from a deterministic to a probabilistic approach using the ensemble simulations (different models, forcings or initial conditions), is still impossible at the high spatial model resolution that is applied.

By averaging the climatic features over a long enough period of time (totally 180 years covering 6 time episodes), the mean state of the past climate is investigated over Iran due to changes in the external forcings. The results reveal that the summer rainfall presents a similar pattern for all time-slices with little changes over Southeast of Iran associated with the monsoon activity. In contrast to the summer rainfall, the winter rainfall patterns show a clear shift from dry conditions during 6 Kyr BP to wetter spells during 1 Kyr BP. This suggests a probable "tipping point" of the two regimes between 3 and 4 Kyr BP coincident with the so called "4.2 Ka climate event" [Booth et al., 2005, Liu and Feng, 2012, Marchant and Hooghiemstra, 2004, Thompson et al., 2002]. Variations in solar insolation, contributes to increased energy within the Earth's climate system. Therefore, the behavior of westerly subtropical jet stream is analysed as a proxy for cyclonic activity and moisture transport during winter seasons over Iran region throughout the past 6,000 years.

Previous studies show that the early Persians, who originated from shores of Caspian Sea, settled in the Iranian plateau ca. 1,700 BC [Durant, 1954, Shoja and Tubbs, 2007], in a phase when the West Asian Subtropical Westerly Jet (WASWJ) is shifted southward and the rainfall enhanced over Iran. It can be concluded that the past winter rainfall patterns over Iran were more sensitive to the WASWJ's meridional gradients than its mean zonal flow. There is an evidence of similar WASWJ shift to PI during the 1 Kyr BP coincident with the Medieval Climate Anomaly (ca 1000 to 1350 AD, [Chen et al., 2010]). The perturbations of zonal flow show an increasing trend since 6 Kyr BP to PI episode, indicating an enhanced cyclonic activity over Iran. There is an evidence of a regime shift of the WASWJ during the 3 Kyr BP, which contributed to the dipole pattern in the rainfall anomaly with positive sign over Southwest Iran and a negative sign over Northwest Iran. It can be concluded that since Mid-Holocene to 3 Kyr BP the WASWJ was shifted to the north and after the 3 Kyr BP period, to the south. This describes the enhanced rainfall amounts over Iran via increased moisture transport and cyclonic activity

after 3 Kyr BP. Further investigations, such as model-proxy comparison, are suggested to shed light on the mystery of moisture changes over Iran during the historical dry or wet spells.

6.5 Outlooks

A set of global and regional models have been used and compared with different proxy data to determine the physical mechanisms controlling the Asian climate dynamics. Here, possible improvements are listed for the modelling approaches presented in this thesis:

– **Intercomparison of model simulations of Mid- and Late-Holocene with recently published proxy data in the CADY project:** With recently published reconstructions from other working groups within the CADY project, target time-slices are now identified that could be compared with simulated model experiments. From the experiences in the first phase of the CADY project (this thesis), useful tools are designed to investigate the physical mechanisms behind the climate regimes.

– **Ensemble Climate Simulations and historical events:** There is a potential for designing a set of new simulations with longer integration period and better resolution for the key events (*e.g.*, 4.2 ky BP event, Mongol invasion of Khwarezmia and Eastern Iran, Fall of Angkor civilization in Cambodia, etc.). The ensemble paleoclimate simulations (different models, different initial conditions) can cover a confident range of the possible climate and increase the confidence of the results.

– **Improved distribution of proxy network:** The climatically sensitive regions in Asia are identified in this study. This information can improve the future site-selection approach for the proxy data collection and sampling. There is still a lack of proxy data over several key regions in Asia (*e.g.*, westerly-dominated Iranian Plateau, monsoon region, Central India, Tibetan Plateau, etc.).

– **Proxy data assimilation in process-based deterministic models:** A novel Inverse Proxy Modelling (IPM) technique, as a model-data fusion approach, can integrate proxy records with models which can capture the physical mechanisms. This can lead to a better combination of proxy data and model simulations and improve the understanding

of driving mechanisms behind the Asian climate dynamics so as to improve the future climate predictions.

Acknowledgments

Over the past three years I have received support from a large number of individuals. My study started with the CADY project that gave me the opportunity to work at the Institute of Meteorology, Free University of Berlin. I would like to express my most sincere gratitude to Prof. Dr. Ulrich Cubasch, my supervisor and mentor who accepted me as his student and made this a thoughtful and enjoyable journey. I would like to thank Prof. Dr. Sahar Sodoudi, who encouraged me to start my study at FU Berlin. Their support over the past three years helped me to move from an idea to a completed study.

I would like to thank sincerely Dr. Kerstin Prömmel for her support, guidance and for correction of the thesis. Special thanks go to my colleagues and friends for many stimulating discussions and constructive criticism, in particular Walter Acevedo, Edoardo Mazza, Emmanuele Russo, Nico Becker, Daniel Befort and Martin Bergemann. I want to continue by thanking the members of the Climate System Modeling Working Group, in particular Dr. Ingo Kirchner, Dr. Stefan Polanski, Bo Huang, Dr. Gerd Burger, Christopher Kadow, Dr. Janina Körper, Dr. Ines Langer and Ines Höschel. Special thanks to Thomas Bergmann for his unconditional good mood and technical supports.

My warm acknowledgments to Prof. Edward R. Cook, Dr. Johann Jungclaus, Dr. Kevin J. Anchukaitis, Dr. Stefan Lauterbach, Dr. Sushma Prasad, Dr. Abdel Hannachi and Dr. Christian Blume.

I owe my sincere gratitude to many people for their support and love during my career, in particular Fariborz Fallah, Azadeh Mina, Fatemeh Zaman, Ahad Ghandchizadeh, Tayebeh Ghandchizadeh, Rahimeh Ghandchizadeh, Reza Azadian, Shima Azadian, Payam Talebitaher, Kati Mina, Pedram Talebitaher, Peyman Ladonni, Hamed Darzi, Kami Ahmadi, A. Ali Saberi, Javad Fallahi, Amir Asgari and Harold Klemp.

I would like to thank my family for the love, support and encouragement I have gotten through the best and worst years of my life.

Finally, I would like to extend my deepest gratitude to Dagmar Müller for her unconditional love, endless patience and emotional support.

This research was supported and funded by the BMBF joint research project CADY Central Asian Climate Dynamics. I thank the individual CADY/CAME teams for permanent support and fruitful discussions.

Bibliography

JB. Adams, ME Mann, and CM Ammann. Proxy evidence for an El Niño-like response to volcanic forcing. *Nature*, 426(6964):274–278, NOV 20 2003. ISSN 0028-0836. doi: 10.1038/nature02101.

RF Adler, GJ Huffman, A Chang, R Ferraro, PP Xie, J Janowiak, B Rudolf, U Schneider, S Curtis, D Bolvin, A Gruber, J Susskind, P Arkin, and E Nelkin. The version-2 global precipitation climatology project (GPCP) monthly precipitation analysis (1979-present). *Journal of Hydrology*, 4(6):1147–1167, DEC 2003. ISSN 1525-755X.

M. A. Altabet, M. J. Higginson, and D. W. Murray. The effect of millennial-scale changes in arabian sea denitrification on atmospheric Co2. *Nature*, 415(6868):159–162, January 2002. doi: 10.1038/415159a.

Caspar M. Ammann, Fortunat Joos, David S. Schimel, Bette L. Otto-Bliesner, and Robert A. Tomas. Solar influence on climate during the past millennium: Results from transient simulations with the NCAR Climate System Model. *Proceedings of the National Academy of Sciences*, 104(10):3713–3718, March 2007. URL http://www.pnas.org/content/104/10/3713.

Aavudai Anandhi and RaviS. Nanjundiah. Performance evaluation of AR4 Climate Models in simulating daily precipitation over the Indian region using skill scores. *Theoretical and Applied Climatology*, 2014. ISSN 0177-798X. URL http://dx.doi.org/10.1007/s00704-013-1043-5.

K. J. Anchukaitis, B. M. Buckley, E. R. Cook, B. I. Cook, R. D. D'Arrigo, and C. M. Ammann. Influence of volcanic eruptions on the climate of the Asian monsoon region. *Geophys. Res. Lett.*, 37(22), 2010. ISSN 1944-8007. URL http://dx.doi.org/10.1029/2010GL044843.

A. Anoop, S. Prasad, B. Plessen, N. Basavaiah, B. Gaye, R. Naumann, P. Menzel, S. Weise, and A. Brauer. Palaeoenvironmental implications of evaporative gaylussite crystals from Lonar Lake, central India. *J. Quaternary Sci.*, 28(4):349–359, 2013. ISSN 1099-1417. URL http://dx.doi.org/10.1002/jqs.2625.

H. M. Archambault, L. F. Bosart, D. Keyser, and A. R. Aiyyer. Influence of large-scale flow regimes on cool-season precipitation in the northeastern United States. *Monthly Weather Review*, 136(8):2945–2963, August 2008. doi: 10.1175/2007MWR2308.1.

S. Asharaf, A. Dobler, and B. Ahrens. Soil Moisture-Precipitation Feedback Processes in the Indian Summer Monsoon Season. *Journal of Hydrometeorology*, 13(5):1461–1474, October 2012. doi: 10.1175/JHM-D-12-06.1.

Augustin. Eight glacial cycles from an Antarctic ice core. *Nature*, 429(6992):623–628, 2004. ISSN 0028-0836. doi: http://dx.doi.org/10.1038/nature02599. 10.1038/nature02599.

P.G. Baines and T.N. Palmer. Rationale for a new physically based parameterization of subgrid scale orographic effects. Technical report, Research Department, CSIRO Division of Atmospheric Research, Aspendale, Australia, 1990.

Xinghua Bao and Fuqing Zhang. Evaluation of NCEPCFSR, NCEPNCAR, ERA-Interim, and ERA-40 Reanalysis Datasets against Independent Sounding Observations over the Tibetan Plateau. *J. Climate*, 26(1):206–214, June 2012. ISSN 0894-8755. URL http://dx.doi.org/10.1175/JCLI-D-12-00056.1.

A. G. Barnston and R. E. Livezey. Classification, Seasonality and Persistence of Low-frequency Atmospheric Circulation Patterns. *Monthly Weather Review*, 115(6):1083–1126, June 1987.

M Belkin and P Niyogi. Laplacian eigenmaps for dimensionality reduction and data representation. *Neural Computation*, 15(6):1373–1396, JUN 2003. ISSN 0899-7667. doi: 10.1162/089976603321780317.

Jason L. Bell, Lisa C. Sloan, and Mark A. Snyder. Regional Changes in Extreme Climatic Events: A Future Climate Scenario. *J. Climate*, 17(1):81–87, January 2004. ISSN 0894-8755.

James B. Benedict and Max Maisch. The little ice age, Jean M. Grove, 1988, Methuen, London and New York. *Geoarchaeology*, 4(4):363–365, 1989. ISSN 1520-6548. URL http://dx.doi.org/10.1002/gea.3340040406.

M. Berberian, C. A. Petrie, D. T. Potts, A. A. Chaverdi, A. Dusting, A. S. Zarchi, L. Week, P. Ghassemi, and R. Noruzi. Archaeoseismicity of the Mounds and Monuments Along the Kazerun Fault (western Zagros, Sw Iranian Plateau) Since the Chalcolithic Period. *Iranica Antiqua*, 49:1–81, 2014. doi: 10.2143/IA.49.0.3009238.

Manuel Berberian, Sdegh Malek Shahmirzdi, Jebra'il Nokandeh, and Morteza Djamali. Archeoseismicity and environmental crises at the Sialk Mounds, Central Iranian

Plateau, since the Early Neolithic. *Journal of Archaeological Science*, 39(9):2845–2858, September 2012. ISSN 0305-4403. URL http://www.sciencedirect.com/science/article/pii/S0305440312001197.

Jonas Berking, Janina Körper, Sebastian Wagner, Ulrich Cubasch, and Brigitta Schtt. Heavy Rainfalls in a Desert(Ed) City: A Climate-Archaeological Case Study From Sudan. In *Climates, Landscapes, and Civilizations*, pages 163–168. American Geophysical Union, 2013. URL http://dx.doi.org/10.1029/2012GM001208.

A. Bhattacharyya, J. Sharma, S. K. Shah, and V. Chaudhary. Climatic changes during the last 1800 yrs BP from Paradise Lake, Sela Pass, Arunachal Pradesh, Northeast Himalaya. *Current Science*, 93(7):983–987, October 2007.

S. Bjoerck and B. Wohlfarth. *Tracking environmental change using lake sediments. Volume 1: Basin analysis, coring, and chronological techniques.*, chapter C14 chronostratigraphic techniques in paleolimnology., pages 205–245. Kluwer, Dordrecht, 2001.

William R. Boos and Zhiming Kuang. Dominant control of the South Asian monsoon by orographic insulation versus plateau heating. *Nature*, 463(7278):218–222, January 2010. ISSN 0028-0836. URL http://dx.doi.org/10.1038/nature08707.

William R. Boos and Zhiming Kuang. Sensitivity of the South Asian monsoon to elevated and non-elevated heating. *Sci. Rep.*, 3, February 2013. URL http://dx.doi.org/10.1038/srep01192.

Robert K. Booth, Stephen T. Jackson, Steven L. Forman, John E. Kutzbach, E. A. Bettis, Joseph Kreigs, and David K. Wright. A severe centennial-scale drought in midcontinental North America 4200 years ago and apparent global linkages. *The Holocene*, 15 (3):321–328, 2005. doi: 10.1191/0959683605hl825ft.

H.P. Borgaonkar, A.B. Sikder, Somaru Ram, and G.B. Pant. El Nio and related monsoon drought signals in 523-year-long ring width records of teak (Tectona grandis L.F.) trees from south India. *Palaeogeography, Palaeoclimatology, Palaeoecology*, 285(12):74–84, January 2010. ISSN 0031-0182. URL http://www.sciencedirect.com/science/article/pii/S0031018209004714.

O. Bothe, K. Fraedrich, and X. H. Zhu. Large-scale circulations and Tibetan Plateau summer drought and wetness in a high-resolution climate model. *International Journal of Climatology*, 31(6):832–846, May 2011. doi: 10.1002/joc.2124.

Adrian W. Bowman and Adelchi Azzalini. *Applied Smoothing Techniques for Data Analysis : The Kernel Approach with S-Plus Illustrations*. Oxford University press, 2004.

J. Brad Adams, Michael E. Mann, and Caspar M. Ammann. Proxy evidence for an El Nino-like response to volcanic forcing. *Nature*, 426(6964):274–278, November 2003. ISSN 0028-0836. URL http://dx.doi.org/10.1038/nature02101.

P. Bretagnon and G. Francou. Planetary theories in rectangular and spherical variables - VSOP 87 solutions. *Astronomy and Astrophysics*, 202:309–315, 1988.

Christopher S. Bretherton, Catherine Smith, and John M. Wallace. An Intercomparison of Methods for Finding Coupled Patterns in Climate Data. *J. Climate*, 5(6):541–560, June 1992. ISSN 0894-8755. URL http://dx.doi.org/10.1175/1520-0442(1992)005<0541:AIOMFF>2.0.CO;2.

K. R. Briffa. Annual climate variability in the Holocene: interpreting the message of ancient trees. *Quaternary Science Reviews*, 19(1-5):87–105, January 2000. doi: 10.1016/S0277-3791(99)00056-6.

Brendan M. Buckley, Kritsadapan Palakit, Khwanchai Duangsathaporn, Prasong Sanguantham, and Patsi Prasomsin. Decadal scale droughts over northwestern Thailand over the past 448 years: links to the tropical Pacific and Indian Ocean sectors. *Climate Dynamics*, 29(1):63–71, JUL 2007. ISSN 0930-7575. doi: 10.1007/s00382-007-0225-1.

Brendan M. Buckley, Kevin J. Anchukaitis, Daniel Penny, Roland Fletcher, Edward R. Cook, Masaki Sano, Le Canh Nam, Aroonrut Wichienkeeo, Ton That Minh, and Truong Mai Hong. Climate as a contributing factor in the demise of Angkor, Cambodia. *Proceedings of the National Academy of Sciences*, 107:6748–6752, March 2010. URL http://www.pnas.org/content/early/2010/03/22/0910827107.

E. J. Burke and S. J. Brown. Evaluating uncertainties in the projection of future drought. *Journal of Hydrometeorology*, 9(2):292–299, April 2008. doi: 10.1175/2007JHM929.1.

Wenju Cai, Simon Borlace, Matthieu Lengaigne, Peter van Rensch, Mat Collins, Gabriel Vecchi, Axel Timmermann, Agus Santoso, Michael J. McPhaden, Lixin Wu, Matthew H. England, Guojian Wang, Eric Guilyardi, and Fei-Fei Jin. Increasing frequency of extreme El Nino events due to greenhouse warming. *Nature Clim. Change*, 4(2):111–116, February 2014. ISSN 1758-678X. URL http://dx.doi.org/10.1038/nclimate2100.

S. Ceccarelli, S. Grando, M. Maatougui, M. Michael, M. Slash, R. Haghparast, M. Rahmanian, A. Taheri, A. Al-Yassin, A. Benbelkacem, M. Labdi, H. Mimoun, and M. Nachit. Plant breeding and climate changes. *Journal of Agricultural Science*, 148:627–637, December 2010. doi: 10.1017/S0021859610000651.

A. Chakraborty, R. S. Nanjundiah, and J. Srinivasan. Role of Asian and African orography in Indian summer monsoon. *Geophys. Res. Lett.*, 29(20), 2002. ISSN 1944-8007. URL http://dx.doi.org/10.1029/2002GL015522.

M. S. Chauhan, R. K. Mazari, and G. Rajagopalan. Vegetation and climate in upper Spiti region, Himachal Pradesh during late Holocene. *Current Science*, 79(3):373–377, August 2000.

F. H. Chen, Z. C. Yu, M. L. Yang, E. Ito, S. M. Wang, D. B. Madsen, X. Z. Huang, Y. Zhao, T. Sato, H. J. B. Birks, I. Boomer, J. H. Chen, C. B. An, and B. Wunnemann. Holocene moisture evolution in arid central Asia and its out-of-phase relationship with Asian monsoon history. *Quaternary Science Reviews*, 27(3-4):351–364, February 2008. doi: 10.1016/j.quascirev.2007.10.017.

Fa-Hu Chen, Jian-Hui Chen, Jonathan Holmes, Ian Boomer, Patrick Austin, John B. Gates, Ning-Lian Wang, Stephen J. Brooks, and Jia-Wu Zhang. Moisture changes over the last millennium in arid central Asia: a review, synthesis and comparison with monsoon region. *Quaternary Science Reviews*, 29:1055–1068, April 2010. ISSN 0277-3791. URL http://www.sciencedirect.com/science/article/pii/S0277379110000077.

Feng Chen, Yu-jiang Yuan, Fa-Hu Chen, Wen-shou Wei, Shu-long Yu, Xiang-jun Chen, Zi-ang Fan, Rui-bo Zhang, Tong-wen Zhang, Hua-ming Shang, and Li Qin. A 426-year drought history for Western Tian Shan, Central Asia, inferred from tree rings and linkages to the North Atlantic and Indo–West Pacific Oceans. *The Holocene*, 23(8): 1095–1104, August 2013. URL http://hol.sagepub.com/content/23/8/1095.abstract.

Jianhui Chen, Fahu Chen, Song Feng, Wei Huang, Jianbao Liu, and Aifeng Zhou. Hydroclimatic changes in China and surroundings during the Medieval Climate Anomaly and Little Ice Age: spatial patterns and possible mechanisms. *Quaternary Science Reviews*, 107(0):98–111, January 2015. ISSN 0277-3791. URL http://www.sciencedirect.com/science/article/pii/S0277379114003990.

Wei Cheng, John C. H. Chiang, and Dongxiao Zhang. Atlantic Meridional Overturning Circulation (AMOC) in CMIP5 Models: RCP and Historical Simulations. *J. Climate*, 26 (18):7187–7197, March 2013. ISSN 0894-8755. URL http://dx.doi.org/10.1175/JCLI-D-12-00496.1.

J. C. H. Chiang, W. Cheng, and C. M. Bitz. Fast teleconnections to the tropical Atlantic sector from Atlantic thermohaline adjustment. *Geophysical Research Letters*, 35(7), April 2008. doi: 10.1029/2008GL033292.

JCH Chiang and DJ Vimont. Analogous Pacific and Atlantic meridional modes of tropical atmosphere-ocean variability. *Journal of Climate*, 17(21):4143–4158, NOV 2004. ISSN 0894-8755. doi: 10.1175/JCLI4953.1.

Peter D. Clift and R. Alan Plumb. *The Asian Monsoon: Causes, History and Effects*. Cambridge University Press, Cambridge, UK, 2008.

Sloan Coats, Jason E. Smerdon, Richard Seager, Benjamin I. Cook, and J. F. Gonzlez-Rouco. Megadroughts in Southwestern North America in ECHO-G Millennial Simulations and Their Comparison to Proxy Drought Reconstructions. *J. Climate*, 26

(19):7635–7649, May 2013. ISSN 0894-8755. URL http://dx.doi.org/10.1175/JCLI-D-12-00603.1.

Mat Collins, Soon-Il An, Wenju Cai, Alexandre Ganachaud, Eric Guilyardi, Fei-Fei Jin, Markus Jochum, Matthieu Lengaigne, Scott Power, Axel Timmermann, Gabe Vecchi, and Andrew Wittenberg. The impact of global warming on the tropical Pacific ocean and El Nino. *Nature Geosciences*, 3(6):391–397, JUN 2010. ISSN 1752-0894. doi: 10.1038/NGEO868.

E. R. Cook, P. J. Krusic, K. J. Anchukaitis, B. M. Buckley, T. Nakatsuka, and M. Sano. Tree-ring reconstructed summer temperature anomalies for temperate East Asia since 800 C.E. *Climate Dynamics*, 41(11-12):2957–2972, 2013a. ISSN 0930-7575. URL http://dx.doi.org/10.1007/s00382-012-1611-x.

Edward R. Cook, Kevin J. Anchukaitis, Brendan M. Buckley, Rosanne D. DArrigo, Gordon C. Jacoby, and William E. Wright. Asian Monsoon Failure and Megadrought During the Last Millennium. *Science*, 328(5977):486–489, April 2010a. URL http://www.sciencemag.org/content/328/5977/486.

Edward R. Cook, Richard Seager, Richard R. Heim, Russell S. Vose, Celine Herweijer, and Connie Woodhouse. Megadroughts in North America: placing IPCC projections of hydroclimatic change in a long-term palaeoclimate context. *J. Quaternary Sci.*, 25(1): 48–61, 2010b. ISSN 1099-1417. URL http://dx.doi.org/10.1002/jqs.1303.

John Cook, Dana Nuccitelli, Sarah A Green, Mark Richardson, Brbel Winkler, Rob Painting, Robert Way, Peter Jacobs, and Andrew Skuce. Quantifying the consensus on anthropogenic global warming in the scientific literature. *Environ. Res. Lett.*, 2013b.

Michael A. A. Cox and Trevor F. Cox. *Multidimensional Scaling*. Springer Handbooks Comp.Statistics. Springer Berlin Heidelberg, 2008. ISBN 978-3-540-33036-3. doi: 10.1007/978-3-540-33037-0_14. URL http://dx.doi.org/10.1007/978-3-540-33037-0_14.

T. M. Cronin, G. S. Dwyer, T. Kamiya, S. Schwede, and D. A. Willard. Medieval Warm Period, Little Ice Age and 20th century temperature variability from Chesapeake Bay. *Global and Planetary Change*, 36:17–29, March 2003. doi: 10.1016/S0921-8181(02)00161-3.

T. J. Crowley, G. Zielinski, B. Vinther, R. Udisti, K. Kreutz, J. Cole-Dai, and E. Castellano. Data-Model Comparison: Volcanism and the Little Ice Age. http://www.pages-igbp.org/products/pages-news/900-16-2-data-model-comparison, 2008a. PAGES Newsletter.

T.J. Crowley, G. Zielinski, B. Vinther, R. Udisti, K. Kreutz, J. Cole-Dai, and J. Castellano. Volcanism and the Little Ice Age, 2008b.

U. Cubasch, J. Waszkewitz, G. Hegerl, and J. Perlwitz. Regional climate changes as simulated in time-slice experiments. 31(2-4):273–304, 1995. ISSN 0165-0009. URL http://dx.doi.org/10.1007/BF01095150.

H. M. Cullen, P. B. deMenocal, S. Hemming, G. Hemming, F. H. Brown, T. Guilderson, and F. Sirocko. Climate change and the collapse of the Akkadian empire: Evidence from the deep sea. *Geology*, 28(4):379–382, April 2000. URL http://geology.gsapubs.org/content/28/4/379.

A. G. Dai. Characteristics and trends in various forms of the Palmer Drought Severity Index during 1900-2008. *Journal of Geophysical Research-atmospheres*, 116, June 2011a. doi: 10.1029/2010JD015541.

A. G. Dai. Drought under global warming: a review. *Wiley Interdisciplinary Reviews-climate Change*, 2(1):45–65, January 2011b. doi: 10.1002/wcc.81.

Aiguo Dai. Increasing drought under global warming in observations and models. *Nature Clim. Change*, 3(1):52–58, January 2013. ISSN 1758-678X. URL http://dx.doi.org/10.1038/nclimate1633.

A. Dallmeyer, M. Claussen, and J. Otto. Contribution of oceanic and vegetation feedbacks to Holocene climate change in monsoonal Asia. *Climate of the Past*, 6(2):195–218, 2010.

A. Dallmeyer, M. Claussen, Y. Wang, and U. Herzschuh. Spatial variability of Holocene changes in the annual precipitation pattern: a model-data synthesis for the Asian monsoon region. *Climate Dynamics*, 40(11-12):2919–2936, 2013. ISSN 0930-7575. URL http://dx.doi.org/10.1007/s00382-012-1550-6.

WilliamA. Dando. Asia, Climates of Siberia, Central and East Asia. In JohnE. Oliver, editor, *Encyclopedia of Earth Sciences Series*, pages 102–114. Springer Netherlands, 2005. URL http://dx.doi.org/10.1007/1-4020-3266-8_19.

R. D'Arrigo, R. Wilson, J. Palmer, P. Krusic, A. Curtis, J. Sakulich, S. Bijaksana, S. Zulaikah, L. O. Ngkoimani, and A. Tudhope. The reconstructed Indonesian warm pool sea surface temperatures from tree rings and corals: Linkages to Asian monsoon drought and El Nino-Southern Oscillation. *Paleoceanography*, 21(3), August 2006. doi: 10.1029/2005PA001256.

Rosanne D'Arrigo, Rob Wilson, and Alexander Tudhope. The impact of volcanic forcing on tropical temperatures during the past four centuries. *Nature Geosci.*, 2(1):51–56, January 2009. ISSN 1752-0894. URL http://dx.doi.org/10.1038/ngeo393.

Rosanne D'Arrigo, Rob Wilson, and Kevin J. Anchukaitis. Volcanic cooling signal in tree ring temperature records for the past millennium. *J. Geophys. Res. Atmos.*, 118

(16):9000–9010, 2013. ISSN 2169-8996. URL http://dx.doi.org/10.1002/jgrd.50692.

A. G. Dawson and G. O'Hare. Ocean-atmosphere circulation and global climate: The El Niño Southern Oscillation. *Geography*, 85:193–208, July 2000.

R. F. Denniston, L. A. Gonzalez, Y. Asmerom, R. H. Sharma, and M. K. Reagan. Speleothem evidence for changes in Indian summer monsoon precipitation over the last similar to 2300 years. *Quaternary Research*, 53(2):196–202, March 2000. doi: 10.1006/qres.1999.2111.

M. K. Dhavalikar. Toward An Ecological Model For Chalcolithic Cultures of Central and Western India. *Journal of Anthropological Archaeology*, 3(2):133–158, 1984. doi: 10.1016/0278-4165(84)90010-2.

Noah S. Diffenbaugh, Jason L. Bell, and Lisa C. Sloan. Simulated changes in extreme temperature and precipitation events at 6ka. *Palaeogeography, Palaeoclimatology, Palaeoecology*, 236(12):151–168, June 2006. ISSN 0031-0182. URL http://www.sciencedirect.com/science/article/pii/S0031018206001374.

Qinghua Ding and Bin Wang. Circumglobal Teleconnection in the Northern Hemisphere Summer. *J. Climate*, 18(17):3483–3505, September 2005. ISSN 0894-8755. URL http://dx.doi.org/10.1175/JCLI3473.1.

Yihui Ding. The variability of the Asian summer monsoon. *Journal of the Meteorological Society of Japan. Ser. II*, 85B:21–54, 2007.

Morteza Djamali, Jacques-Louis De Beaulieu, NaomiF. Miller, Valrie Andrieu-Ponel, Philippe Ponel, Razieh Lak, Nasser Sadeddin, Hossein Akhani, and Hassan Fazeli. Vegetation history of the SE section of the Zagros Mountains during the last five millennia; a pollen record from the Maharlou Lake, Fars Province, Iran. *Vegetation History and Archaeobotany*, 18(2):123–136, 2009. ISSN 0939-6314. URL http://dx.doi.org/10.1007/s00334-008-0178-2.

A. Dobler and B. Ahrens. Precipitation by a regional climate model and bias correction in Europe and South Asia. *Meteorologische Zeitschrift*, 17(4):499–509, 2008. doi: 10.1127/0941-2948/2008/0306.

W. Durant. *The story of Civilization: Book 1: Our Oriental Heritage*. New York: Simon and Schuster, 1954.

D. R. Easterling, G. A. Meehl, C. Parmesan, S. A. Changnon, T. R. Karl, and L. O. Mearns. Climate extremes: Observations, modeling, and impacts. *Science*, 289(5487): 2068–2074, September 2000. doi: 10.1126/science.289.5487.2068.

Lisa L. Ely, Yehouda Enzel, Victor R. Baker, Vishwas S. Kale, and Sheila Mishra. Changes in the magnitude and frequency of late Holocene monsoon floods on the Narmada River, central India. *Geological Society of America Bulletin*, 108(9):1134–1148, September 1996. URL http://gsabulletin.gsapubs.org/content/108/9/1134.

Julien Emile-Geay, Kimberly M. Cobb, Michael E. Mann, and Andrew T. Wittenberg. Estimating Central Equatorial Pacific SST Variability over the Past Millennium. Part II: Reconstructions and Implications. *J. Climate*, 26(7):2329–2352, December 2012. ISSN 0894-8755. URL http://dx.doi.org/10.1175/JCLI-D-11-00511.1.

Matthew H. England, Shayne McGregor, Paul Spence, Gerald A. Meehl, Axel Timmermann, Wenju Cai, Alex Sen Gupta, Michael J. McPhaden, Ariaan Purich, and Agus Santoso. Recent intensification of wind-driven circulation in the Pacific and the ongoing warming hiatus. *Nature Clim. Change*, 4(3):222–227, March 2014. ISSN 1758-678X. URL http://dx.doi.org/10.1038/nclimate2106.

Edward Ott Eugenia Kalnay, Brian Hunt and Istvan Szunyogh. *Predictability of Weather and Climate-Chapter : Ensemble forecasting and data assimilation: two problems with the same solution?* Cambridge University Press, 2006. URL http://dx.doi.org/10.1017/CBO9780511617652.008.

B. Fallah and U. Cubasch. A comparison of model simulations of Asian mega-droughts during the past millennium with proxy reconstructions. *Clim. Past Discuss.*, 10(3): 2685–2716, June 2014. ISSN 1814-9359. URL http://www.clim-past-discuss.net/10/2685/2014/.

E. M. Fischer, J. Luterbacher, E. Zorita, S. F. B. Tett, C. Casty, and H. Wanner. European climate response to tropical volcanic eruptions over the last half millennium. *Geophys. Res. Lett.*, 34(5), 2007. ISSN 1944-8007. URL http://dx.doi.org/10.1029/2006GL027992.

N. Fischer and J. H. Jungclaus. Evolution of the seasonal temperature cycle in a transient Holocene simulation: orbital forcing and sea-ice. *Clim. Past*, 7(4):1139–1148, November 2011. ISSN 1814-9332. URL http://www.clim-past.net/7/1139/2011/.

Dominik Fleitmann, Stephen J. Burns, Augusto Mangini, Manfred Mudelsee, Jan Kramers, Igor Villa, Ulrich Neff, Abdulkarim A. Al-Subbary, Annett Buettner, Dorothea Hippler, and Albert Matter. Holocene ITCZ and Indian monsoon dynamics recorded in stalagmites from Oman and Yemen (Socotra). *Quaternary Science Reviews*, 26(12):170–188, January 2007. ISSN 0277-3791. URL http://www.sciencedirect.com/science/article/pii/S0277379106002265.

H. Flohn. Contributions to a Meteorology of the Tibetan Highlands. Paper 130, National Environmental Satellite Center, ESSA, Colorado State University Fort Collins, Colorado, 1968.

J. C. Fontes, F. Gasse, and E. Gibert. Holocene environmental changes in Lake Bangong basin (western Tibet) .1. Chronology and stable isotopes of carbonates of a Holocene lacustrine core. *Palaeogeography Palaeoclimatology Palaeoecology*, 120(1-2):25–47, February 1996. doi: 10.1016/0031-0182(95)00032-1.

J.P.F. Fortuin and H. Kelder. An ozone climatology based on ozonesonde and satellite measurements. *Journal of Geophysical Research: Atmospheres*, 103:31709–31734, 1988.

David Frank, Jan Esper, Eduardo Zorita, and Rob Wilson. A noodle, hockey stick, and spaghetti plate: a perspective on high-resolution paleoclimatology. *WIREs Clim Chg*, 1(4):507–516, 2010. ISSN 1757-7799. URL http://dx.doi.org/10.1002/wcc.53.

C. Franzke, I. Horenko, A. J. Majda, and R. Klein. Systematic Metastable Atmospheric Regime Identification in an AGCM. *Journal of the Atmospheric Sciences*, 66(7):1997–2012, July 2009. doi: 10.1175/2009JAS2939.1.

Christian L. E. Franzke. Warming trends: Nonlinear climate change. *Nature Clim. Change*, 4(6):423–424, June 2014. ISSN 1758-678X. URL http://dx.doi.org/10.1038/nclimate2245.

S. Gadgil. The Indian monsoon and its variability. *Annual Review of Earth and Planetary Sciences*, 31:429–467, 2003. doi: 10.1146/annurev.earth.31.100901.141251.

Yanhong Gao, Lan Cuo, and Yongxin Zhang. Changes in Moisture Flux over the Tibetan Plateau during 19792011 and Possible Mechanisms. *J. Climate*, 27(5):1876–1893, November 2013. ISSN 0894-8755. URL http://dx.doi.org/10.1175/JCLI-D-13-00321.1.

A Giannini, R Saravanan, and P Chang. Oceanic forcing of Sahel rainfall on interannual to interdecadal time scales. *Science*, 302(5647):1027–1030, NOV 7 2003. ISSN 0036-8075. doi: 10.1126/science.1089357.

F. Giorgi and L. O. Mearns. Probability of regional climate change based on the Reliability Ensemble Averaging (REA) method. *Geophys. Res. Lett.*, 30(12), 2003. ISSN 1944-8007. URL http://dx.doi.org/10.1029/2003GL017130.

N.E. Graham, C.M. Ammann, D. Fleitmann, K.M. Cobb, and J. Luterbacher. Support for global climate reorganization during the Medieval Climate Anomaly. 37 (5-6):1217–1245, 2011. ISSN 0930-7575. URL http://dx.doi.org/10.1007/s00382-010-0914-z.

J. M. Gregory, K. W. Dixon, R. J. Stouffer, A. J. Weaver, E. Driesschaert, M. Eby, T. Fichefet, H. Hasumi, A. Hu, J. H. Jungclaus, I. V. Kamenkovich, A. Levermann, M. Montoya, S. Murakami, S. Nawrath, A. Oka, A. P. Sokolov, and R. B. Thorpe. A

model intercomparison of changes in the Atlantic thermohaline circulation in response to increasing atmospheric Co2 concentration. *Geophysical Research Letters*, 32(12), June 2005. doi: 10.1029/2005GL023209.

H. I. Griffiths, A. Schwalb, and L. R. Stevens. Environmental change in southwestern Iran: the Holocene ostracod fauna of Lake Mirabad. *Holocene*, 11(6):757–764, 2001. doi: 10.1191/09596830195771.

Richard H. Grove. The Great El Nio of 178993 and its Global Consequences: Reconstructing an Extreme Climate Event in World Environmental History. *The Medieval History Journal*, 10(1-2):75–98, 2007. doi: 10.1177/097194580701000203. URL http://mhj.sagepub.com/content/10/1-2/75.abstract.

Wei Gu, Chongyin Li, Weijing Li, Wen Zhou, and Johnny C. L. Chan. Interdecadal unstationary relationship between NAO and east China's summer precipitation patterns. *Geophys. Res. Lett.*, 36(13), July 2009. ISSN 1944-8007. URL http://dx.doi.org/10.1029/2009GL038843.

Anil K. Gupta, David M. Anderson, and Jonathan T. Overpeck. Abrupt changes in the Asian southwest monsoon during the Holocene and their links to the North Atlantic Ocean. *Nature*, 421(6921n):354–357, January 2003. ISSN 0028-0836. URL http://dx.doi.org/10.1038/nature01340.

A. Hannachi. Tropospheric planetary wave dynamics and mixture modeling: Two preferred regimes and a regime shift. *Journal of the Atmospheric Sciences*, 64(10):3521–3541, October 2007. doi: 10.1175/JAS4045.1.

A. Hannachi and A.G. Turner. Isomap nonlinear dimensionality reduction and bimodality of Asian monsoon convection. *Geophys. Res. Lett.*, 40(8):1653–1658, 2013. ISSN 1944-8007. URL http://dx.doi.org/10.1002/grl.50351.

J. Hansen, R. Ruedy, M. Sato, and K. Lo. Global Surface Temperature Change. *Reviews of Geophysics*, 48, DEC 14 2010. ISSN 8755-1209. doi: 10.1029/2010RG000345.

I. Harris, P.D. Jones, T.J. Osborn, and D.H. Lister. Updated high-resolution grids of monthly climatic observations the CRU TS3.10 Dataset. *Int. J. Climatol.*, 34(3): 623–642, 2014. ISSN 1097-0088. URL http://dx.doi.org/10.1002/joc.3711.

S Hastenrath and L Greishar. Changing predictibility of Indian monsoon rainfall anomalies. *Proceedings of The Indian Academy of Sciences–Earth and Planetary Sciences*, 102(1): 35–47, MAR 1993. ISSN 0253-4126.

G. C. Hegerl, T. J. Crowley, M. Allen, W. T. Hyde, H. N. Pollack, J. Smerdon, and E. Zorita. Detection of human influence on a new, validated 1500-year temperature reconstruction. *Journal of Climate*, 20(4):650–666, February 2007. doi: 10.1175/JCLI4011.1.

Gabriele C. Hegerl, Hans von Storch, Klaus Hasselmann, Benjamin D. Santer, Ulrich Cubasch, and Philip D. Jones. Detecting Greenhouse-Gas-Induced Climate Change with an Optimal Fingerprint Method. *J. Climate*, 9(10):2281–2306, October 1996. ISSN 0894-8755. URL http://dx.doi.org/10.1175/1520-0442(1996)009<2281:DGGICC>2.0.CO;2.

Isaac M. Held and Mingfang Ting. Orographic versus Thermal Forcing of Stationary Waves: The Importance of the Mean Low-Level Wind. *J. Atmos. Sci.*, 47(4): 495–500, February 1990. ISSN 0022-4928. URL http://dx.doi.org/10.1175/1520-0469(1990)047<0495:OVTFOS>2.0.CO;2.

RW Higgins, A Leetmaa, and VE Kousky. Relationships between climate variability and winter temperature extremes in the United States. *Journal of Climate*, 15(13):1555–1572, JUL 2002. ISSN 0894-8755.

M Hoerling, J Hurrell, and J Eischeid. Mediterranean climate change and Indian ocean warming. *Nuovo Cimento Della Societa Italiana Di Fisica C-Geophysics and Space Physics*, 29(1):99–104, JAN-FEB 2006. ISSN 1124-1896. Workshop on Historical Reconstruction of Climate Variability and Change in Mediterranean Regions, Bologna, ITALY, OCT 05-06, 2004.

M. P. Hoerling and A. Kumar. Atmospheric response patterns associated with tropical forcing. *Journal of Climate*, 15(16):2184–2203, August 2002.

D. Hofer, C. C. Raible, and T. F. Stocker. Variations of the Atlantic meridional overturning circulation in control and transient simulations of the last millennium. *Clim. Past*, 7 (1):133–150, February 2011. ISSN 1814-9332. URL http://www.clim-past.net/7/133/2011/.

James R. Holton and Gregory J. Hakim. *An Introduction to Dynamic Meteorology, 5th Edition*. Academic Press, 2012.

Brian J. Hoskins and David J. Karoly. The Steady Linear Response of a Spherical Atmosphere to Thermal and Orographic Forcing. *J. Atmos. Sci.*, 38(6):1179–1196, June 1981. ISSN 0022-4928.

Norden E. Huang, Zheng Shen, Steven R. Long, Manli C. Wu, Hsing H. Shih, Quanan Zheng, Nai-Chyuan Yen, Chi Chao Tung, and Henry H. Liu. The empirical mode decomposition and the Hilbert spectrum for nonlinear and non-stationary time series analysis. *Proceedings of the Royal Society of London. Series A: Mathematical, Physical and Engineering Sciences*, 454(1971):903–995, March 1998. URL http://rspa.royalsocietypublishing.org/content/454/1971/903.

James W. Hurrell. Decadal Trends in the North Atlantic Oscillation: Regional Temperatures and Precipitation. *Science*, 269(5224):676–679, 1995. doi: 10.1126/science.269.5224.676. URL http://www.sciencemag.org/content/269/5224/676.abstract.

IPCC. IPCC climate change: The physical science basis. Technical report, Cambridge University Press, 2007.

A. S. Issar and M. Zohar, editors. *Climate Change - Environment and Civilization in the Middle East*, volume XXII. Springer, 2004.

F. Ji, Z. H. Wu, J. P. Huang, and E. P. Chassignet. Evolution of land surface air temperature trend. *Nature Climate Change*, 4(6):462–466, June 2014. doi: 10.1038/NCLIMATE2223.

IT Jolliffe, M Uddin, and SK Vines. Simplified EOFs - three alternatives to rotation. *Climate Research*, 20(3):271–279, APR 26 2002. ISSN 0936-577X. doi: 10.3354/cr020271.

P. D. Jones, T. J. Osborn, and K. R. Briffa. The Evolution of Climate Over the Last Millennium. *Science*, 292(5517):662–667, April 2001. URL http://www.sciencemag.org/content/292/5517/662.

Gerlinde Jung, Matthias Prange, and Michael Schulz. Uplift of Africa as a potential cause for Neogene intensification of the Benguela upwelling system. *Nature Geosci*, September 2014. ISSN 1752-0908. URL http://dx.doi.org/10.1038/ngeo2249.

J. H. Jungclaus, S. J. Lorenz, C. Timmreck, C. H. Reick, V. Brovkin, K. Six, J. Segschneider, M. A. Giorgetta, T. J. Crowley, J. Pongratz, N. A. Krivova, L. E. Vieira, S. K. Solanki, D. Klocke, M. Botzet, M. Esch, V. Gayler, H. Haak, T. J. Raddatz, E. Roeckner, R. Schnur, H. Widmann, M. Claussen, B. Stevens, and J. Marotzke. Climate and carbon-cycle variability over the last millennium. *Climate of the Past*, 6(5):723–737, 2010. doi: 10.5194/cp-6-723-2010.

E. Kalnay, M. Kanamitsu, R. Kistler, W. Collins, D. Deaven, L. Gandin, M. Iredell, S. Saha, G. White, J. Woollen, Y. Zhu, A. Leetmaa, R. Reynolds, M. Chelliah, W. Ebisuzaki, W. Higgins, J. Janowiak, K. C. Mo, C. Ropelewski, J. Wang, Roy Jenne, and Dennis Joseph. The NCEP/NCAR 40-Year Reanalysis Project. *Bull. Amer. Meteor. Soc.*, 77 (3):437–471, March 1996. ISSN 0003-0007. URL http://dx.doi.org/10.1175/1520-0477(1996)077<0437:TNYRP>2.0.CO;2.

Jed O. Kaplan, Kristen M. Krumhardt, Erle C. Ellis, William F. Ruddiman, Carsten Lemmen, and Kees Klein Goldewijk. Holocene carbon emissions as a result of anthropogenic land cover change. *The Holocene*, December 2010. URL http://hol.sagepub.com/content/early/2010/12/24/0959683610386983.

R. Kar, P. S. Ranhotra, A. Bhattacharyya, and B. Sekar. Vegetation vis-a-vis climate and glacial fluctuations of the Gangotri Glacier since the last 2000 years. *Current Science*, 82(3):347–351, February 2002.

Alireza Karimi, Manfred Frechen, Hossein Khademi, Martin Kehl, and Ahmad Jalalian. Chronostratigraphy of loess deposits in northeast Iran. *Quaternary International*, 234 (12):124–132, April 2011. ISSN 1040-6182. URL http://www.sciencedirect.com/science/article/pii/S1040618209002626.

F. Kaspar and U. Cubasch. Simulation of East African precipitation patterns with the regional climate model CLM. *Meteorologische Zeitschrift*, 17(4):511–517, 2008. doi: 10.1127/0941-2948/2008/0299.

M. Kehl. Quaternary Climate Change In Iran - the State of Knowledge. *Erdkunde*, 63(1): 1–17, January 2009. doi: 10.3112/erdkunde.2009.01.01.

M. Kehl, M. Frechen, and A. Skowronek. Nature and age of Late Quaternary basin fill deposits in the basin of Persepolis/Southern Iran. *Quaternary International*, 196:57–70, March 2009. doi: 10.1016/j.quaint.2008.06.007.

Farhad Khormali, Shadi Ghergherechi, Martin Kehl, and Shamsollah Ayoubi. Soil formation in loess-derived soils along a subhumid to humid climate gradient, northeastern iran. *Geoderma*, 179180(0):113–122, June 2012. ISSN 0016-7061. URL http://www.sciencedirect.com/science/article/pii/S0016706112000705.

R. H. Kripalani, J. H. Oh, and H. S. Chaudhari. Response of the East Asian summer monsoon to doubled atmospheric CO2: Coupled climate model simulations and projections under IPCC AR4. 87(1-4):1–28, 2007a. ISSN 0177-798X. URL http://dx.doi.org/10.1007/s00704-006-0238-4.

R. H. Kripalani, J. H. Oh, A. Kulkarni, S. S. Sabade, and H. S. Chaudhari. South Asian summer monsoon precipitation variability: Coupled climate model simulations and projections under IPCC AR4. 90(3-4):133–159, 2007b. ISSN 0177-798X. URL http://dx.doi.org/10.1007/s00704-006-0282-0.

K. Krishna Kumar, Martin Hoerling, and Balaji Rajagopalan. Advancing dynamical prediction of Indian monsoon rainfall. *Geophys. Res. Lett.*, 32(8), 2005. ISSN 1944-8007. URL http://dx.doi.org/10.1029/2004GL021979.

K Krishna Kumar, B Rajagopalan, M Hoerling, G Bates, and M Cane. Unraveling the mystery of Indian monsoon failure during El Niño. *Science*, 314:115–119, OCT 6 2006. ISSN 0036-8075; 1095-9203. doi: 10.1126/science.1131152.

V. Krishnamurthy and J. Shukla. Intraseasonal and seasonally persisting patterns of Indian monsoon rainfall. *Journal of Climate*, 20(1):3–20, January 2007. doi: 10.1175/JCLI3981.1.

T. N. Krishnamurti, C. M. Kishtawal, Timothy E. LaRow, David R. Bachiochi, Zhan Zhang, C. Eric Williford, Sulochana Gadgil, and Sajani Surendran. Improved Weather

and Seasonal Climate Forecasts from Multimodel Superensemble. *Science*, 285(5433): 1548–1550, September 1999. URL http://www.sciencemag.org/content/285/5433/1548.

T. N. Krishnamurti, C. M. Kishtawal, Zhan Zhang, Timothy LaRow, David Bachiochi, Eric Williford, Sulochana Gadgil, and Sajani Surendran. Multimodel Ensemble Forecasts for Weather and Seasonal Climate. *J. Climate*, 13(23):4196–4216, December 2000. ISSN 0894-8755.

R. Krishnan, Vinay Kumar, M. Sugi, and J. Yoshimura. Internal Feedbacks from Monsoon-Midlatitude Interactions during Droughts in the Indian Summer Monsoon. *J. Atmos. Sci.*, 66(3):553–578, March 2009. ISSN 0022-4928. URL http://dx.doi.org/10.1175/2008JAS2723.1.

N. A. Krivova, L. Balmaceda, and S. K. Solanki. Reconstruction of solar total irradiance since 1700 from the surface magnetic flux. *Astronomy and Astrophysics*, 467(1):335–346, 2007. URL http://dx.doi.org/10.1051/0004-6361:20066725.

Jong-Seong Kug, Soon-Il An, Yoo-Geun Ham, and In-Sik Kang. Changes in El Niño and La Niña teleconnections over North Pacific-America in the global warming simulations. *Theoretical and applied climatology*, 100(3-4):275–282, MAY 2010. ISSN 0177-798X. doi: 10.1007/s00704-009-0183-0.

Arun Kumar, Mingyue Chen, Martin Hoerling, and Jon Eischeid. Do extreme climate events require extreme forcings? *Geophys. Res. Lett.*, 40(13):3440–3445, 2013. ISSN 1944-8007. URL http://dx.doi.org/10.1002/grl.50657.

H.H. Lamb. The early medieval warm epoch and its sequel. *Palaeogeography, Palaeoclimatology, Palaeoecology*, 1(0):13–37, 1965. ISSN 0031-0182. URL http://www.sciencedirect.com/science/article/pii/0031018265900040.

S. J. Lambert and G. J. Boer. CMIP1 evaluation and intercomparison of coupled climate models. 17(2-3):83–106, 2001. ISSN 0930-7575. URL http://dx.doi.org/10.1007/PL00013736.

Stefan Lauterbach, Roman Witt, Birgit Plessen, Peter Dulski, Sushma Prasad, Jens Mingram, Gerd Gleixner, Sabine Hettler-Riedel, Martina Stebich, Bernhard Schnetger, Antje Schwalb, and Anja Schwarz. Climatic imprint of the mid-latitude Westerlies in the Central Tian Shan of Kyrgyzstan and teleconnections to North Atlantic climate variability during the last 6000 years. *The Holocene*, June 2014. URL http://hol.sagepub.com/content/early/2014/06/04/0959683614534741.abstract.

YunGon Lee, Chang-Hoi Ho, Jhoon Kim, and Jinwon Kim. Potential impacts of northeastern Eurasian snow cover on generation of dust storms in northwestern China during

spring. 41(3-4):721–733, 2013. ISSN 0930-7575. URL http://dx.doi.org/10.1007/s00382-012-1522-x.

Rebecca Legatt, Igor V. Polyakov, Uma S. Bhatt, Xiangdong Zhang, and Roman V. Bekryaev. North Atlantic variability driven by stochastic forcing in a simple model. *2012*, 64, 2012. URL http://www.tellusa.net/index.php/tellusa/article/view/18695.

S. Legutke and R. Voss. The Hamburg atmosphere-ocean coupled model ECHO-G. Technical report, German Climate Computer Center (DKRZ)., 1999.

Alan P. Leonardi, Steven L. Morey, and James J. O'Brien. Interannual Variability in the Eastern Subtropical North Pacific Ocean. *J. Phys. Oceanogr.*, 32(6):1824–1837, June 2002. ISSN 0022-3670.

Jinbao Li, Shang-Ping Xie, Edward R. Cook, Gang Huang, Rosanne D'Arrigo, Fei Liu, Jian Ma, and Xiao-Tong Zheng. Interdecadal modulation of El Nino amplitude during the past millennium. *Nature Clim. Change*, 1(2):114–118, May 2011. ISSN 1758-678X. URL http://dx.doi.org/10.1038/nclimate1086.

Jinbao Li, Shang-Ping Xie, Edward R. Cook, Mariano S. Morales, Duncan A. Christie, Nathaniel C. Johnson, Fahu Chen, Rosanne D/'Arrigo, Anthony M. Fowler, Xiaohua Gou, and Keyan Fang. El Niño modulations over the past seven centuries. *Nature Clim. Change*, 3(9):822–826, September 2013. ISSN 1758-678X. URL http://dx.doi.org/10.1038/nclimate1936.

V. Lieberman, editor. *Southeast Asia in Global Context*. Cambridge University Press, Cambridge, 2009.

E. Lioubimtseva, R. Cole, J.M. Adams, and G. Kapustin. Impacts of climate and land-cover changes in arid lands of Central Asia. *Journal of Arid Environments*, 62(2):285–308, July 2005. ISSN 0140-1963. URL http://www.sciencedirect.com/science/article/pii/S0140196304002496.

Fenggui Liu and Zhaodong Feng. A dramatic climatic transition at 4000 cal. yr BP and its cultural responses in Chinese cultural domains. *The Holocene*, 2012. doi: 10.1177/0959683612441839. URL http://hol.sagepub.com/content/early/2012/04/12/0959683612441839.abstract.

Xingqi Liu, Hailiang Dong, Xiangdong Yang, Ulrike Herzschuh, Enlou Zhang, Jan-Berend W. Stuut, and Yongbo Wang. Late Holocene forcing of the Asian winter and summer monsoon as evidenced by proxy records from the northern QinghaiTibetan Plateau. *Earth and Planetary Science Letters*, 280(14):276–284, April 2009. ISSN 0012-821X. URL http://www.sciencedirect.com/science/article/pii/S0012821X09000752.

Y-H. Liu, G. M. Henderson, C-Y. Hu, A. J. Mason, N. Charnley, K. R. Johnson, and S-C. Xie. Links between the East Asian monsoon and North Atlantic climate during the 8,200 year event. *Nature Geosci*, 6(2):117–120, February 2013. ISSN 1752-0894. URL http://dx.doi.org/10.1038/ngeo1708.

Lennart Ljung. *System Identification: Theory for the users.* Printice-Hall, Inc., 1999.

E. N. Lorenz. How Complicated Is Circulation of Earths Atmosphere. *Annals of the New York Academy of Sciences*, 163(A1), 1969. doi: 10.1111/j.1749-6632.1969.tb13033.x.

Edward N. Lorenz. The predictability of a flow which possesses many scales of motion. *Tellus A*, 21(3), 2011. URL http://www.tellusa.net/index.php/tellusa/article/view/10086.

F. Lott and M. J. Miller. A new subgrid-scale orographic drag parametrization: Its formulation and testing. *Quarterly Journal of the Royal Meteorological Society*, 123 (537):101–127, January 1997. doi: 10.1256/smsqj.53703.

Arup Maharatna. *The demography of famines: an Indian historical perspective*. Oxford University Press, 1996.

M. E. Mann and P. D. Jones. Global surface temperatures over the past two millennia. *Geophysical Research Letters*, 30(15), August 2003. doi: 10.1029/2003GL017814.

M. E. Mann, R. S. Bradley, and M. K. Hughes. Northern hemisphere temperatures during the past millennium: Inferences, uncertainties, and limitations. *Geophysical Research Letters*, 26(6):759–762, March 1999. doi: 10.1029/1999GL900070.

M. E. Mann, Z. H. Zhang, M. K. Hughes, R. S. Bradley, S. K. Miller, S. Rutherford, and F. B. Ni. Proxy-based reconstructions of hemispheric and global surface temperature variations over the past two millennia. *Proceedings of the National Academy of Sciences of the United States of America*, 105(36):13252–13257, September 2008. doi: 10.1073/pnas.0805721105.

Michael E. Mann, Mark A. Cane, Stephen E. Zebiak, and Amy Clement. Volcanic and Solar Forcing of the Tropical Pacific over the Past 1000 Years. *J. Climate*, 18(3):447–456, February 2005. ISSN 0894-8755. URL http://dx.doi.org/10.1175/JCLI-3276.1.

Robert Marchant and Henry Hooghiemstra. Rapid environmental change in african and south american tropics around 4000 years before present: a review. *Earth-Science Reviews*, 66(34):217–260, August 2004. ISSN 0012-8252. URL http://www.sciencedirect.com/science/article/pii/S0012825204000042.

Annarita Mariotti. How ENSO impacts precipitation in southwest central Asia. *Geophys. Res. Lett.*, 34(16), 2007. ISSN 1944-8007. URL http://dx.doi.org/10.1029/2007GL030078.

G. Marland, T.A. Boden, and R.J. Andres. Global, Regional, and National Fossil Fuel CO2 Emissions. In *A Compendium of Data on Global Change*. Oak Ridge National Laboratory, U.S. Department of Energy, Oak Ridge, Tenn., U.S.A., 2008.

S. J. Marsland, H. Haak, J. H. Jungclaus, M. Latif, and F. Roske. The Max-Planck-Institute global ocean/sea ice model with orthogonal curvilinear coordinates. *Ocean Modelling*, 5(2):91–127, 2003. doi: 10.1016/S1463-5003(02)00015-X.

C. Marzin, N. Kallel, M. Kageyama, J.-C. Duplessy, and P. Braconnot. Glacial fluctuations of the Indian monsoon and their relationship with North Atlantic abrupt climate change: new data and climate experiments. *Clim. Past Discuss.*, 8(6):6269–6308, December 2012. ISSN 1814-9359. URL http://www.clim-past-discuss.net/8/6269/2012/.

Geoffrey McLachlan and David Peel. General Introduction. In *Finite Mixture Models*, pages 1–39. John Wiley & Sons, Inc., 2005. URL http://dx.doi.org/10.1002/0471721182.ch1.

J. F. McManus, R. Francois, J. M. Gherardi, L. D. Keigwin, and S. Brown-Leger. Collapse and rapid resumption of Atlantic meridional circulation linked to deglacial climate changes. *Nature*, 428(6985):834–837, April 2004. doi: 10.1038/nature02494.

M. J. McPhaden. Genesis and evolution of the 1997-98 El Niño. *Science*, 283(5404): 950–954, February 1999a. doi: 10.1126/science.283.5404.950.

MJ McPhaden. El Niño - the child prodigy of 1997-98. *Nature*, 398(6728), APR 15 1999b. ISSN 0028-0836. doi: 10.1038/19193.

G. A. Meehl, A. X. Hu, and C. Tebaldi. Decadal Prediction in the Pacific Region. *Journal of Climate*, 23(11):2959–2973, June 2010. doi: 10.1175/2010JCLI3296.1.

Gerald A. Meehl and Aixue Hu. Megadroughts in the Indian Monsoon Region and Southwest North America and a Mechanism for Associated Multidecadal Pacific Sea Surface Temperature Anomalies. *J. Climate*, 19(9):1605–1623, May 2006. ISSN 0894-8755. URL http://dx.doi.org/10.1175/JCLI3675.1.

Gerald A. Meehl, Julie M. Arblaster, Katja Matthes, Fabrizio Sassi, and Harry van Loon. Amplifying the Pacific Climate System Response to a Small 11-Year Solar Cycle Forcing. *Science*, 325(5944):1114–1118, 2009. doi: 10.1126/science.1172872. URL http://www.sciencemag.org/content/325/5944/1114.abstract.

Gerald A. Meehl, Aixue Hu, Julie M. Arblaster, John Fasullo, and Kevin E. Trenberth. Externally Forced and Internally Generated Decadal Climate Variability Associated with the Interdecadal Pacific Oscillation. *Journal of Climate*, 26(18):7298–7310, SEP 2013. ISSN 0894-8755. doi: 10.1175/JCLI-D-12-00548.1.

P. Menzel, B. Gaye, M. G. Wiesner, S. Prasad, M. Stebich, B. K. Das, A. Anoop, N. Riedel, and N. Basavaiah. Influence of bottom water anoxia on nitrogen isotopic ratios and amino acid contributions of recent sediments from small eutrophic lonar lake, central india. *Limnology and Oceanography*, 58(3):1061–1074, May 2013. doi: 10.4319/lo.2013.58.3.1061.

Ruping Mo. Efficient Algorithms for Maximum Covariance Analysis of Datasets with Many Variables and Fewer Realizations: A Revisit. *J. Atmos. Oceanic Technol.*, 20 (12):1804–1809, December 2003. ISSN 0739-0572.

A. Moberg, D. M. Sonechkin, K. Holmgren, N. M. Datsenko, and W. Karlen. Highly variable Northern Hemisphere temperatures reconstructed from low- and high-resolution proxy data. *Nature*, 433(7026):613–617, February 2005. doi: 10.1038/nature03265.

Thomas Moelg, Fabien Maussion, and Dieter Scherer. Mid-latitude westerlies as a driver of glacier variability in monsoonal High Asia. *Nature Clim. Change*, 4(1):68–73, January 2014. ISSN 1758-678X. URL http://dx.doi.org/10.1038/nclimate2055.

Raphael Neukom, Joelle Gergis, David J. Karoly, Heinz Wanner, Mark Curran, Julie Elbert, Fidel Gonzalez-Rouco, Braddock K. Linsley, Andrew D. Moy, Ignacio Mundo, Christoph C. Raible, Eric J. Steig, Tas van Ommen, Tessa Vance, Ricardo Villalba, Jens Zinke, and David Frank. Inter-hemispheric temperature variability over the past millennium. *Nature Clim. Change*, 4(5):362–367, May 2014. ISSN 1758-678X. URL http://dx.doi.org/10.1038/nclimate2174.

T. N. Palmer. Extended-Range Atmospheric Prediction and the Lorenz Model. *Bull. Amer. Meteor. Soc.*, 74(1):49–65, January 1993. ISSN 0003-0007.

T. N. Palmer. Chaos and predictability in forecasting the monsoons. *Indian National Science Acadmy*, (60):57–66, 1994.

T. N. Palmer, Brankovi, and D. S. Richardson. A probability and decision-model analysis of PROVOST seasonal multi-model ensemble integrations. *Q.J.R. Meteorol. Soc.*, 126 (567):2013–2033, 2000. ISSN 1477-870X. URL http://dx.doi.org/10.1002/qj.49712656703.

T. N. Palmer, A. Doring, and G. Seregin. The real butterfly effect. *Nonlinearity*, 27(9), September 2014. doi: 10.1088/0951-7715/27/9/R123.

W. C. Palmer. Meteorological Drought. *U.S. Weather Bureau, Washington, D.C. 20852*, 3(3):1–10, 1965.

H. S. Park and B. J. Sohn. Recent trends in changes of vegetation over East Asia coupled with temperature and rainfall variations. *Journal of Geophysical Research-atmospheres*, 115, July 2010. doi: 10.1029/2009JD012752.

Hyo-Seok Park, John C. H. Chiang, and Simona Bordoni. The Mechanical Impact of the Tibetan Plateau on the Seasonal Evolution of the South Asian Monsoon. *J. Climate*, 25(7):2394–2407, October 2011. ISSN 0894-8755. URL http://dx.doi.org/10.1175/JCLI-D-11-00281.1.

J. Paul, F. Fortuin, and Hennie Kelder. An ozone climatology based on ozonesonde and satellite measurements. *J. Geophys. Res.*, 103(D24):31709–31734, 1998. ISSN 2156-2202. URL http://dx.doi.org/10.1029/1998JD200008.

C Penland and L Matrosova. Prediction of tropical Atlantic sea surface temperatures using linear inverse modeling. *Journal of Climate*, 11(3):483–496, MAR 1998. ISSN 0894-8755. doi: 10.1175/1520-0442(1998)011⟨0483:POTASS⟩2.0.CO;2.

JoaquimG. Pinto, Mark Reyers, and Uwe Ulbrich. The variable link between PNA and NAO in observations and in multi-century CGCM simulations. *Climate Dynamics*, 36(1-2):337–354, 2011. ISSN 0930-7575. URL http://dx.doi.org/10.1007/s00382-010-0770-x.

S. Polanski, A. Rinke, and K. Dethloff. Validation of the HIRHAM-Simulated Indian Summer Monsoon Circulation. *Advances In Meteorology*, 2010. doi: 10.1155/2010/415632.

S. Polanski, B. Fallah, S. Prasad, and U. Cubasch. Simulation of the Indian monsoon and its variability during the last millennium. *Clim. Past Discuss.*, 9(1):703–740, February 2013. ISSN 1814-9359. URL http://www.clim-past-discuss.net/9/703/2013/.

Stefan Polanski, Bijan Fallah, Daniel J. Befort, Sushma Prasad, and Ulrich Cubasch. Regional moisture change over India during the past Millennium: A comparison of multi-proxy reconstructions and climate model simulations. *Global and Planetary Change*, 122 (0):176–185, November 2014. ISSN 0921-8181. URL http://www.sciencedirect.com/science/article/pii/S0921818114001817.

J. Pongratz, C. Reick, T. Raddatz, and M. Claussen. A reconstruction of global agricultural areas and land cover for the last millennium. *Global Biogeochem. Cycles*, 22(3), 2008. ISSN 1944-9224. URL http://dx.doi.org/10.1029/2007GB003153.

C. Ponton, L. Giosan, T. I. Eglinton, D. Q. Fuller, J. E. Johnson, P. Kumar, and T. S. Collett. Holocene aridification of India. *Geophysical Research Letters*, 39, February 2012. doi: 10.1029/2011GL050722.

Sushma Prasad and Yehouda Enzel. Holocene paleoclimates of india. *Quaternary Research*, 66(3):442–453, November 2006. ISSN 0033-5894. URL http://www.sciencedirect.com/science/article/pii/S0033589406000755.

Sushma Prasad, A. Anoop, N. Riedel, S. Sarkar, P. Menzel, N. Basavaiah, R. Krishnan, D. Fuller, B. Plessen, B. Gaye, U. Rhl, H. Wilkes, D. Sachse, R. Sawant, M.G. Wiesner, and M. Stebich. Prolonged monsoon droughts and links to Indo-Pacific warm pool: A Holocene record from Lonar Lake, central India. *Earth and Planetary Science Letters*, 391(0):171–182, April 2014. ISSN 0012-821X. URL http://www.sciencedirect.com/science/article/pii/S0012821X14000594.

James J. Price, Robert A. Weller, and Rebecca R. Schuldich. Wind-Driven Ocean Currents and Ekman Transport. *Science*, 238(4833):1534–1538, 1987. doi: 10.1126/science.238.4833.1534. URL http://www.sciencemag.org/content/238/4833/1534.abstract.

Kerstin Proemmel, Ulrich Cubasch, and Frank Kaspar. A regional climate model study of the impact of tectonic and orbital forcing on African precipitation and vegetation. *Palaeogeography Palaeoclimatology Palaeoecology*, 369:154–162, January 2013. doi: 10.1016/j.palaeo.2012.10.015.

T. J. Raddatz, C. H. Reick, W. Knorr, J. Kattge, E. Roeckner, R. Schnur, K. G. Schnitzler, P. Wetzel, and J. Jungclaus. Will the tropical land biosphere dominate the climate-carbon cycle feedback during the twenty-first century? *Climate Dynamics*, 29(6):565–574, November 2007. doi: 10.1007/s00382-007-0247-8.

S. Rahmstorf. Ocean circulation and climate during the past 120,000 years. *Nature*, 419 (6903):207–214, September 2002. doi: 10.1038/nature01090.

Balaji Rajagopalan and Peter Molnar. Signatures of Tibetan Plateau heating on Indian summer monsoon rainfall variability. *J. Geophys. Res. Atmos.*, 118(3):1170–1178, 2013. ISSN 2169-8996. URL http://dx.doi.org/10.1002/jgrd.50124.

V. Ramaswamy, M. D. Schwarzkopf, W. J. Randel, B. D. Santer, B. J. Soden, and G. L. Stenchikov. Anthropogenic and Natural Influences in the Evolution of Lower Stratospheric Cooling. *Science*, 311(5764):1138–1141, 2006. doi: 10.1126/science.1122587. URL http://www.sciencemag.org/content/311/5764/1138.abstract.

E. Ramezani, M. R. M. Mohadjer, H. D. Knapp, H. Ahmadi, and H. Joosten. The late-holocene vegetation history of the central caspian (hyrcanian) forests of northern iran. *Holocene*, 18(2):307–321, February 2008. doi: 10.1177/0959683607086768.

N. A. Rayner, D. E. Parker, E. B. Horton, C. K. Folland, L. V. Alexander, D. P. Rowell, E. C. Kent, and A. Kaplan. Global analyses of sea surface temperature, sea ice, and night marine air temperature since the late nineteenth century. *J. Geophys. Res.*, 108 (D14), 2003. ISSN 2156-2202. URL http://dx.doi.org/10.1029/2002JD002670.

T. Raziei, P. Daneshkar, and B. Saghfian. Annual rainfall trend in arid and semi-arid regions of iran. In *ICID 21st European Regional Conference*, Frankfurt (Oder) and Slubice - Germany and Poland, 2005. 21st European Regional Conference 2005.

Kira Rehfeld, Norbert Marwan, SebastianF.M. Breitenbach, and Jrgen Kurths. Late Holocene Asian summer monsoon dynamics from small but complex networks of paleoclimate data. 41(1):3–19, 2013. ISSN 0930-7575. URL http://dx.doi.org/10.1007/s00382-012-1448-3.

G. Rilling, P. Flandrin, P. Goncalves, and J.M. Lilly. Bivariate Empirical Mode Decomposition. *Signal Processing Letters, IEEE*, 14(12):936–939, 2007. ISSN 1070-9908.

D. Rind, R. Suozzo, N. K. Balachandran, and M. J. Prather. Climate Change and the Middle Atmosphere .1. the Doubled Co2 Climate. *Journal of the Atmospheric Sciences*, 47(4):475–494, February 1990. doi: 10.1175/1520-0469(1990)047⟨0475:CCATMA⟩2.0.CO;2.

B. Rockel, A. Will, and A. Hense. The Regional Climate Model COSMO-CLM(CCLM). *Meteorologische Zeitschrift*, 17(4):347–348, 2008. doi: 10.1127/0941-2948/2008/0309.

E. Roeckner, K. Arpe, L. Bengtsson, M. Christoph, M. Claussen, L. Dmenil, M. Esch, M. Giorgetta, U. Schlese, and U. Schulzweida. The atmospheric general circulation model ECHAM4: model description and simulation of present-day climate. Technical report, Max Planck Institut für Meteorologie., 1996.

E. Roeckner, R. Brokopf, M. Esch, M. Giorgetta, S. Hagemann, L. Kornblueh, E. Manzini, U. Schlese, and U. Schulzweida. Sensitivity of Simulated Climate to Horizontal and Vertical Resolution in the ECHAM5 Atmosphere Model. *J. Climate*, 19(16):3771–3791, August 2006. ISSN 0894-8755. URL http://dx.doi.org/10.1175/JCLI3824.1.

J. C. Rogers and M. N. Raphael. Meridional Eddy Sensible Heat Fluxes In the Extremes of the Pacific North-american Teleconnection Pattern. *Journal of Climate*, 5(2):127–139, February 1992.

C. F. Ropelewski and M. S. Halpert. Global and Regional Scale Precipitation Patterns Associated With the El-niño Southern Oscillation. *Monthly Weather Review*, 115(8):1606–1626, August 1987.

I. Ross, P. J. Valdes, and S. Wiggins. ENSO dynamics in current climate models: an investigation using nonlinear dimensionality reduction. *Nonlinear Processes in Geophysics*, 15(2):339–363, 2008. ISSN 1023-5809.

Daniel J. Rowlands, David J. Frame, Duncan Ackerley, Tolu Aina, Ben B. B. Booth, Carl Christensen, Matthew Collins, Nicholas Faull, Chris E. Forest, Benjamin S. Grandey, Edward Gryspeerdt, Eleanor J. Highwood, William J. Ingram, Sylvia Knight, Ana Lopez, Neil Massey, Frances McNamara, Nicolai Meinshausen, Claudio Piani, Suzanne M. Rosier, Benjamin M. Sanderson, Leonard A. Smith, Daithi A. Stone, Milo Thurston, Kuniko Yamazaki, Y. Hiro Yamazaki, and Myles R. Allen. Broad range of 2050 warming

from an observationally constrained large climate model ensemble. *Nature Geosci*, 5(4):256–260, April 2012. ISSN 1752-0894. URL http://dx.doi.org/10.1038/ngeo1430.

Paolo M. Ruti, Valerio Lucarini, Alessandro Dell'Aquila, Sandro Calmanti, and Antonio Speranza. Does the subtropical jet catalyze the midlatitude atmospheric regimes? *Geophys. Res. Lett.*, 33(6), 2006. ISSN 1944-8007. URL http://dx.doi.org/10.1029/2005GL024620.

Kazuyuki Saito, Tetsuzo Yasunari, and Kumiko Takata. Relative Roles of Large-Scale Orography and Land Surface Processes in the Global Hydroclimate. Part II: Impacts on Hydroclimate over Eurasia. *J. Hydrometeor*, 7(4):642–659, August 2006. ISSN 1525-755X. URL http://dx.doi.org/10.1175/JHM516.1.

Masaki Sano, Brendan M. Buckley, and Tatsuo Sweda. Tree-ring based hydroclimate reconstruction over northern Vietnam from Fokienia hodginsii: eighteenth century megadrought and tropical Pacific influence. *Climate Dynamics*, 33(2-3):331–340, AUG 2009. ISSN 0930-7575. doi: 10.1007/s00382-008-0454-y.

B. D. Santer, K. E. Taylor, T. M. L. Wigley, T. C. Johns, P. D. Jones, D. J. Karoly, J. F. B. Mitchell, A. H. Oort, J. E. Penner, V. Ramaswamy, M. D. Schwarzkopf, R. J. Stouffer, and S. Tett. A search for human influences on the thermal structure of the atmosphere. *Nature*, 382(6586):39–46, July 1996. URL http://dx.doi.org/10.1038/382039a0.

B. D. Santer, M. F. Wehner, T. M. L. Wigley, R. Sausen, G. A. Meehl, K. E. Taylor, C. Ammann, J. Arblaster, W. M. Washington, J. S. Boyle, and W. Brggemann. Contributions of Anthropogenic and Natural Forcing to Recent Tropopause Height Changes. *Science*, 301(5632):479–483, July 2003. URL http://www.sciencemag.org/content/301/5632/479.

J. Sanwal, B. S. Kotlia, C. Rajendran, S. M. Ahmad, K. Rajendran, and M. Sandiford. Climatic variability in Central Indian Himalaya during the last similar to 1800 years: Evidence from a high resolution speleothem record. *Quaternary International*, 304: 183–192, August 2013. doi: 10.1016/j.quaint.2013.03.029.

Saswati Sarkar, Heinz Wilkes, Sushma Prasad, Achim Brauer, Nils Riedel, Martina Stebich, Nathani Basavaiah, and Dirk Sachse. Spatial heterogeneity in lipid biomarker distributions in the catchment and sediments of a crater lake in central India. *Organic Geochemistry*, 66(0):125–136, January 2014. ISSN 0146-6380. URL http://www.sciencedirect.com/science/article/pii/S0146638013002532.

Tomonori Sato, Maki Tsujimura, Tsutomu Yamanaka, Hiroyuki Iwasaki, Atsuko Sugimoto, Michiaki Sugita, Fujio Kimura, Gombo Davaa, and Dambaravjaa Oyunbaatar. Water sources in semiarid northeast Asia as revealed by field observations and isotope transport

model. *J. Geophys. Res.*, 112(D17), 2007. ISSN 2156-2202. URL http://dx.doi.org/10.1029/2006JD008321.

Jrme Saulire, David James Brayshaw, Brian Hoskins, and Michael Blackburn. Further Investigation of the Impact of Idealized Continents and SST Distributions on the Northern Hemisphere Storm Tracks. *J. Atmos. Sci.*, 69(3):840–856, September 2011. ISSN 0022-4928. URL http://dx.doi.org/10.1175/JAS-D-11-0113.1.

Q. Schiermeier. Climate models fail to 'predict' US droughts. *Nature*, 496(7445):284–284, April 2013.

Armin Schmidt, Mark Quigley, Morteza Fattahi, Ghasem Azizi, Mehran Maghsoudi, and Hassan Fazeli. Holocene settlement shifts and palaeoenvironments on the central iranian plateau: Investigating linked systems. *The Holocene*, 21(4):583–595, June 2011a. URL http://hol.sagepub.com/content/21/4/583.abstract.

G. A. Schmidt, J. H. Jungclaus, C. M. Ammann, E. Bard, P. Braconnot, T. J. Crowley, G. Delaygue, F. Joos, N. A. Krivova, R. Muscheler, B. L. Otto-Bliesner, J. Pongratz, D. T. Shindell, S. K. Solanki, F. Steinhilber, and L. E. A. Vieira. Climate forcing reconstructions for use in PMIP simulations of the Last Millennium (v1.0). *Geosci. Model Dev.*, 4(1):33–45, January 2011b. ISSN 1991-9603. URL http://www.geosci-model-dev.net/4/33/2011/.

G. A. Schmidt, J. H. Jungclaus, C. M. Ammann, E. Bard, P. Braconnot, T. J. Crowley, G. Delaygue, F. Joos, N. A. Krivova, R. Muscheler, B. L. Otto-Bliesner, J. Pongratz, D. T. Shindell, S. K. Solanki, F. Steinhilber, and L. E. A. Vieira. Climate forcing reconstructions for use in PMIP simulations of the Last Millennium (v1.1). *Geosci. Model Dev.*, 5(1):185–191, January 2012. ISSN 1991-9603. URL http://www.geosci-model-dev.net/5/185/2012/.

Gavin A. Schmidt, Max Kelley, Larissa Nazarenko, Reto Ruedy, Gary L. Russell, Igor Aleinov, Mike Bauer, Susanne E. Bauer, Maharaj K. Bhat, Rainer Bleck, Vittorio Canuto, Yong-Hua Chen, Ye Cheng, Thomas L. Clune, Anthony Del Genio, Rosalinda de Fainchtein, Greg Faluvegi, James E. Hansen, Richard J. Healy, Nancy Y. Kiang, Dorothy Koch, Andy A. Lacis, Allegra N. LeGrande, Jean Lerner, Ken K. Lo, Elaine E. Matthews, Surabi Menon, Ron L. Miller, Valdar Oinas, Amidu O. Oloso, Jan P. Perlwitz, Michael J. Puma, William M. Putman, David Rind, Anastasia Romanou, Makiko Sato, Drew T. Shindell, Shan Sun, Rahman A. Syed, Nick Tausnev, Kostas Tsigaridis, Nadine Unger, Apostolos Voulgarakis, Mao-Sung Yao, and Jinlun Zhang. Configuration and assessment of the GISS ModelE2 contributions to the CMIP5 archive. *J. Adv. Model. Earth Syst.*, 6(1):141–184, 2014. ISSN 1942-2466. URL http://dx.doi.org/10.1002/2013MS000265.

Siegfried Schubert, David Gutzler, Hailan Wang, Aiguo Dai, Tom Delworth, Clara Deser, Kirsten Findell, Rong Fu, Wayne Higgins, Martin Hoerling, Ben Kirtman, Randal Koster, Arun Kumar, David Legler, Dennis Lettenmaier, Bradfield Lyon, Victor Magana, Kingtse Mo, Sumant Nigam, Philip Pegion, Adam Phillips, Roger Pulwarty, David Rind, Alfredo Ruiz-Barradas, Jae Schemm, Richard Seager, Ronald Stewart, Max Suarez, Jozef Syktus, Mingfang Ting, Chunzai Wang, Scott Weaver, and Ning Zeng. A US CLIVAR Project to assess and compare the responses of global climate models to drought-related SST forcing patterns: Overview and results. *Journal of Climate*, 22(19):5251–5272, OCT 2009. ISSN 0894-8755. doi: 10.1175/2009JCLI3060.1.

A. P. Schurer, S. F. B. Tett, and G. C. Hegerl. Small influence of solar variability on climate over the past millennium. *Nature Geoscience*, 7(2):104–108, February 2014. doi: 10.1038/NGEO2040.

R. Seager. The turn of the century North American drought: Global context, dynamics, and past analogs. *Journal of Climate*, 20(22):5527–5552, November 2007. doi: 10.1175/2007JCLI1529.1.

R Seager, Y Kushnir, C Herweijer, N Naik, and J Velez. Modeling of tropical forcing of persistent droughts and pluvials over western North America: 1856-2000. *Journal of Climate*, 18(19):4065–4088, OCT 1 2005. ISSN 0894-8755. doi: 10.1175/JCLI3522.1.

S. Sengupta and A. Sarkar. Stable isotope evidence of dual (Arabian Sea and Bay of Bengal) vapour sources in monsoonal precipitation over north India. *Earth and Planetary Science Letters*, 250(3-4):511521, October 2006. doi: 10.1016/j.epsl.2006.08.011.

Rajib Shaw and Huy Nguyen. *Droughts in Asian Monsoon Region*. Emerald Group Publishing, 2011.

J. Sheffield and E. F. Wood. Projected changes in drought occurrence under future global warming from multi-model, multi-scenario, IPCC AR4 simulations. *Climate Dynamics*, 31(1):79–105, July 2008a. doi: 10.1007/s00382-007-0340-z.

J. Sheffield and E. F. Wood. Global trends and variability in soil moisture and drought characteristics, 1950-2000, from observation-driven simulations of the terrestrial hydrologic cycle. *Journal of Climate*, 21(3):432–458, February 2008b. doi: 10.1175/2007JCLI1822.1.

Caiming Shen, Wei-Chyung Wang, Zhixin Hao, and Wei Gong. Exceptional drought events over eastern China during the last five centuries. *Climate Change*, 85(3-4):453–471, 2007. ISSN 0165-0009. URL http://dx.doi.org/10.1007/s10584-007-9283-y.

Feng Shi, Bao Yang, Aurelien Mairesse, Lucien von Gunten, Jianping Li, Achim Braeuning, Fengmei Yang, and Xia Xiao. Northern Hemisphere temperature reconstruction during

the last millennium using multiple annual proxies. *Climate Research*, 56(3):231–244, 2013. ISSN 0936-577X. doi: 10.3354/cr01156.

M. M. Shoja and R. S. Tubbs. The history of anatomy in persia. *Journal of Anatomy*, 210(4):359–378, April 2007. doi: 10.1111/j.1469-7580.2007.00711.x.

A. Sinha, M. Berkelhammer, L. Stott, M. Mudelsee, H. Cheng, and J. Biswas. The leading mode of Indian summer monsoon precipitation variability during the last millennium. *Geophysical Research Letters*, 38:L15703, August 2011a. doi: 10.1029/2011GL047713.

Ashish Sinha, Lowell Stott, Max Berkelhammer, Hai Cheng, R. Lawrence Edwards, Brendan Buckley, Mark Aldenderfer, and Manfred Mudelsee. A global context for megadroughts in monsoon asia during the past millennium. *Quaternary Science Reviews*, 30(12):47–62, January 2011b. ISSN 0277-3791. URL http://www.sciencedirect.com/science/article/pii/S0277379110003598.

Julia Slingo and Tim Palmer. Uncertainty in weather and climate prediction. *Philosophical Transactions of the Royal Society A: Mathematical, Physical and Engineering Sciences*, 369(1956):4751–4767, 2011. doi: 10.1098/rsta.2011.0161. URL http://rsta.royalsocietypublishing.org/content/369/1956/4751.abstract.

TM Smith and RW Reynolds. Extended reconstruction of global sea surface temperatures based on coads data (1854-1997). *Journal of Climate*, 16(10):1495–1510, MAY 15 2003. ISSN 0894-8755. doi: 10.1175/1520-0442-16.10.1495.

Sahar Sodoudi, Alimohammad Noorian, Manfred Geb, and Eberhard Reimer. Daily precipitation forecast of ecmwf verified over iran. *Theoretical and Applied Climatology*, 99(1-2):39–51, 2010. ISSN 0177-798X. URL http://dx.doi.org/10.1007/s00704-009-0118-9.

S. K. Solanki, I. G. Usoskin, B. Kromer, M. Schussler, and J. Beer. Unusual activity of the sun during recent decades compared to the previous 11,000 years. *Nature*, 431 (7012):1084–1087, October 2004. ISSN 0028-0836. URL http://dx.doi.org/10.1038/nature02995.

K. R. Sperber and T. N. Palmer. Interannual tropical rainfall variability in general circulation model simulations associated with the atmospheric model intercomparison project. *Journal of Climate*, 9(11):2727–2750, November 1996.

M. Srokosz, M. Baringer, H. Bryden, S. Cunningham, T. Delworth, S. Lozier, J. Marotzke, and R. Sutton. Past, Present, and Future Changes in the Atlantic Meridional Overturning Circulation. *Bull. Amer. Meteor. Soc.*, 93(11):1663–1676, March 2012. ISSN 0003-0007. URL http://dx.doi.org/10.1175/BAMS-D-11-00151.1.

M. Staubwasser, F. Sirocko, P. M. Grootes, and M. Segl. Climate change at the 4.2 ka BP termination of the Indus valley civilization and Holocene south Asian monsoon variability. *Geophys. Res. Lett.*, 30(8):1425, 2003. ISSN 1944-8007. URL http://dx.doi.org/10.1029/2002GL016822.

F. Steinhilber, J. Beer, and C. Frhlich. Total solar irradiance during the Holocene. *Geophys. Res. Lett.*, 36(19), 2009. ISSN 1944-8007. URL http://dx.doi.org/10.1029/2009GL040142.

C. Stepanek and G. Lohmann. Modelling mid-pliocene climate with COSMOS. *Geosci. Model Dev.*, 5(5):1221–1243, October 2012. ISSN 1991-9603. URL http://www.geosci-model-dev.net/5/1221/2012/.

J. Steppeler, G. Doms, U. Schattler, H. W. Bitzer, A. Gassmann, U. Damrath, and G. Gregoric. Meso-gamma scale forecasts using the nonhydrostatic model LM. *Meteorology and Atmospheric Physics*, 82(1-4):75–96, 2003. doi: 10.1007/s00703-001-0592-9.

Lora R. Stevens, Emi Ito, Antje Schwalb, and Herbert E. Wright Jr. Timing of atmospheric precipitation in the Zagros Mountains inferred from a multi-proxy record from Lake Mirabad, Iran. *Quaternary Research*, 66(3):494–500, November 2006. ISSN 0033-5894. URL http://www.sciencedirect.com/science/article/pii/S0033589406000937.

LoraR. Stevens, Morteza Djamali, Valrie Andrieu-Ponel, and Jacques-Louis de Beaulieu. Hydroclimatic variations over the last two glacial/interglacial cycles at Lake Urmia, Iran. 47(4):645–660, 2012. ISSN 0921-2728. URL http://dx.doi.org/10.1007/s10933-012-9588-3.

T.F. Stocker, D. Qin, G.-K. Plattner, M. Tignor, S.K. Allen, J. Boschung, A. Nauels, Y. Xia, V. Bex, and P.M. Midgley. IPCC, 2013: Climate Change 2013: The Physical Science Basis. Contribution of Working Group I to the Fifth Assessment Report of the Intergovernmental Panel on Climate Change. Technical report, Cambridge University Press, Cambridge, United Kingdom and New York, NY, USA, 2013.

R. J. Stouffer, J. Yin, J. M. Gregory, K. W. Dixon, M. J. Spelman, W. Hurlin, A. J. Weaver, M. Eby, G. M. Flato, H. Hasumi, A. Hu, J. H. Jungclaus, I. V. Kamenkovich, A. Levermann, M. Montoya, S. Murakami, S. Nawrath, A. Oka, W. R. Peltier, D. Y. Robitaille, A. Sokolov, G. Vettoretti, and S. L. Weber. Investigating the causes of the response of the thermohaline circulation to past and future climate changes. *Journal of Climate*, 19(8):1365–1387, April 2006. doi: 10.1175/JCLI3689.1.

G. Strandberg, E. Kjellstrm, A. Poska, S. Wagner, M.-J. Gaillard, A.-K. Trondman, A. Mauri, B. A. S. Davis, J. O. Kaplan, H. J. B. Birks, A. E. Bjune, R. Fyfe, T. Giesecke, L. Kalnina, M. Kangur, W. O. van der Knaap, U. Kokfelt, P. Kune, M. Latał owa,

L. Marquer, F. Mazier, A. B. Nielsen, B. Smith, H. Sepp, and S. Sugita. Regional climate model simulations for Europe at 6 and 0.2 k BP: sensitivity to changes in anthropogenic deforestation. *Clim. Past*, 10(2):661–680, March 2014. ISSN 1814-9332. URL http://www.clim-past.net/10/661/2014/.

C. J. Stubenrauch, W. B. Rossow, S. Kinne, S. Ackerman, G. Cesana, H. Chepfer, L. Di Girolamo, B. Getzewich, A. Guignard, A. Heidinger, B. C. Maddux, W. P. Menzel, P. Minnis, C. Pearl, S. Platnick, C. Poulsen, J. Riedi, S. Sun-Mack, A. Walther, D. Winker, S. Zeng, and G. Zhao. Assessment of global cloud datasets from satellites: Project and database initiated by the GEWEX radiation panel. *Bull. Amer. Meteor. Soc.*, 94(7):1031–1049, January 2013. ISSN 0003-0007. URL http://dx.doi.org/10.1175/BAMS-D-12-00117.1.

Jianqi Sun and Huijun Wang. Changes of the connection between the summer North Atlantic Oscillation and the East Asian summer rainfall. *J. Geophys. Res.*, 117(D8), 2012. ISSN 2156-2202. URL http://dx.doi.org/10.1029/2012JD017482.

H. S. Sundqvist, Q. Zhang, A. Moberg, K. Holmgren, H. Krnich, J. Nilsson, and G. Brattstrm. Climate change between the mid and late Holocene in northern high latitudes – Part 1: Survey of temperature and precipitation proxy data. *Clim. Past*, 6(5):591–608, September 2010. ISSN 1814-9332. URL http://www.clim-past.net/6/591/2010/.

H. Tang, A. Micheels, J. Eronen, and M. Fortelius. Regional climate model experiments to investigate the Asian monsoon in the Late Miocene. *Clim. Past*, 7(3):847–868, August 2011. ISSN 1814-9332. URL http://www.clim-past.net/7/847/2011/.

Hui Tang. *The spatio-temporal evolution of the Asian monsoon climate in the Late Miocene and its causes: A regional climate model study.* PhD thesis, Faculty of Science of the University of Helsinki, 2013.

Hui Tang, JussiT. Eronen, Arne Micheels, and Bodo Ahrens. Strong interannual variation of the Indian summer monsoon in the Late Miocene. 41(1):135–153, 2013a. ISSN 0930-7575. URL http://dx.doi.org/10.1007/s00382-012-1655-y.

Hui Tang, Arne Micheels, JussiT. Eronen, Bodo Ahrens, and Mikael Fortelius. Asynchronous responses of East Asian and Indian summer monsoons to mountain uplift shown by regional climate modelling experiments. 40(5-6):1531–1549, 2013b. ISSN 0930-7575. URL http://dx.doi.org/10.1007/s00382-012-1603-x.

D. Tanre, J. F. Geleyn, and J. M. Slingo. *Aerosols and Their Climatic Effects*, chapter First results of the introduction of an advanced aerosolradiation interaction in the ECMWF low resolution global model, pages 133–177. Deepak Publishing, 1984a.

D. Tanre, J.-F. Geleyn, and J.M. Slingo. *First results of the introduction of an advanced aerosol-radiation interaction in the ECMWF low resolution global model.*, chapter he, pages 137–177. Deepak Publishing, Hampton, VA., 1984b.

JB Tenenbaum, V de Silva, and JC Langford. A global geometric framework for nonlinear dimensionality reduction. *Science*, 290:2319–2323, DEC 22 2000. ISSN 0036-8075. doi: 10.1126/science.290.5500.2319.

Lonnie G. Thompson, Ellen Mosley-Thompson, Mary E. Davis, Keith A. Henderson, Henry H. Brecher, Victor S. Zagorodnov, Tracy A. Mashiotta, Ping-Nan Lin, Vladimir N. Mikhalenko, Douglas R. Hardy, and Jrg Beer. Kilimanjaro ice core records: Evidence of holocene climate change in tropical africa. *Science*, 298(5593):589–593, 2002. doi: 10.1126/science.1073198. URL http://www.sciencemag.org/content/298/5593/589.abstract.

R. S. Thompson and K. H. Anderson. Biomes of western North America at 18,000, 6000 and 0 c-14 yr BP reconstructed from pollen and packrat midden data. *Journal of Biogeography*, 27(3):555–584, May 2000. doi: 10.1046/j.1365-2699.2000.00427.x.

Jessica E. Tierney and Peter B. deMenocal. Abrupt shifts in Horn of Africa Hydroclimate Since the Last Glacial Maximum. *Science*, 342(6160):843–846, November 2013. URL http://www.sciencemag.org/content/342/6160/843.

A Timmermann, M Latif, A Grotzner, and R Voss. Modes of climate variability as simulated by a coupled general circulation model. Part I: ENSO-like climate variability and its low-frequency modulation. *Climate Dynamics*, 15(8):605–618, AUG 1999. ISSN 0930-7575. doi: 10.1007/s003820050304.

Matthias Tomczak and J. Stuart Godfrey. *Regional Oceanography: an Introduction*. Daya Publishing House, 2004.

KE Trenberth and DP Stepaniak. Indices of El Niño evolution. *Journal of Climate*, 14(8):1697–1701, 2001. ISSN 0894-8755. doi: 10.1175/1520-0442(2001)014⟨1697:LIOENO⟩2.0.CO;2.

Kevin E. Trenberth and John T. Fasullo. An apparent hiatus in global warming? *Earth's Future*, 1(1):19–32, 2013. ISSN 2328-4277. URL http://dx.doi.org/10.1002/2013EF000165.

A. G. Turner and A. Hannachi. Is there regime behavior in monsoon convection in the late 20th century? *Geophysical Research Letters*, 37, August 2010. doi: 10.1029/2010GL044159.

CarolineC. Ummenhofer, RosanneD. DArrigo, KevinJ. Anchukaitis, BrendanM. Buckley, and EdwardR. Cook. Links between Indo-pacific climate variability and drought in

the Monsoon Asia Drought Atlas. 40(5-6):1319–1334, 2013. ISSN 0930-7575. URL http://dx.doi.org/10.1007/s00382-012-1458-1.

S. M. Uppala, P. W. Kaellberg, A. J. Simmons, U. Andrae, V. Da Costa Bechtold, M. Fiorino, J. K. Gibson, J. Haseler, A. Hernandez, G. A. Kelly, X. Li, K. Onogi, S. Saarinen, N. Sokka, R. P. Allan, E. Andersson, K. Arpe, M. A. Balmaseda, A. C. M. Beljaars, L. Van De Berg, J. Bidlot, N. Bormann, S. Caires, F. Chevallier, A. Dethof, M. Dragosavac, M. Fisher, M. Fuentes, S. Hagemann, E. Hlm, B. J. Hoskins, L. Isaksen, P. A. E. M. Janssen, R. Jenne, A. P. Mcnally, J.-F. Mahfouf, J.-J. Morcrette, N. A. Rayner, R. W. Saunders, P. Simon, A. Sterl, K. E. Trenberth, A. Untch, D. Vasiljevic, P. Viterbo, and J. Woollen. The ERA-40 re-analysis. *Q.J.R. Meteorol. Soc.*, 131(612): 2961–3012, 2005. ISSN 1477-870X. URL http://dx.doi.org/10.1256/qj.04.176.

M. Vellinga and R. A. Wood. Global climatic impacts of a collapse of the Atlantic thermohaline circulation. *Climatic Change*, 54(3):251–267, August 2002. doi: 10.1023/A:1016168827653.

Sergio M. Vicente-Serrano, Santiago Begueraa, and Juan I. Lopez-Moreno. Comment on characteristics and trends in various forms of the palmer drought severity index (pdsi) during 1900–2008 by Aiguo Dai. *J. Geophys. Res.*, 116(D19), 2011. ISSN 2156-2202. URL http://dx.doi.org/10.1029/2011JD016410.

L. E. A. Vieira and S. K. Solanki. Evolution of the solar magnetic flux on time scales of years tomillenia. *A&A*, 509, January 2010. URL http://dx.doi.org/10.1051/0004-6361/200913276.

Sebastian Wagner, Martin Widmann, Julie Jones, Torsten Haberzettl, Andreas Lcke, Christoph Mayr, Christian Ohlendorf, Frank Schbitz, and Bernd Zolitschka. Transient simulations, empirical reconstructions and forcing mechanisms for the Mid-holocene hydrological climate in southern Patagonia. 29(4):333–355–, 2007. ISSN 0930-7575. URL http://dx.doi.org/10.1007/s00382-007-0229-x.

E. R. Wahl and C. Morrill. Climate Change Toward Understanding and Predicting Monsoon Patterns. *Science*, 328(5977):437–438, April 2010. doi: 10.1126/science.1188926.

J. M. Wallace and D. S. Gutzler. Teleconnections In the Geopotential Height Field During the Northern Hemisphere Winter. *Monthly Weather Review*, 109(4):784–812, 1981.

John M. Wallace, Catherine Smith, and Christopher S. Bretherton. Singular Value Decomposition of Wintertime Sea Surface Temperature and 500-mb Height Anomalies. *J. Climate*, 5(6):561–576, June 1992. ISSN 0894-8755.

R.P.D. Walsh, R. Glaser, and S. Militzer. The climate of Madras during the eighteenth century. *Int. J. Climatol.*, 19(9):1025–1047, 1999. ISSN 1097-0088.

B. Wang. *The Asian Monsoon*. Springer/Praxis Publishing Co, Berlin, 2006.

Bin Wang, Renguang Wu, and K-M. Lau. Interannual Variability of the Asian Summer Monsoon: Contrasts between the Indian and the Western North PacificEast Asian Monsoons. *J. Climate*, 14(20):4073–4090, October 2001a. ISSN 0894-8755.

D. Wang, C. Menz, T. Simon, C. Simmer, and C. Ohlwein. Regional dynamical downscaling with CCLM over East Asia. *Meteorology and Atmospheric Physics*, 121(1-2): 39–53, July 2013. doi: 10.1007/s00703-013-0250-z.

Guiling Wang. Agricultural drought in a future climate: results from 15 global climate models participating in the IPCC 4th assessment. 25(7-8):739–753, 2005. ISSN 0930-7575. URL http://dx.doi.org/10.1007/s00382-005-0057-9.

P. X. Wang, S. Clemens, L. Beaufort, P. Braconnot, G. Ganssen, Z. M. Jian, P. Kershaw, and M. Sarnthein. Evolution and variability of the Asian monsoon system: state of the art and outstanding issues. *Quaternary Science Reviews*, 24(5-6):595–629, March 2005a. doi: 10.1016/j.quascirev.2004.10.002.

Y. J. Wang, H. Cheng, R. L. Edwards, Z. S. An, J. Y. Wu, C. C. Shen, and J. A. Dorale. A high-resolution absolute-dated Late Pleistocene monsoon record from Hulu Cave, China. *Science*, 294(5550):2345–2348, December 2001b. doi: 10.1126/science.1064618.

Yongbo Wang, Xingqi Liu, and Ulrike Herzschuh. Asynchronous evolution of the Indian and East Asian Summer Monsoon indicated by Holocene moisture patterns in monsoonal central Asia. *Earth-Science Reviews*, 103(34):135–153, December 2010. ISSN 0012-8252. URL http://www.sciencedirect.com/science/article/pii/S0012825210001169.

Yongjin Wang, Hai Cheng, R. Lawrence Edwards, Yaoqi He, Xinggong Kong, Zhisheng An, Jiangying Wu, Megan J. Kelly, Carolyn A. Dykoski, and Xiangdong Li. The Holocene Asian Monsoon: Links to Solar Changes and North Atlantic Climate. *Science*, 308(5723):854–857, May 2005b. URL http://www.sciencemag.org/content/308/5723/854.

K. Wasylikowa. Palaeoecology of lake zeribar, iran, in the pleniglacial, lateglacial and holocene, reconstructed from plant macrofossils. *Holocene*, 15(5):720–735, July 2005. doi: 10.1191/0959683605hl846rp.

R. S. Webb, C. E. Rosenzweig, and E. R. Levine. Specifying Land Surface Characteristics In General-circulation Models - Soil-profile Data Set and Derived Water-holding Capacities. *Global Biogeochemical Cycles*, 7(1):97–108, March 1993. doi: 10.1029/92GB01822.

P. J. Webster, V. O. Magaa, T. N. Palmer, J. Shukla, R. A. Tomas, M. Yanai, and T. Yasunari. Monsoons: Processes, predictability, and the prospects for prediction. *J.*

Geophys. Res., 103(C7):14451–14510, 1998. ISSN 2156-2202. URL http://dx.doi.org/10.1029/97JC02719.

N. Wells, S. Goddard, and M. J. Hayes. A self-calibrating Palmer Drought Severity Index. *Journal of Climate*, 17(12):2335–2351, June 2004. doi: 10.1175/1520-0442(2004)017⟨2335:ASPDSI⟩2.0.CO;2.

Patrick Wetzel, Ernst Maier-Reimer, Michael Botzet, Johann Jungclaus, Noel Keenlyside, and Mojib Latif. Effects of Ocean Biology on the Penetrative Radiation in a Coupled Climate Model. *J. Climate*, 19(16):3973–3987, August 2006. ISSN 0894-8755. URL http://dx.doi.org/10.1175/JCLI3828.1.

Katharine M. Willett, Nathan P. Gillett, Philip D. Jones, and Peter W. Thorne. Attribution of observed surface humidity changes to human influence. *Nature*, 449(7163):710–712, October 2007. ISSN 0028-0836. URL http://dx.doi.org/10.1038/nature06207.

Rob Wilson, Edward Cook, Rosanne D'Arrigo, Nadja Riedwyl, Michael N. Evans, Alexander Tudhope, and Rob Allan. Reconstructing ENSO: the influence of method, proxy data, climate forcing and teleconnections. *J. Quaternary Sci.*, 25(1):62–78, 2010. ISSN 1099-1417. URL http://dx.doi.org/10.1002/jqs.1297.

J. Wolff, E. Maier-Reimer, and S. Legutke. The hamburg primitive equation model hope. Technical report, German Climate Computer Center (DKRZ), 1997.

Maier-Reimer E. Legutke S. Wolff, J. The Hamburg Primitive Equation Model HOPE. Technical report, German Climate Computer Center (DKRZ), 1997.

T. Woollings, J. M. Gregory, J. G. Pinto, M. Reyers, and D. J. Brayshaw. Response of the North Atlantic storm track to climate change shaped by ocean-atmosphere coupling. *Nature Geosci*, 5(5):313–317, May 2012. ISSN 1752-0894. URL http://dx.doi.org/10.1038/ngeo1438.

Guoxiong Wu, Yimin Liu, Qiong Zhang, Anmin Duan, Tongmei Wang, Rijin Wan, Xin Liu, Weiping Li, Zaizhi Wang, and Xiaoyun Liang. The Influence of Mechanical and Thermal Forcing by the Tibetan Plateau on Asian Climate. *J. Hydrometeor*, 8(4):770–789, August 2007. ISSN 1525-755X. URL http://dx.doi.org/10.1175/JHM609.1.

Guoxiong Wu, Yimin Liu, Bian He, Qing Bao, Anmin Duan, and Fei-Fei Jin. Thermal Controls on the Asian Summer Monsoon. *Sci. Rep.*, 2, May 2012. URL http://dx.doi.org/10.1038/srep00404.

Dong Xiao, Ping Zhao, Yue Wang, Qinhua Tian, and Xiuji Zhou. Millennial-scale phase relationship between North Atlantic deep-level temperature and Qinghai-Tibet Plateau temperature and its evolution since the Last Interglaciation. *Chinese Science Bulletin*, 59(1):75–81, 2014. doi: 10.1007/s11434-013-0028-1. URL http://csb.scichina.com:8080/kxtbe.

Gao Ya, Wang Huijun, and Li Shuanglin. Influences of the Atlantic Ocean on the summer precipitation of the southeastern Tibetan Plateau. *J. Geophys. Res. Atmos.*, 118 (9):3534–3544, 2013. ISSN 2169-8996. URL http://dx.doi.org/10.1002/jgrd.50290.

Bao Yang, Achim Braeuning, Kathleen R. Johnson, and Shi Yafeng. General characteristics of temperature variation in China during the last two millennia. *Geophys. Res. Lett.*, 29(9):38–1–38–4, 2002. ISSN 1944-8007. URL http://dx.doi.org/10.1029/2001GL014485.

M. Yanni and G.-X. Wu. *Effects of the Tibetan Plateau, in The Asian Monsoon*. Springer, 2006.

T. Yasunari, K. Saito, and K. Takata. Relative roles of large-scale orography and land surface processes in the global hydroclimate. Part I: Impacts on monsoon systems and the tropics. *Journal of Hydrometeorology*, 7(4):626–641, August 2006. doi: 10.1175/JHM515.1.

Sang-Wook Yeh, Jong-Seong Kug, Boris Dewitte, Min-Ho Kwon, Ben P. Kirtman, and Fei-Fei Jin. El Niño in a changing climate. *Nature*, 461(7263), SEP 24 2009. ISSN 0028-0836. doi: 10.1038/nature08316.

D. X. Yuan, H. Cheng, R. L. Edwards, C. A. Dykoski, M. J. Kelly, M. L. Zhang, J. M. Qing, Y. S. Lin, Y. J. Wang, J. Y. Wu, J. A. Dorale, Z. S. An, and Y. J. Cai. Timing, duration, and transitions of the Last Interglacial Asian Monsoon. *Science*, 304(5670): 575–578, April 2004. doi: 10.1126/science.1091220.

P. Z. Zhang, H. Cheng, R. L. Edwards, F. H. Chen, Y. J. Wang, X. L. Yang, J. Liu, M. Tan, X. F. Wang, J. H. Liu, C. L. An, Z. B. Dai, J. Zhou, D. Z. Zhang, J. H. Jia, L. Y. Jin, and K. R. Johnson. A Test of Climate, Sun, and Culture Relationships from an 1810-Year Chinese Cave Record. *Science*, 322(5903):940–942, November 2008. doi: 10.1126/science.1163965.

Q. Zhang, H. S. Sundqvist, A. Moberg, H. Krnich, J. Nilsson, and K. Holmgren. Climate change between the mid and late holocene in northern high latitudes; part 2: Model-data comparisons. *Clim. Past*, 6(5):609–626, September 2010. ISSN 1814-9332. URL http://www.clim-past.net/6/609/2010/.

Rong Zhang and Thomas L. Delworth. Impact of Atlantic multidecadal oscillations on India/Sahel rainfall and Atlantic hurricanes. *Geophys. Res. Lett.*, 33(17), 2006. ISSN 1944-8007. URL http://dx.doi.org/10.1029/2006GL026267.

Y Zhang, JM Wallace, and DS Battisti. ENSO-like interdecadal variability: 1900-93. *Journal of Climate*, 10(5):1004–1020, MAY 1997. ISSN 0894-8755. doi: 10.1175/1520-0442(1997)010⟨1004:ELIV⟩2.0.CO;2.

Yong Zhao, MinZhong Wang, AnNing Huang, HongJun Li, Wen Huo, and Qing Yang. Relationships between the West Asian subtropical westerly jet and summer precipitation in northern Xinjiang. 116(3-4):403–411, 2014. ISSN 0177-798X. URL http://dx.doi.org/10.1007/s00704-013-0948-3.

E. Zorita, J. F. Gonzlez-Rouco, H. von Storch, J. P. Montvez, and F. Valero. Natural and anthropogenic modes of surface temperature variations in the last thousand years. *Geophys. Res. Lett.*, 32(8), 2005. ISSN 1944-8007. URL http://dx.doi.org/10.1029/2004GL021563.

Appendix A

Citations to Previously Published Work

Large portion of Chapter 1 and 2 have been published as the following papers:

> **Bijan Fallah** and Ulrich Cubasch, "A comparison of model simulations of Asian mega-droughts during the past millennium with proxy reconstructions.", Clim. Past Discuss., Copernicus Publications, http://www.clim-past.net/11/253/2015/cp-11-253-2015.html, 2014, 10, 2685-2716.

> Polanski, S.; **Fallah, B.**; Befort, D. J.; Prasad, S. and Cubasch, U.: "Regional moisture change over India during the past Millennium: A comparison of multi-proxy reconstructions and climate model simulations", Global and Planetary Change,http://dx.doi.org/10.1016/j.gloplacha.2014.08.016 , 2014, 122, 176-185.

The whole chapter 3 is published as the following paper:

> **Bijan Fallah**, Sahar Sodoudi and Ulrich Cubasch, " Westerly jet stream and past millennium climate change in Arid Central Asia simulated by COSMO-CLM model.", Theoretical and Applied Climatology, http://link.springer.com/article/10.1007/s00704-015-1479-x#, 2015.

Chapter 4 is under review as the following paper:

> **Bijan Fallah**, Ulrich Cubasch, Kerstin Prömmel and Sahar Sodoudi, "A numerical model study on the behaviour of Asian summer monsoon due to orographic forcing of Tibetan Plateau.", under review by Climate Dynamics.

Chapter 5 is under review as the following paper:

> **Bijan Fallah**, Sahar Sodoudi, Emmanuele Russo, Ingo kirchner and Ulrich Cubasch, "Towards modeling the regional rainfall changes over Iran due to the climate forcing of the past 6,000 years.", under review by Quaternary International.

Appendix B

Abbreviations

ACA Arid Central Asia . . . 3
AGCM Atmosphere only Global Circulation Model . . . 29
AOGCM Atmosphere Ocean Global Circulation Model . . . 29
CMZ Core Monsoon Zone . . . 33
COSMOS COmmunity earth System ModelS . . . 29
CRU TS 3.21 Climatic Research Unit Time-Series Version 3.21 . . . 4
CTRL Control . . . 57
ECHAM5 ECMWF operational forecast model cycle 36 and a comprehensive parameterisation package developed at HAMburg version 5 . . . 29
ECMWF European Centre for Medium-Range Weather Forecasts . . . 36
EMD Empirical Mode Decomposition . . . 30
EOF Empirical Orthogonal Function . . . 29
GCM Global Circulation Model . . . 7
GHG Green-House Gas . . . 57
GPCP Global Precipitation Climatology Project
HAMOCC HAMburg Ocean Carbon Cycle . . . 58
IPCC Intergovernmental Panel for Climate Change Fourth Assessment Reports . . . 5
ISM Indian Summer Monsoon . . . 33
ISM Indian Summer Monsoon . . . 33
ITCZ Inter-Tropical Convergence Zone . . . 33
LIA Little Ice Age . . . 5
MADA Monsoon Asian Drought Atlas . . . 30

MCA Medieval Climate Anomaly 5
MPI-ESM Max Planck Institute for Meteorology Earth System Model 57
MPI-M Max Planck Institute for Meteorology 58
MPI-OM Max Planck Institute Ocean Model 29
NCAR National Center for Atmospheric Research
NCDC National Climate Data Center 5
NCEP National Centers for Environmental Prediction
NOTP No Tibetan Plateau 57
OLR Outgoing Long wave Radiation 23
PC Principal Component 23
PDF Probability Density Function 23
PDSI Palmer Drought Severity Index 29
PI Post Industrial 32
SST Seas Surface Temperature 3
TP Tibetan Plateau 8